THE UNIVERSITY OF CHICAGO

FROM ENERGY TRANSFER TO ISOMERIZATION: LOCAL PROTEIN STRUCTURE DICTATES OUTCOME OF PHOTOBIOLOGICAL EXCITED STATE DYNAMICS

A DISSERTATION SUBMITTED TO

THE FACULTY OF THE DIVISION OF THE PHYSICAL SCIENCES

AND

THE FACULTY OF THE DIVISION OF THE BIOLOGICAL SCIENCES

AND THE PRITZKER SCHOOL OF MEDICINE

IN CANDIDACY FOR THE DEGREE OF

DOCTOR OF PHILOSOPHY

GRADUATE PROGRAM IN BIOPHYSICAL SCIENCES

BY

MOIRA LYNN FLANAGAN

CHICAGO, ILLINOIS

DECEMBER 2016

To my loving and amazing sister, Alice Patricia Flanagan

Table of Contents

LIST OF FIGURES vi

LIST OF SCHEMES viii

ABSTRACT ix

ACKNOWLEDGEMENTS xi

1 INTRODUCTION 1
- 1.1 Motivation: The Potential of Photochemistry 1
- 1.2 Two-Dimensional Spectroscopy of Pigment-Protein Complexes 3
  - 1.2.1 Overview of Two-Dimensional Electronic Spectroscopy . . . 3
  - 1.2.2 2DES of Pigment-Protein Complexes 9
- 1.3 The Photosynthetic Reaction Center from *Rhodobacter sphaeroides* . . . 11
  - 1.3.1 Overview of Photosynthesis in Purple Bacteria 11
  - 1.3.2 Energy Transfer in Bacterial Photosynthesis 14
  - 1.3.3 The Bacterial RC as a Model System for Energy Transfer . . 15
- 1.4 Bacteriophytochromes: Function and Photoisomerization 16
  - 1.4.1 Bacteriophytochrome Dynamics and Function 16
  - 1.4.2 Conical Intersections in Bacteriophytochromes 19
- 1.5 Outline of Dissertation 20
- 1.6 References 21

2 PHOTOISOMERIZATION IN BACTERIOPHYTOCHROMES: HOMOGENEOUS MULTI-STEP DYNAMICS OBSERVED DESPITE A HETEROGENEOUS ENSEMBLE OF GROUND STATE CONFORMATION 25
- 2.1 Abstract 25
- 2.2 Introduction 26
- 2.3 Methods 30
  - 2.3.1 Spectroscopy 30
  - 2.3.2 Sample Preparation 31
- 2.4 Results and Discussion 33
  - 2.4.1 $P_r \rightarrow$Lumi-R Conversion of P2 33
  - 2.4.2 $P_r \rightarrow$Lumi-R Conversion of Pa 43
  - 2.4.3 $P_{fr} \rightarrow$Lumi-F Conversion of P2 45
  - 2.4.4 $P_{fr} \rightarrow$Lumi-F Conversion of Pa 47
- 2.5 Conclusion 47
- 2.6 Acknowledgements 50
- 2.7 References 50

3 CHARACTERIZATION OF A SYNTHETIC LIGHT HARVESTING 56

COMPLEX . . . . . .
3.1 Introduction 56
3.2 Results and Discussion 59
3.2.1 Absorption Spectra of the Light Harvesting Complexes . . . 59
3.2.2 2DES of Outer Ring and Alexa Fluor 594 as a Control 67
3.3 Conclusion 70
3.4 Methods 71
3.4.1 Sample Preparation 71
3.4.2 Spectroscopy 71
3.5 Acknowledgements 72
3.6 References 72

4 MUTATIONS TO *R. SPHAEROIDES* REACTION CENTER PERTURB ENERGY LEVELS AND VIBRONIC COUPLING BUT NOT OBSERVED ENERGY TRANSFER RATES 74
4.1 Abstract 74
4.2 Introduction 75
4.3 Methods 77
4.3.1 Sample Preparation 77
4.3.2 Spectroscopy 77
4.4 Results 78
4.4.1 Spectroscopy of Mutant Reaction Centers. 78
4.4.2 Reaction Center Coherences 81
4.5 Discussion 84
4.5.1 Energy Transfer Dynamics. 84
4.5.2 Vibrational Coupling 87
4.6 Conclusion 96
4.7 Viewing this work in the context of Electronic Coherences and Coherent Energy Transfer 98
4.8 Acknowledgements 101
4.9 References 102

5 PROPOSED DIRECTIONS FOR FUTURE RESEARCH 109
5.1 Introduction: Understanding Photochemistry 109
5.2 Bacteriorhodopsin: Exploring Conical Intersections. 110
5.2.1 Mutations that Perturb Isomer Control 114
5.3 Nucleosomes: 2DES of Labeled Proteins to Probe Biology. 116
5.4 Conclusion 120
5.5 References 121
6 CONCLUSION 123
6.1 References 126

List of Figures

Figure 1.1 Pulse characterization of 2DES 5
Figure 1.2 Mock 2D spectrum 7
Figure 1.3 Representative Feynman diagrams of third-order photon echo nonlinear pathways 8
Figure 1.4 Illustration of solvation dynamics of a chromophore 11
Figure 1.5 Chromophores map to spectroscopic features in the Reaction Center 13
Figure 1.6 Bacteriophytochrome structure and function 17
Figure 2.1 Absorption spectra of the purification of P2 32
Figure 2.2 Absorption spectra of P2 and Pa and laser spectrum. 33
Figure 2.3 2DES of P2 in the P_r state at long waiting times 34
Figure 2.4 2DES and dynamics of P2 in the P_r state at short times 35
Figure 2.5 Beating signals of P2 in the P_r→Lumi-R process 36
Figure 2.6 Decay Associated Spectra (DAS) support a homogeneous dynamic model for the P2 P_r→Lum-R conversion 38
Figure 2.7 Proposed model of the P_r→Lumi-R conversion in P2 41
Figure 2.8 Two alternative models to describe dynamics of P2 in the P_r→Lumi-R conversion 42
Figure 2.9 Dynamics of P_r→Lumi-R conversion in Pa closely resemble P2 44
Figure 2.10 2DES and dynamics of P2 in the mixture of P_{fr} and P_r 44
Figure 2.11 Beating signals of P2 in the mixed P_{fr}→Lumi-F and P_r→Lumi-R Processes 46
Figure 2.12 A proposed scheme showing the photodynamics of P_{fr}→Lumi-F conversion 48
Figure 3.1 Structure of the TMV-based synthetic light-harvesting complex 58
Figure 3.2 Comparison of absorption spectra of LH2 and the TMV based light-harvesting systems with their free chromophores 61
Figure 3.3 Narrowing of Outer Ring with decreasing temperature when compared to narrowing of the Mono Ring indicates exchange narrowing due to coupling 63
Figure 3.4 Lineshape model and experimental absorption data 66
Figure 3.5 Excited state vibrations observed in the Outer Ring 2DES 68
Figure 3.6 The coupled Outer Ring decays faster then free Alexa Fluor 69
Figure 4.1 The *R. sphaeroides* Reaction Center complex mutants' structure and absorption spectra 76

Figure 4.2 Rephasing 2DES and Dynamics of Mutant Reaction Centers 80
Figure 4.3 Coherence amplitude and decay rate enhancement at crosspeak locations . 82
Figure 4.4 Dynamics and Coherences from narrow bandwidth laser spectrum 83
Figure 4.5 Decay Associated Spectra for wild type and mutant RCs 86
Figure 4.6 Power spectra reveal vibration-exciton coupling 88
Figure 4.7 Beat map for WT Reaction Center using narrow laser bandwidth 89
Figure 4.8 Feynman Diagrams associated with beating within 2D rephasing spectra of the Reaction Center 91
Figure 4.9 Power spectra of beating in mutant *R. sphaeroides* show changes in vibronic coupling with perturbations to P band transition energy 93
Figure 4.10 Full power spectra of beating in mutant *R. sphaeroides* 95
Figure 5.1 Structure of bacteriorhodopsin from *Halobacter salinarum* 112
Figure 5.2 Retinal isomerization in solution 113
Figure 5.3 The eleven residues within 6 Å of the retinal chromophore 115
Figure 5.4 Scheme for transcription factor access to the DNA packaged into nucleosomes 116
Figure 5.5 Structure and proposed labeling of a mononucleosome 118

List of Schemes

Scheme 2.1 The inter-conversion of biliverdin-IXα between the P_r (15Za) and P_{fr} (15Ea) states 30

Abstract

Photoactive proteins have been studied as a fascinating link between chemistry and biology. The structured environment of the protein both drives specific photochemical reactions and converts the energy from photo-reactions, such as isomerizations, into biological function and signaling. This dissertation presents work that spectroscopically probes the link between energy dynamics and protein function and structure in the photosynthetic reaction center from *R. sphaeroides*, a synthetic light harvesting complex, and the bacteriophytochromes RpBphP2 from *R. palustris* and PaBphP from *P. aeruginosa*. In each of these three systems, chromophores are embedded inside a larger apo-protein. The immediate solvation environment around the chromophore is static compared to a solvent like water and cannot rearrange in response to absorption of light and subsequent change in electronic structure. To investigate the photochemistry itself, the protein's influence on the reaction must be fully understood. Does the relationship between the protein and the chromophore drive the photochemistry by constraining the electrostatic environment? Using two-dimensional electronic spectroscopy (2D-ES), in which the absorption and emission energies of the system are mapped onto two axes, it is feasible to observe differences across an ensemble of complexes each in microscopically different conformations and untangle congested spectra. Chapter 2 presents a study in which the photochemistry and biological function of bacteriophytochromes are shown to persist through significant environmental fluctuations. In chapter 3, a synthetic light harvesting system based on the idea that the protein provides a scaffold for light harvesting is investigated. The system does exhibit noticeable excited state interactions, but does not display the coherent energy transfer characteristic of photosynthetic light harvesting complexes. Chapter 4 presents work that endeavor to perturb energy transfer in the photosynthetic reaction center in purple bacteria.

Incredibly, the complex is able to retain ultrafast energy transfer despite highly disruptive mutations, and we provide evidence that the energy gaps between excitonic states are compensated by the vibrational modes of the bacteriochlorophyll molecules, meaning that the chromophore's intricate vibrational structure in exploited for energy transfer. Finally, this dissertation concludes with proposals for future directions to investigate photochemistry in biology and biology with photochemistry.

Acknowledgements

This dissertation would not exist without the help of many others whom I am very grateful towards. First of all, Professor Greg Engel has been a great mentor and advisor to me. Not only did he believe in me when I certainly did not, he has happily stood by me, allowing me to make my own decisions, and sometimes mistakes, without judgment (as long as I learned a lesson!). Greg, I have all that to thank you for and I haven't even mentioned all you have done to help me develop as a teacher! I have learned so much from you about science, academia, teaching, and management. Thank you.

The Engel research group is an amazing group of people, and I could not have accomplished this work without **all** of them. In particular, I would like to thank Justin Caram and Gitt Panitchayangkoon for taking me under your respective wings when I needed it, and Sara Massey and Nick Williams for talking through ideas and being plain ol' buddies. I would like to thank Cheng "Wave" Wang for working with me on the bacteriophytochrome project, and Phil Long for his work on the Reaction Center project.

I would like to thank my cohort, Caitlin Trejo, Charlie Wright, David Weinstein and Ivy Fitzgerald, for helping me figure out grad school, cell bio, and the biophysics lab course. Michele Wittels, the graduate program in Biophysical Sciences administrator, has become a mentor and friend to me, and I could not have pursued my own goals without her.

I have worked with and collaborated with many people while I have been here at the University of Chicago, and I am grateful to all of them. Most importantly, I am very grateful to my committee members Professors Sean Crosson, Laurie Butler and Andrei Tokmakoff for your time, help, and guidance. I would also like to thank Professors Laurie Mets and Bob Haselkorn for your mentorship and guidance, Professor Keith Moffat for his work on the

bacteriophytochrome project and his assistance in writing a manuscript accessible across the relevant fields, and Professor Yamuna Krishnan for allowing me to help you design a fun and engaging chemistry course.

Many of my friends and loved ones have helped me accomplish this work and get through the more stressful moments in graduate school. I would like to thank my friends Lily Swartz, Jessica Schwartz, Jessi Meliza, Ann Fitzpatrick, and Courtney Sobers, and my loving partner Aaron Wilson for all the support, love and laughter. My mom Robin, my dad Tim, and my brother Brian have all reached out across the distances that temporarily separate us to love and support me. In particular, I need to thank my little sister, Alice, who has no idea how much her love, encouragement, and pure joy for life have helped me accomplish the work presented in this dissertation. She thinks that I am her inspiration, but I would like to record here and forever that I would not have become the woman and scientist that I am or accomplish the things that I have without her. Thank you for your love, Alice.

Chapter 1:

Introduction

1.1 Motivation: The Potential of Photochemistry

Two of the biggest challenges facing our society in the present day are finding renewable resources of energy and developing a way to store said energy[1]. Because the sun provides 120,000 terawatts of daily power, solar energy has become a popular developing branch of technology[2]. In nature, photosynthetic processes in plants and bacteria shoulder this task of harvesting and storing light energy in ATP and hydrocarbon covalent bonds[3]. It is vital to understand how proteins are able to control and tune these processes in order to design our own efficient solar harvesting. Additionally, photochemistry is implicated in many high-energy bond-forming reactions. Therefore, photochemistry may become integral for energy storage technologies, but the same conditions that produce photo-induced high-energy bonds in the lab also result in bond breakages in a seemingly uncontrollable way. Throughout the intersection of photochemistry and biology, pigment-protein complexes perform these high-energy solar powered tasks reliably and with control. Understanding how pigment-protein complexes are able to control reactivity could change photochemistry and its role in synthesis. With society's energy needs increasing, fossil fuels depleting, and climate change on the rise, research efforts towards understanding the design principles underlying photochemistry and photosynthesis have been strengthened over the last few decades[4-7]. In this work, I contribute to this effort by detangling the roles of protein and chromophore in photobiology.

Light-initiated chemical processes comprise a unique branch of chemistry in which control of the reactivity is not straightforward. Photochemical reactions tend to have multiple products, and therefore direct control over these reactions has proven elusive. As scientists, we strive to uncover "design principles" with predictive power that fully describe natural phenomena. Fortunately, biology has given us functional and controlled photochemistry in the form of pigment-protein complexes that we can learn from. Evolution has been optimizing photochemistry and photosynthesis for billions of years, and we can learn from results we observe in the present[8]. It is not necessarily easily accomplished, but we can learn from what nature produced for us. Fortunately, evolution's millennia of guesswork can help us skip some of that work and provide educated guesses and predictions.

Photodynamics in biology are great for learning about the chemistry, but in order to take any generality about the photochemistry away from researching these pigment-protein complexes, we need to know what role the biology or protein plays in these systems, and whether those roles are separable from the photochemistry itself. For instance, biological systems are hot (37 °C), and while this property of biological photochemistry definitely influences the dynamics, one can reasonably guess that it is not the driving force behind every photodynamic process since much more energy is gained from a single absorbed photon. Another strategy that nature introduces is to embed chromophores into apo-protein structure. The relationship between system and bath, chromophore and solvent, is a very old question. There is a large body of work investigating and describing these interactions and how the properties of the solvent molecule relate to the photo-physics of the chromophore. In the case of pigment-protein complexes, this becomes an even more interesting problem. The immediate environment surrounding the chromophore is much more static than the liquid solvents we usually think of. Proteins are much

larger and much slower at responding than small solvent molecules. On the timescale of many light-initiated processes, there is very little protein rearrangement, so the chromophore experiences a remarkably solid, unyielding solvation environment[9]. Is this rigid environment necessary for energy transfer or photochemistry, or is it simply a consequence of biology's available tools and materials? In this dissertation, I employ two-dimensional electronic spectroscopy to elucidate the pigment-protein relationship in driving photochemistry.

1.2 Two-Dimensional Spectroscopy of Pigment-Protein Complexes

1.2.1 Overview of Two-Dimensional Electronic Spectroscopy

Two-dimensional electronic spectroscopy (2DES) is an ideal tool to investigate biological photochemistry because it resolves congested spectra typical of many pigment-protein complexes with femtosecond time resolution (10 fs typical pulse width) and broadband spectral resolution onto two axes giving path information[10-14]. Photochemical reactions in biology progress on a wide range of timescales, but many critical steps occur on femtosecond to hundreds of picosecond timescales, a range not accessible by many techniques. In bacterial photosynthetic complexes, energy transfer steps can be as fast as 100 fs and up to 800 ps[15, 16], while isomerizations in rhodopsins and phytochromes range from 50 fs to a few picoseconds[8, 17, 18]. Traditional spectroscopies with the same time resolution have been developed, but 2D spectroscopies are unique in that they correlate specific excitation energies with their respective fates after time evolution of the system. That is, with 2DES, it is possible to match input energy with output energy to get specific path information about the excited state. The ability to correlate energies provides heterogeneity information and allows more specific assignments of

signals and features. 2DES allows us to analyze the trajectory of each individual subpopulation across an ensemble of complexes separately to better understand the system of interest.

It is critical to understand how the technique probes and measures a system in order to understand what information it provides about the sample. Electrons define chemistry and photochemistry is included. When light interacts with matter, as oscillating electromagnetic radiation, it acts as a force field on the valence electrons[19]. The light radiation oscillates at the frequency corresponding to its energy and as it interacts with matter, it pushes and pulls on the molecule's electrons. If the energy of the oscillating field is near resonant with the energy of an allowed transition of the valence electrons, it may be absorbed by the electron and promote it to a higher energy excited state. Excited electrons are pushed further from equilibrium than an atom or molecule's ground state configuration. How this electron evolves along the excited state and ultimately relaxes radiatively, or nonradiatively back to the ground state is the subject of much of the research that employs 2DES[20].

2DES is powerful time-resolved broadband spectroscopy that utilizes nonlinear, four wave mixing[10-14, 20-22]. The four phase-stabilized ultrafast broadband pulses each interact with the sample in a particular order (Fig. 1.1). The first two pulses are separated by the *coherence time* while the time between the second and third pulse is defined as the *waiting time*, analogous to the delay time in pump probe spectroscopies. The fourth pulse is highly attenuated to prevent nonlinear interactions with the sample and is aligned to propagate in the same direction as the signal pulse. The fourth pulse interferes with the signal to provide time information. The four pulses are focused onto the sample to a single point from a boxcar geometry, or from the four corners of a square (Fig. 1.1b). The signal is only constructive in a

single phase-matched direction that coincides with the local oscillator direction. This physically separates signal from the incoming pulses and noise, giving better signal to noise.

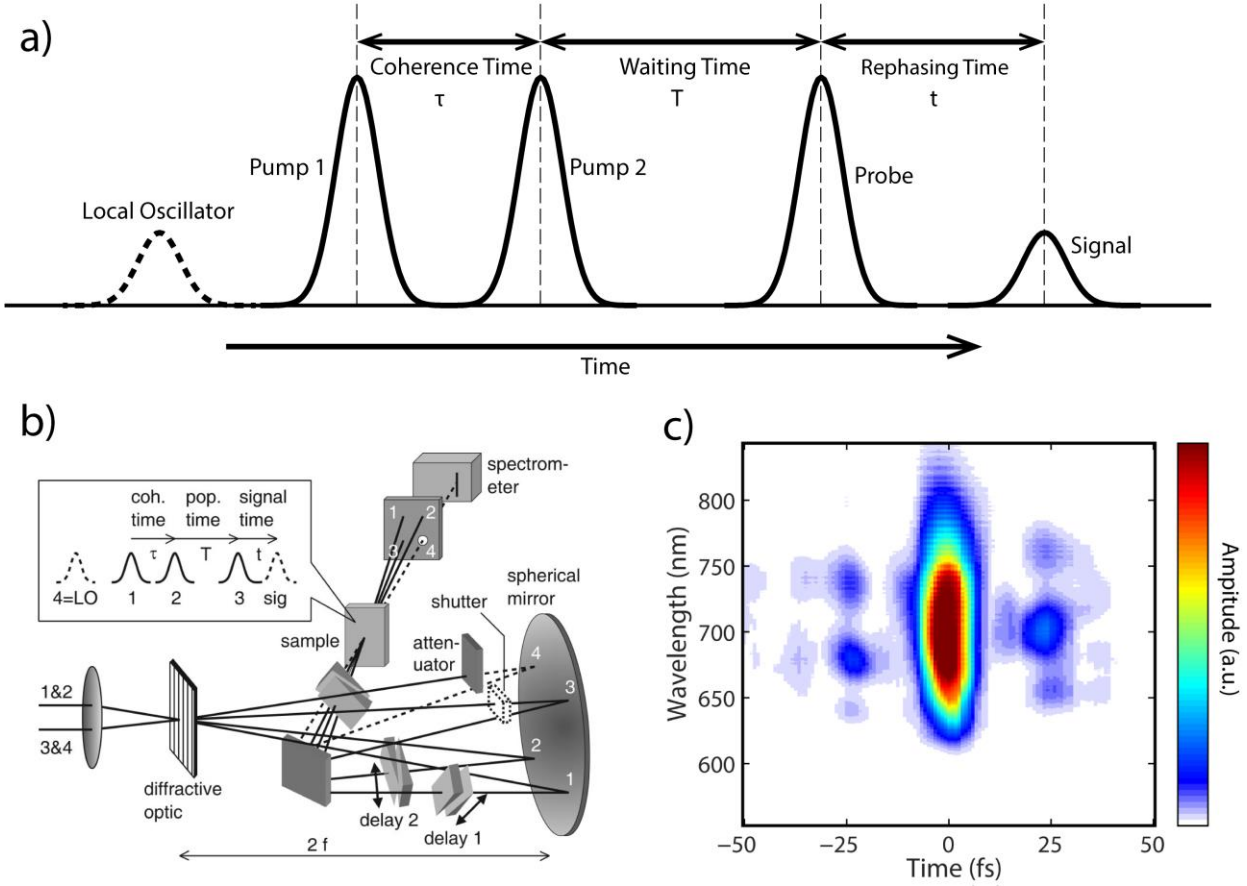

Figure 1.1: Pulse characterization of 2DES (a) Pulse sequences required for 2DES techniques. (b) experimental setup for the spectrometer described in Ref. [23]. Pulses 1 and 2 act as the pump beam that initializes the photochemical process. As the waiting time (also referred to as the delay time) progresses, the system evolves. When pulse 3 interacts with the system, the system evolution is halted, and the ability for the system to retain memory of the initial state is tested by the production of a photon echo after time *t*. The photon echo signal is heterodyne detected by interfering with a highly attenuated local oscillator pulse and imaged with wavelength resolution on a CCD camera. Figure is reproduced with permission from Ref. [23]. (c) Transient-grating Frequency Resolved Optical Grating (TG-FROG)[24] characterization of a typical short, broadband pulse.

For each waiting time, the coherence time is varied over the experimental interval, typically 100-400 fs in 1 or 4 fs steps and signal is collected and integrated. The coherence time

acts as a filter, selectively allowing pathways with resonant transition energies, and data is collected for the range of coherence times to collect path information for the full range of transition energies. That is, with the first pulse, phase evolution is initiated, but with the second, it is halted and photochemistry is allowed to evolve for a set waiting time. The third pulse tests the ability of the ensemble to get back to its initial state or rephase. Essentially, it starts the ensemble to evolve back to its original state. If the system is capable of rephasing, the system constructively interferes to create a macroscopic polarization across the sample, which emits a photon echo signal[11]. Together, the intensity, time of rephasing, and spectrum of the signal create a full picture of the evolution in the waiting time. In 2DES, the photon echo is interfered with the local oscillator and wavelength or frequency resolved and recorded *for each* coherence time. The end result is a 2D plot of interferograms that contains all the necessary information though it must be extracted with some simple analysis[25].

The 2D interferogram is discrete Fourier transformed across the energy (wavelength) axis into a plot with two time axes: the coherence time and the *rephasing time*, or the time between the third pulse and the signal acquisition[7]. In this form, it is easy to isolate the signal from the local oscillator and scattered light that made it to the camera. Once the signal is isolated, it is then two dimensional Fourier transformed such that its two axes are coherence frequency and rephasing frequency, which can be thought of as the frequency of light absorbed by a member of the ensemble (coherence frequency) and the frequency of light emitted after the delay time by the same wave packet[23]. This results in a 2D plot that can correlates input energy and output energy (Fig. 1.2). In this plot, the peaks along the diagonal denote spectroscopic features that have retained their memory from the beginning of the experiment. Off-diagonal peaks, or *crosspeaks*, denote energy transfer from the feature with the energy of the coherence frequency

towards a feature with the energy of the rephasing frequency[13]. Negative features denote excited state absorption while positive features represent both stimulated emission and ground state bleach pathways[23].

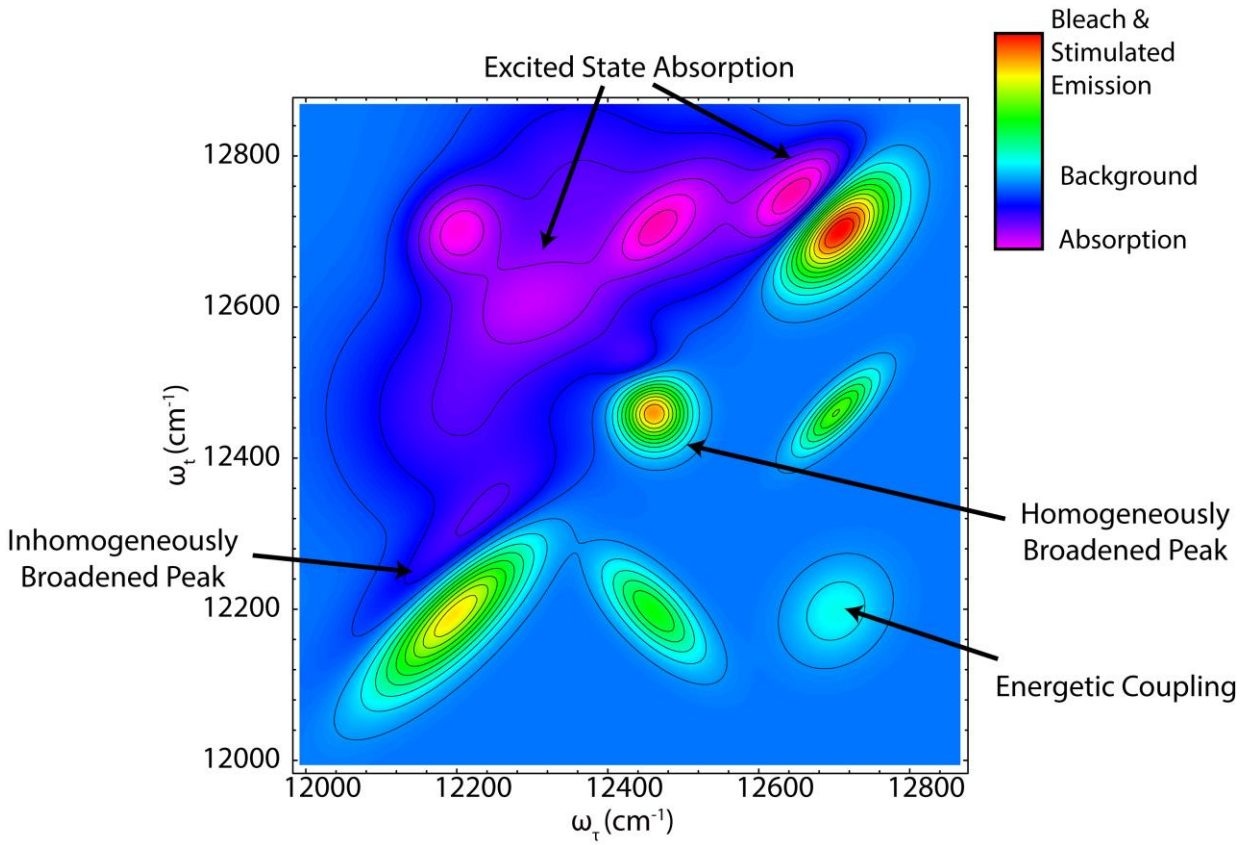

Figure 1.2: Mock 2D spectrum to illustrate types of features in 2DES. Features that are inhomogeneously broadened appear elongated along the central diagonal while peaks that expand equally in all directions show homogeneous broadening. Cross peaks represent coupling, transfer, and excited state absorption. Figure is reproduced with permission from Ref. [20].

The final 2D spectrum is a combination of signals from many different pathways and unraveling the contributions is one of the major hurdles in performing 2DES experiments. The signal in the 2DES spectrum originates from the interaction of the incident electric field of the laser pulse with the collective polarization of all the dipoles in the ensemble[20]. The oscillation of the polarization, induced by the oscillating electric field causes the emission of a signal

field[25]. The third order polarization, the relevant polarization for 2DES, can be expressed in terms of the sample's response function, $R^{(3)}(\tau_1, \tau_2, \tau_3)$ as

$$P^{(3)}(t) = \iiint_0^\infty R^{(3)}(\tau_1,\tau_2,\tau_3)E(t-\tau_1-\tau_2-\tau_3)E(t-\tau_2-\tau_3)E(t-\tau_3)d\tau_1 d\tau_2 d\tau_3$$

The response function, $R^{(3)}(\tau_1, \tau_2, \tau_3)$ describes the polarization due to a set of interactions, and there are many third order response functions that happen simultaneously in an experiment,[25] and hence each response function leads to signal from a unique set of interactions.[26] It can be difficult keeping track of all the response functions and what interactions they represent, so in this dissertation, we will use Feynman diagram as a shorthand.

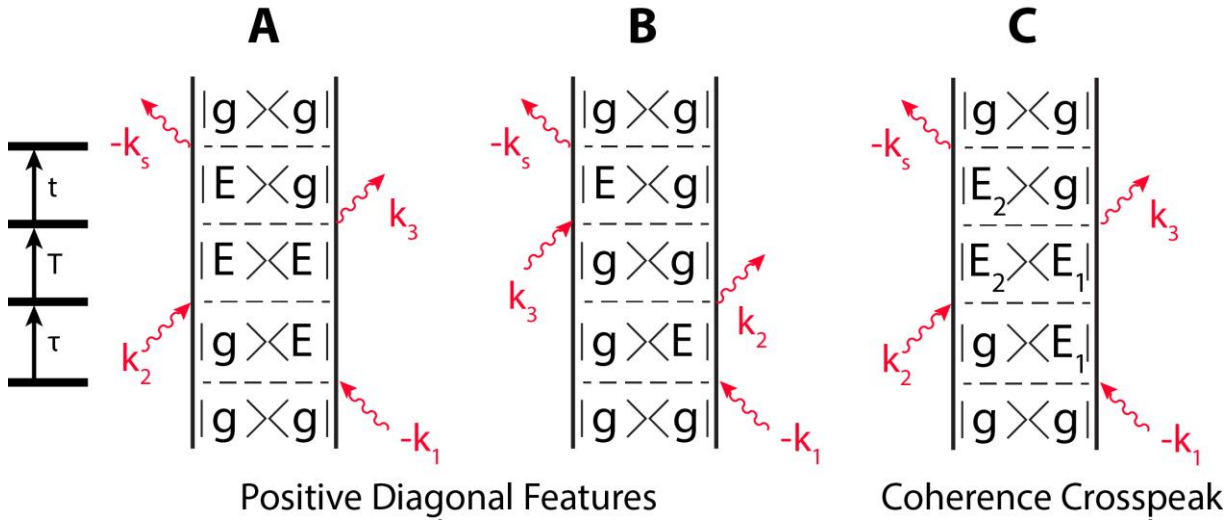

Figure 1.3: Representative Feynman diagrams of third-order photon echo nonlinear pathways. Time is indicated on the left as moving upward in the diagrams. The ground state is indicated by 'g' and accessible excited states by 'E', 'E_1' or 'E_2'. Diagram A shows a stimulated emission pathway, Diagram B shows a ground state bleach pathway and diagram C shows a stimulated emission beating crosspeak pathway[26].

Feynman diagrams encode all of the time dependent interaction and state information in a convenient visual manner (Fig. 1.3). By convention time progresses upwards in the diagram, and each interaction is represented by an arrow—pointed inward for absorption and away for

emission. For instance, the first pulse interaction is represented as the $-k_1$ arrow at the bottom of the diagrams in Fig 3. The density matrix elements represented as the outer product *bra-ket* notation, e.g. $|g\rangle\langle g|$, describe the state of the ensemble participating in this particular pathway. With each interaction, the state of the ensemble is perturbed. With these diagrams in hand, it is straightforward to dissect all of the possible pathways contributing to a particular signal. For example, the Feynman diagrams A and B in Fig. 1.3 both represent pathways that would contribute to a diagonal peak in the 2D spectrum, but arise from evolution on two different potential energy surfaces during the waiting time, T. However, in diagram C, the input energy is the difference between g and E_1 but the signal, $-k_s$, is the energy difference between E_2 and g. Therefore, diagram C represents a crosspeak signal between E_1 and E_2. Diagram C also shows a pathway in which the ensemble evolves in a coherence during the waiting time. A coherence is when an ensemble cannot be described as being in a mixture of pure states, but rather in a superposition of two states, E_1 and E_2 in diagram C. This results in an oscillation in the intensity of the 2DES signal at the frequency of the energy difference between E_1 and E_2.

1.2.2 2DES of Pigment-Protein Complexes

In this dissertation, I will be discussing the purple bacteria reaction center, two bacteriophytochromes, and a synthetic light harvesting system and 2DES data of their respective excited state dynamics. Here, I would like to discuss the basic principles of pigment-protein complexes and how to think of them in regards to spectroscopy. A pigment-protein complex is defined as any protein or protein fragment that has a chromophore associated with it either non-covalently embedded within or covalently attached to a side chain. Interestingly, these complexes rely on chromophore's interaction with a photon for their *biological* function. For example, the pigment-protein complex rhodopsin, which is responsible for our vision, needs its

chromophore retinal to undergo photo-induced isomerization in order to start a signaling cascade communicating that light was observed[18].

Proteins their constituent amino acid side chains are always in motion, but at a much slower timescale than photochemical reactions take place. When a chromophore absorbs a photon in a polar solvent (like water), the surrounding solvent molecules are no longer in the lowest energy arrangement, and therefore rearrange quickly to accommodate this new dipole (Fig. 1.4)[27]. However, a protein environment surrounding a chromophore does not have as many degrees of freedom which should indicate that the choice of amino acids directly surrounding the chromophore are very important for determining its spectroscopic properties. That is, the protein motion is effectively "frozen" on the timescale of 2DES experiments. Additionally, the relatively static nature of the surrounding protein means that slight differences in conformations in the ensemble will be resonant with slightly different transition energies. In an absorption spectra, this manifests as a wider absorption peak, but so do ultrafast relaxation processes that occur in every member of the population. 2DES can distinguish between these two spectral broadening mechanisms since it separates the absorption axis from the transition energy at a later time when the experiment is probed[9, 28]. In 2DES, differences in protein conformations that result in a range of transition energies, or *inhomogeneous broadening*, will manifest as a diagonally elongated peak. That is, a single pigment protein complex that absorbs on the blue edge of the ensemble spectroscopic peak will still be on the blue edge later as long as the time to change conformation[28] is longer than the experiment. Broadening that results from ultrafast relaxation processes and the randomized nature of the bath is called *homogeneous* broadening and manifests as a peak that expands evenly in all directions as time progresses resulting in a very round peak.

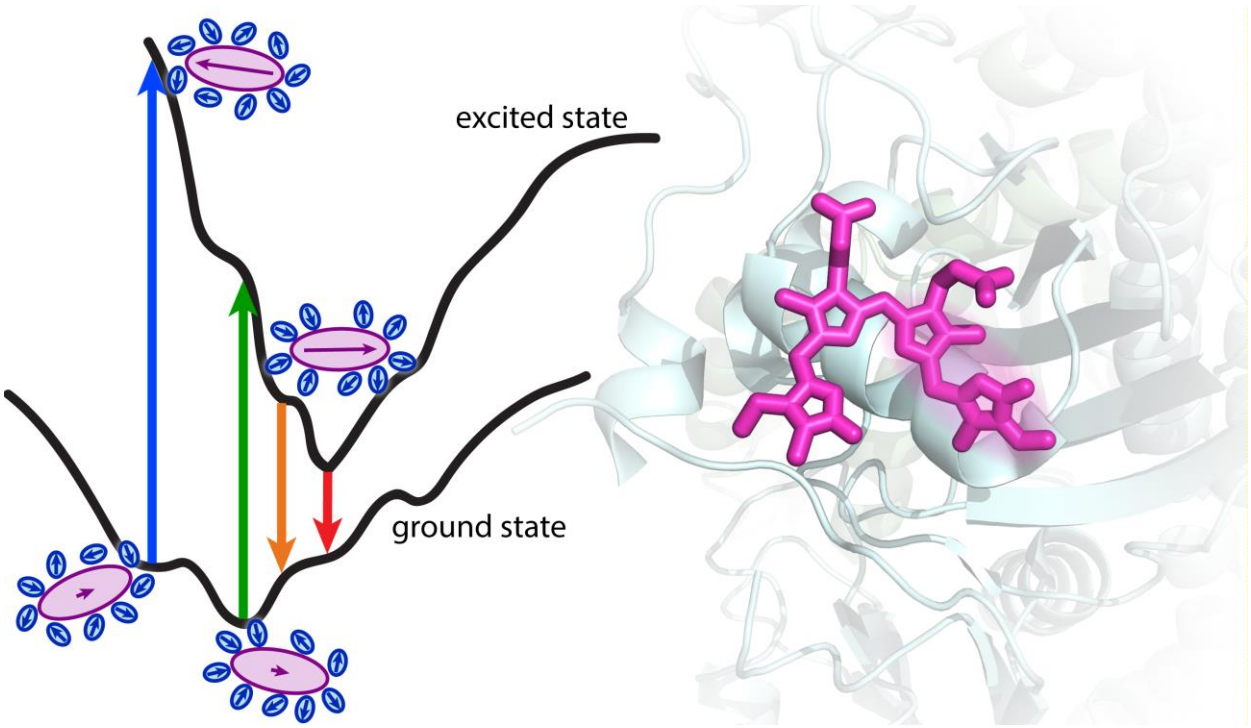

Figure 1.4: Two dimensional projection illustration of solvation dynamics of a chromophore in solution and how solvation differs when a chromophore is embedded in a relatively static and structured apoprotein.

1.3 The Photosynthetic Reaction Center from *Rhodobacter sphaeroides*

1.3.1 Overview Of Photosynthesis In Purple Bacteria

Photosynthesis is the canonical example of the intersection of photochemistry and biology, and has been around in one form or another long before multicellular life came into being[29]. Significant work has gone into understanding photosynthesis and designing photosynthesis-inspired devices to harvest light into useful energy[2, 7, 8, 30, 31]. It is important to understand the processes that have evolved to carry out each step of photosynthesis if we want to infer design principles from the millions of years of trial and error evolution. It is most common to think of carbon fixation or how plants emit oxygen when one hears the word

photosynthesis, but in this work, I will only address the first few steps of light absorption and energy transfer, which all occur before any traditional chemistry, like the splitting of water , begins to occur. In recent years, there have been suggestions that quantum mechanical effects may assist the efficiency and speed of energy transfer in the initial steps of photosynthesis[7, 32], and in Chapter 4 of this dissertation, I investigate how the relationship between the protein and its chromophores influences this initial light absorbing and energy transfer process in the purple bacteria *Rhodobacter sphaeroides.*

Unlike algae and higher plants, photosynthesis in purple bacteria is not an oxygenic photosynthetic process and lacks the carbon fixation cycle, like that of algae and higher plants[29]. Rather, it is a relatively simple system of light harvesting, charge separation, electron transport, and ATP synthesis. *R. sphaeroides* possess the capability to grow both aerobically with aerobic respiration and anaerobic with anaerobic photosynthesis. The cells form invaginations in the membrane called chromatophores that contain two light harvesting complexes, LH1 and LH2, a reaction center (RC), cytochrome bc1, and ATP synthase[8]. Light harvesting complexes LH2 absorb far-red (800 nm and 850 nm) photons and the energy is transferred through the LH2 network until it reaches an LH1/RC complex. LH1 wraps around two RC complexes in a figure eight shape. The energy transfers to the LH1 and then undergoes a slightly uphill transfer to the special pair bacteriochlorophylls in the reaction center. Charge separation occurs in the RC, and the electron is transferred across the membrane within the RC to the antiporter cytochrome bc1 complexes where it travels downhill across the membrane in exchange for a proton used to power ATP synthase. Lastly, an electron is replaced onto the special pair of a RC by a cytochrome complex[8]. Since the reaction center is the focus of chapter 4 of this dissertation, it is worth narrowing our focus to describe the reaction center.

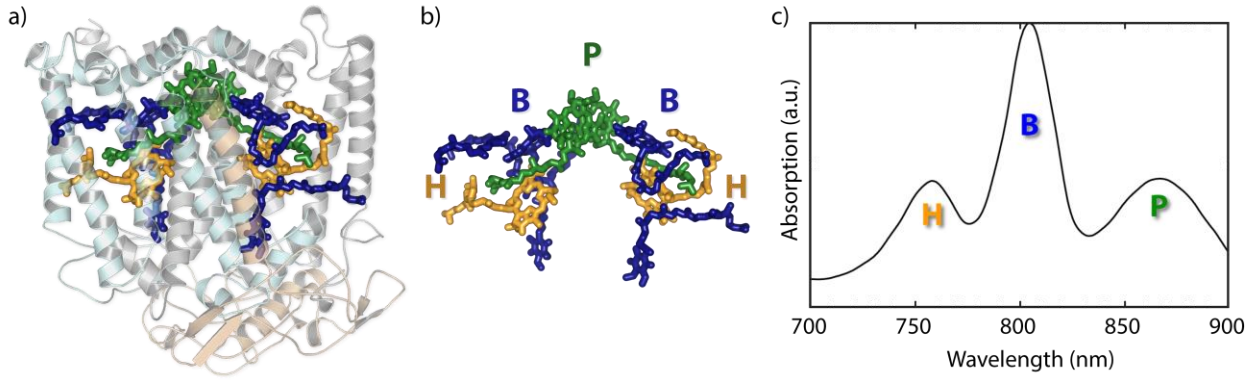

Figure 1.5: Chromophores easily map to spectroscopic features in the RC. (a) The full reaction center protein surrounding non-covalently embedded chromophores (b) Rendering of representative RC cofactor as they appear within the larger protein structure. (c) Absorption spectrum of the RC at room temperature with absorption peaks labeled with the constituent chromophores.

The reaction center (RC) is made of three polypeptides folded into the transmembrane complex shown in Fig. 1.5. Inside the protein matrix, there are two quasi-symmetric branches of chromophores. There are two tightly coupled bacteriochlorophyll molecules at the top of the complex in Fig. 1.5 called the special pair that comprises the P feature on the absorption spectrum in Fig. 1.5. The special pair is followed by two bacteriochlorophylls, one on each side of the branched configuration. These are called the accessory bacteriochlorophylls and correspond to the spectroscopic feature marked B in Fig. 1.5. After the accessory bacteriochlorophylls, each branch has a bacteriopheophytin, which corresponds to the H peak in the absorption spectrum. Finally, each branch has a quinone on the cytoplasmic side of the complex. The RC acts as the charge separation complex *in vivo*. That is, after the absorption of energy either from LH1 or from absorption of a photon, the excited state P* easily loses an electron to the neighboring chromophores, overwhelmingly to the A side of the branched structure. The exact path of transfer is still debated in the field, but the electron eventually makes it to the A quinone and is subsequently transferred to the B side quinone. After two electrons

make it to the B side quinone, properly a quinol, it is ejected from the complex and replaced with a quinone. The electrons on the quinol later help the cytochrome bc1 complex pump protons to power ATP synthase.

1.3.2 Energy Transfer in Bacterial Photosynthesis

The majority of energy transfer in the photosynthetic light harvesting of purple bacteria occurs through Förster resonance energy transfer (FRET) hops from complex to complex. FRET occurs when electrostatic coupling between the transition dipoles of the exciton states in question is weaker than the environmental fluctuations. Immediately upon absorption of a photon, the excitation loses energy to the bath and relaxes to its lowest vibrational state. The efficiency and speed of energy transfer through FRET is determined by the coupling strength, the dipole strengths of both the donor, and acceptor states, the fluorescence lifetime of the donor and the spectral overlap between the emission spectrum of the donor and absorption spectrum of the acceptor. More overlap in the two spectra means that there is a greater probability of energy transferring between isoenergetic states and is therefore faster. FRET occurs on the time scales of nano to milliseconds, so a FRET decay process is also competing with a radiative decay. The fluorescence lifetime of the donor must be longer than the time of energy transfer.

When coupling between exciton states is much stronger than coupling between the system and bath, Redfield theory describes energy transfer very differently. Instead of hopping between a donor and acceptor, energy begins delocalized and as time progresses and fluctuations from the bath influence the delocalized state, it localizes onto one or a few chromophores. This process occurs much faster than FRET and relies on interactions with the bath to relax to a final state. However, coupling between chromophores within photosynthetic complexes in purple

bacteria is between the Redfield and FRET regimes and the transport of energy from the site of absorption to the reaction center must be considered distinctly.

Bacteriochlorophylls within the light harvesting and reaction center complexes in *R. sphaeroides* are arranged such that the coupling between excitons is approximately equivalent to coupling to the bath. The photosynthetic complexes live in the happy medium of delocalization across many chromophores and interactions with the environment that cause decoherence. This behavior has been categorized as coherent resonance energy transfer (CRET) since it uses the coherences of the Redfield regime, but results in transport not just localization. This category of energy transfer is thought to be responsible for energy transfer within photosynthetic complexes while FRET governs transfer between complexes. Chapter 4 of this dissertation will focus on properties of energy transfer in the purple bacteria reaction center and how the excitons interact with their environment.

1.3.3 The Bacterial RC As A Model System For Energy Transfer

The RC complex is also capable of light harvesting and energy transfer in addition to its core function, electron transfer. In fact, one of the important reasons for the multitude of light harvesting complexes in purple bacteria is simply to increase the surface area for absorption without the cell having to produce many of the metabolically expensive RCs. Because of the RC's ability to perform all three bacteriochlorophyll tasks, the RC is often used as a model system for all three processes, and will be used as a model system for energy transfer in chapter 4 of this dissertation. Unlike LH2 and LH1, the complexes primarily responsible for photosynthetic light harvesting and energy transfer in *R. sphaeroides* which each have many bacteriochlorophylls congested into a single spectroscopic peak, the reaction center has three very distinct spectroscopic features within our bandwidth that are each composed of two

chromophores per complex (Fig. 1.5). This feature of the reaction center makes it an ideal complex for dissecting spectroscopic signatures and assigning dynamics and populations to the correct molecules. All of the chromophores in the RC are capable of light absorption, but energy transfer typically occurs downhill in energy from H to B to P, the *opposite* direction as electron transfer.

1.4 Bacteriophytochromes: Function and Photo-isomerization

1.4.1 Bacteriophytochrome Dynamics and Function

Chlorophylls and bacteriochlorophylls are not the only important pigments in biology. There are many examples of pigment-protein complexes that absorb light, undergo a conformation change, and initiate a signaling pathway. One of the most ubiquitous examples of photo-isomerization in biology is class (bacterio)phytochrome proteins. In this dissertation, I will discuss two bacteriophytochromes, but the closely related plant phytochromes are also of great interest to researchers across chemistry and biology (Fig. 1.6). Bacteriophytochromes have a linear tetrapyrrole covalently attached to a conserved cysteine and embedded within the larger complex[33-35]. Bacteriophytochromes form homodimers *in vivo* and undergo a large-scale rearrangement of the entire protein complex upon isomerization of its chromophore. Neighboring proteins recognize this conformation change and this leads to changes in expression of light sensitive genes or circadian rhythm processes.

In chapter 2 of this dissertation, I will discuss the isomerization dynamics in two bacteriophytochromes RpBphP2 (P2) from *Rhodopseudomonas palustris* and PaBphB (Pa) from *Pseuodomonas aeruginosa.* P2 is a bacteriophytochrome highly representative of the class of proteins. It adopts a red (~700 nm) state (P_r) in the dark and is converted to a far-red (~750 nm)

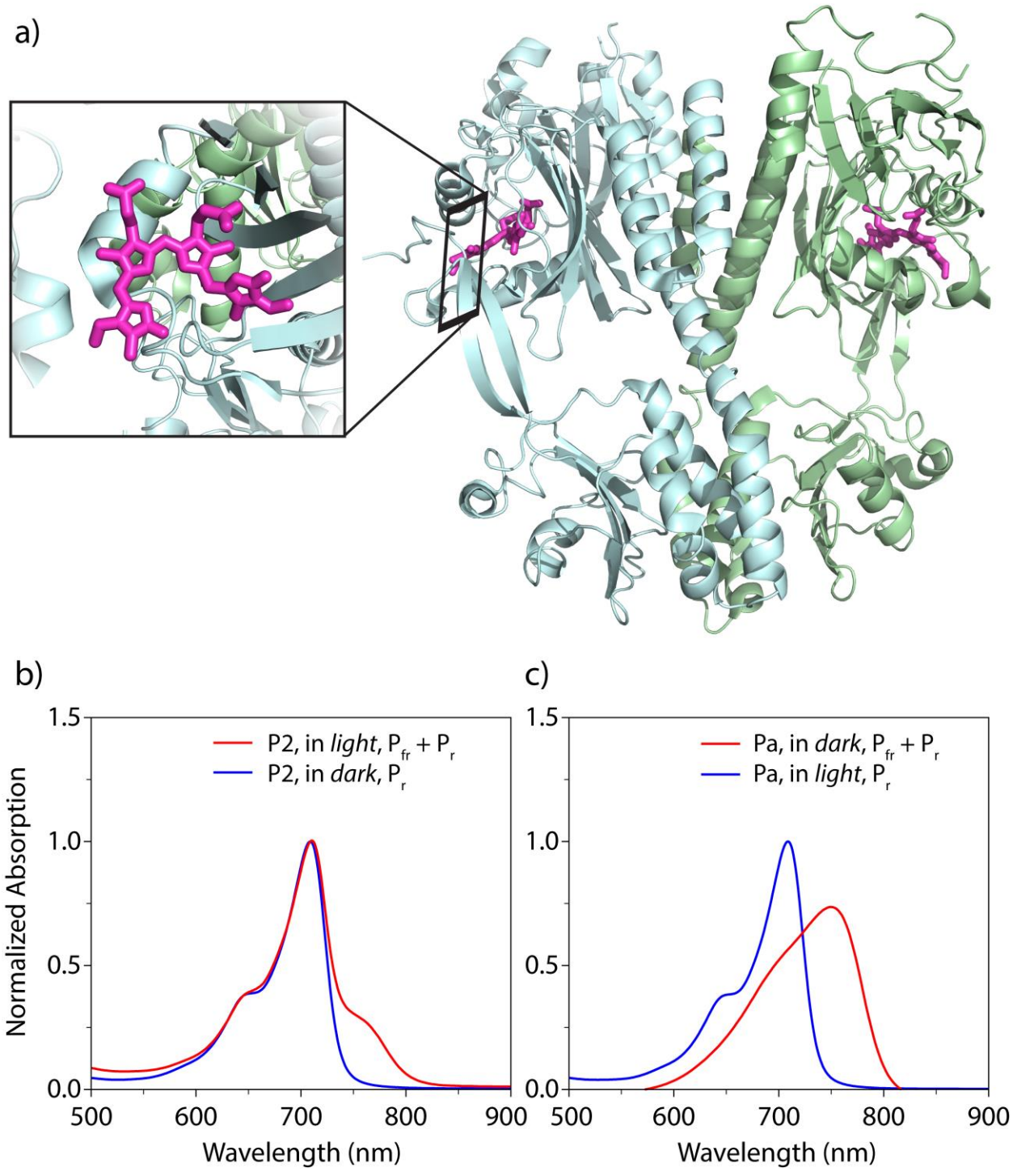

Figure 1.6: Bacteriophytochrome structure and function. (a) P2 bacteriophytochrome with biliverdin inset. Isomerization causes the D-ring to flip and the protein structure responds with a large rearrangement. (b) absorption of both P2 and Pa in both their P_r and P_{fr} states.

state (P_{fr}) upon illumination with far-red light (Fig. 1.6b). *R. palustris* is an aquatic photosynthetic bacterium that is often found beneath layers of phytoplankton. Because phytoplankton absorb strongly in the visible, *R. palustris* has evolved to collect light in the wavelengths far red of 800 nm with its LH2 complex that absorbs light centered at 860 nm (Note that this is distinct from LH2 in *R. sphaeroides).* However, *R. palustris* is also able to express an LH4 complex that absorbs light centered at 800 nm, where much more light would be available in the absence of the phytoplankton layer. Since it is metabolically expensive to produce both complexes at all times, the organism has developed a way to only express LH4 when visible light is available. P2, in coordination with RpBphP3 (P3), a very similar bacteriophytochrome, act as an "AND" gate to detect available visible light indicating the depletion of the algae and cyanobacteria layers above[36]. The cell is able to upregulate LH4 in response to auto-phosphorylation of both complexes P2 and P3 due to $P_r \rightarrow P_{fr}$ conversion. LH4 then enables the cell to collect much more light energy when it is available.

Unlike P2 and most other bacteriophytochromes, Pa from *P. aeruginosa* adopts a P_{fr} state in the dark and converts to P_r in the presence of light. The reason for both the backwards photoconversion cycle as well as the biological function for this phytochrome are still under investigation[37]. Phytochromes are usually associated with photosynthetic machinery regulation, as in *R. palustris*, but *P. aeruginosa* is not a photosynthetic bacterium. Another bacteriophytochrome, DrBphP (Dr) with the same unusual photocycle as Pa has been discovered in *Deinococcus radiodurans*[38]. This bacteriophytochrome has been linked to carotenoid synthesis as photoprotection, but *P. aeruginosa* does not have any carotenoids so Dr and Pa bacteriophytochromes cannot have the same function. Pa has been linked as a contributor to

quorum sensing, but why a light sensor is necessary in quorum sensing and what role Pa plays specifically are still unknown[37].

Both P2 and Pa bacteriophytochromes have a biliverdin molecule, a linear tetrapyrrole, covalently embedded inside the protein and both undergo a $P_r \leftrightarrow P_{fr}$ conversion cycle in response to light. How this isomerization proceeds in a fluctuating and noisy environment is the focus of chapter 2 of this dissertation. Presently, there are two competing proposals for this isomerization in the field[39]. In one model, the isomerization proceeds entirely on the excited state. There is a local minimum on the excited state potential energy surface above the isomerization product and the excitation decays when it becomes locally stuck in that well. In the other hypothesis, isomerization occurs through both the excited and then the ground state. The system evolves away from the Franck-Condon region on the excited state but then decays at an avoided crossing or conical intersection between the two isomer product wells. The direction of reaction after decay to the ground state determines the product.

1.4.2 Conical Intersections in Bacteriophytochromes

The isomerizations of chromophores within (bacterio)phytochromes are thought to convert through a mixed excited and ground state process by passing through a conical intersection[39, 40]. When the Born-Oppenheimer approximation that allows the separation of electronic and nuclear motion breaks down, it is possible for two adjacent potential energy surfaces touch[41-45]. In fact, these degenerate points are very common and are found across photochemistry[46]. When this intersection is viewed in two relevant nuclear coordinates, it occurs at a single point and the resulting double cone shape of the two energy surfaces give conical intersections their name. In the other N-2 available dimensions, this intersection appears as a seam connecting the two adjacent potential energy surfaces.

Conical intersections provide us with a new way to think about photochemistry. The conical intersection point connects many different product wells in the lower energy surface and often, many of these wells are accessible from the degeneracy[47]. The degeneracy also allows ultrafast decay from excited to ground state and thus, the relative energies of the multiple product wells become practically obsolete. Rather, the momentum of the decaying wavepacket as it passes through the intersection point is more likely to determine the product formation. Therefore, the reliability of conical intersection reactions in pigment-protein complexes is most likely due to a consistent "push" or vibration, which sends the decaying wavepacket towards the same product well each time it absorbs a photon. That is, conical intersections can hypothetically be controlled by manipulation of the two branching nuclear coordinates that define the single point degeneracy. The C_{15}=C_{16} isomerization in both P2 and Pa bacteriophytochromes occurs with a higher quantum yield than biliverdin without an apo-protein indicating that the protein surrounding the chromophore is able to evolve and influence the reactivity of its chromophore through the conical intersection decay. In order to understand the design principles of photoreceptor proteins, it is essential to isolate and understand the essential motion that controls reactivity.

1.5 Outline of Dissertation

The aim of the research in this dissertation is to uncover the core design principles that govern photon-initiated dynamics or reactions in biological systems. Here, I present 2DES studies that probe the persistence of photochemistry in nature. In chapter 2, I discuss two bacteriophytochrome proteins. In both of these proteins, excited state dynamics proceed reliably regardless of fluctuations and small conformation differences showing that they are robust to the

heat and random fluctuations inseparable from a living environment. In chapter 3, I investigate a synthetic light harvesting system built with specific design principles in mind. I ask if the design considered in this system is sufficient to recreate coherent energy transfer and efficient, ultrafast light harvesting. Photosynthetic energy transfer and light harvesting is further investigated in chapter 4, where I present the results when point mutations to the chromophore binding pocket are introduced and the chromophore solvation environment changes drastically. Interestingly, we find that energy transfer is able to survive large changes to the electronic environment and discuss possible explanations for this surprising result.

1.6 References

[1] T.M.I. Mahlia, T.J. Saktisandan, A. Jannifar, M.H. Hasan, H.S.C. Matseelar, A review of available methods and development on energy storage; technology update, Renew Sust Energ Rev 33 (2014) 532-545.

[2] G.W. Crabtree, N.S. Lewis, Solar energy conversion, Phys Today 60 (2007) 37-42.

[3] E. Rabinowitch, Govindjee, Photosynthesis, Wiley, New York,, 1969.

[4] T. Brixner, J. Stenger, H.M. Vaswani, M. Cho, R.E. Blankenship, G.R. Fleming, Two-dimensional spectroscopy of electronic couplings in photosynthesis, Nature 434 (2005) 625-628.

[5] E. Harel, G.S. Engel, Quantum coherence spectroscopy reveals complex dynamics in bacterial light-harvesting complex 2 (LH2), Proceedings of the National Academy of Sciences of the United States of America 109 (2012) 706-711.

[6] E.E. Ostroumov, R.M. Mulvaney, R.J. Cogdell, G.D. Scholes, Broadband 2D Electronic Spectroscopy Reveals a Carotenoid Dark State in Purple Bacteria, Science 340 (2013) 52-56.

[7] G.S. Engel, T.R. Calhoun, E.L. Read, T.K. Ahn, T. Mancal, Y.C. Cheng, R.E. Blankenship, G.R. Fleming, Evidence for wavelike energy transfer through quantum coherence in photosynthetic systems, Nature 446 (2007) 782-786.

[8] R.E. Blankenship, Molecular mechanisms of photosynthesis, Second edition. ed., Wiley/Blackwell, Chichester, West Sussex, 2014.

[9] X.J. Jordanides, M.J. Lang, X.Y. Song, G.R. Fleming, Solvation dynamics in protein environments studied by photon echo spectroscopy, Journal of Physical Chemistry B 103 (1999) 7995-8005.

[10] S. Mukamel, Principles of nonlinear optical spectroscopy, Oxford University Press, New York, 1995.

[11] T. Brixner, T. Mancal, I.V. Stiopkin, G.R. Fleming, Phase-stabilized two-dimensional electronic spectroscopy, J Chem Phys 121 (2004) 4221-4236.

[12] M.L. Cowan, J.P. Ogilvie, R.J.D. Miller, Two-dimensional spectroscopy using diffractive optics based phased-locked photon echoes, Chemical Physics Letters 386 (2004) 184-189.

[13] J.D. Hybl, A.A. Ferro, D.M. Jonas, Two-dimensional Fourier transform electronic spectroscopy, J Chem Phys 115 (2001) 6606-6622.

[14] D.M. Jonas, Two-dimensional femtosecond spectroscopy, Annu Rev Phys Chem 54 (2003) 425-463.

[15] D.C. Arnett, C.C. Moser, P.L. Dutton, N.F. Scherer, The first events in photosynthesis: Electronic coupling and energy transfer dynamics in the photosynthetic reaction center from Rhodobacter sphaeroides, J Phys Chem B 103 (1999) 2014-2032.

[16] X.J. Jordanides, G.D. Scholes, G.R. Fleming, The mechanism of energy transfer in the bacterial photosynthetic reaction center, J Phys Chem B 105 (2001) 1652-1669.

[17] Y. Yang, M. Linke, T. von Haimberger, J. Hahn, R. Matute, L. González, P. Schmieder, K. Heyne, Real-Time Tracking of Phytochrome's Orientational Changes During Pr Photoisomerization, Journal of the American Chemical Society 134 (2012) 1408-1411.

[18] L.A. Peteanu, R.W. Schoenlein, Q. Wang, R.A. Mathies, C.V. Shank, The 1st Step in Vision Occurs in Femtoseconds - Complete Blue and Red Spectral Studies, Proc Natl Acad Sci U S A 90 (1993) 11762-11766.

[19] D.J. Griffiths, Introduction to electrodynamics, 3rd ed., Prentice Hall, Upper Saddle River, N.J., 1999.

[20] M.H. Cho, T. Brixner, I. Stiopkin, H. Vaswani, G.R. Fleming, Two dimensional electronic spectroscopy of molecular complexes, J Chin Chem Soc-Taip 53 (2006) 15-24.

[21] B. AM, T. DB, S. GD, Crossing disciplines - A view on two-dimensional optical spectroscopy, Ann. Phys. (Berlin) 526 (2013) 31-49.

[22] H. Zheng, J.R. Caram, P.D. Dahlberg, B.S. Rolczynski, S. Viswanathan, D.S. Dolzhnikov, A. Khadivi, D.V. Talapin, G.S. Engel, Dispersion-free continuum two-dimensional electronic spectrometer, Appl Opt 53 (2014) 1909-1917.

[23] T. Brixner, T. Mancal, I.V. Stiopkin, G.R. Fleming, Phase-stabilized two-dimensional electronic spectroscopy, J Chem Phys 121 (2004) 4221-4236.

[24] J.N. Sweetser, D.N. Fittinghoff, R. Trebino, Transient-grating frequency-resolved optical gating, Opt Lett 22 (1997) 519-521.

[25] M. Cho, Two-Dimensional Optical Spectroscopy, CRC Press, Boca Raton, FL, 2009.

[26] T.L. Jansen, J. Knoester, Waiting time dynamics in two-dimensional infrared spectroscopy, Acc Chem Res 42 (2009) 1405-1411.

[27] G.R. Fleming, M.H. Cho, Chromophore-solvent dynamics, Annu Rev Phys Chem 47 (1996) 109-134.

[28] A.F. Fidler, E. Harel, P.D. Long, G.S. Engel, Two-Dimensional Spectroscopy Can Distinguish between Decoherence and Dephasing of Zero-Quantum Coherences, J Phys Chem A 116 (2012) 282-289.

[29] R.E. Blankenship, Molecular Mechanisms of Photosynthesis, Blackwell Science, Oxford U.K./Malden MA, 2002.

[30] K.A. Fransted, J.R. Caram, D. Hayes, G.S. Engel, Two-Dimensional Electronic Spectroscopy of Bacteriochlorophyll a in Solution: Elucidating the Coherence Dynamics of the Fenna-Matthews-Olson Complex Using its Chromophore as a Control, J Chem Phys 127 (2012) 125101.

[31] G.B. Griffin, P.M. Lundin, B.S. Rolczynski, A. Linkin, R.D. McGillicuddy, Z. Bao, G.S. Engel, Ultrafast energy transfer from rigid, branched side-chains into a conjugated, alternating copolymer, J Chem Phys 140 (2014) 034903.

[32] G. Panitchayangkoon, D. Hayes, K.A. Fransted, J.R. Caram, E. Harel, J. Wen, R.E. Blankenship, G.S. Engel, Long-lived quantum coherence in photosynthetic complexes at physiological temperature, Proc Natl Acad Sci U S A 107 (2010) 12766-12770.

[33] W.L. Butler, K.H. Norris, H.W. Siegelman, S.B. Hendricks, Detection, Assay, and Preliminary Purification of the Pigment Controlling Photoresponsive Development of Plants, Proceedings of the National Academy of Sciences of the United States of America 45 (1959) 1703-1708.

[34] M.S. Davis, A. Forman, J. Fajer, Ligated chlorophyll cation radicals: Their function in photosystem II of plant photosynthesis, Proceedings of the National Academy of Sciences of the United States of America 76 (1979) 4170-4174.

[35] J. Hughes, T. Lamparter, F. Mittmann, E. Hartmann, W. Gartner, A. Wilde, T. Borner, A prokaryotic phytochrome, Nature 386 (1997) 663-663.

[36] E. Giraud, L. Fardoux, N. Fourrier, L. Hannibal, B. Genty, P. Bouyer, B. Dreyfus, A. Vermeglio, Bacteriophytochrome controls photosystem synthesis in anoxygenic bacteria, Nature 417 (2002) 202-205.

[37] K. Barkovits, B. Schubert, S. Heine, M. Scheer, N. Frankenberg-Dinkel, Function of the bacteriophytochrome BphP in the RpoS/Las quorum-sensing network of Pseudomonas aeruginosa, Microbiology 157 (2011) 1651-1664.

[38] S.J. Davis, A.V. Vener, R.D. Vierstra, Bacteriophytochromes: Phytochrome-like photoreceptors from nonphotosynthetic eubacteria, Science 286 (1999) 2517-2520.

[39] P.W. Kim, N.C. Rockwell, L.H. Freer, C.-W. Chang, S.S. Martin, J.C. Lagarias, D.S. Larsen, Unraveling the Primary Isomerization Dynamics in Cyanobacterial Phytochrome Cph1 with Multipulse Manipulations, The Journal of Physical Chemistry Letters 4 (2013) 2605-2609.

[40] K.C. Toh, E.A. Stojković, I.H.M. van Stokkum, K. Moffat, J.T.M. Kennis, Proton-transfer and hydrogen-bond interactions determine fluorescence quantum yield and photochemical efficiency of bacteriophytochrome, Proceedings of the National Academy of Sciences 107 (2010) 9170-9175.

[41] E. Teller, Internal Conversion in Polyatomic Molecules, Israel J Chem 7 (1969) 227-241.

[42] M. Baer, Beyond Born-Oppenheimer : Conical intersections and electronic non-adiabatic coupling terms, Wiley, Hoboken, N.J., 2006.

[43] W. Domcke, D. Yarkony, H. Köppel, Conical intersections : electronic structure, dynamics & spectroscopy, World Scientific, River Edge, NJ, 2004.

[44] W. Domcke, D. Yarkony, H. Köppel, Conical intersections : theory, computation and experiment, World Scientific, Singapore ; Hackensack, NJ, 2011.

[45] D.R. Yarkony, Diabolical conical intersections, Rev Mod Phys 68 (1996).

[46] G.A. Worth, L.S. Cederbaum, Beyond Born-Oppenheimer: Molecular dynamics through a conical intersection, Annu Rev Phys Chem 55 (2004) 127-158.

[47] F. Bernardi, M. Olivucci, M.A. Robb, Potential energy surface crossings in organic photochemistry, Chem Soc Rev 25 (1996) 321-328.

Chapter 2:

Photoisomerization in Bacteriophytochromes: Homogeneous Multi-step Dynamics Observed despite a Heterogeneous Ensemble of Ground State Conformation

Adapted from: Wang C, Flanagan ML, McGillicuddy RD, Zheng H, Ginzburg AR, Yang X, Moffatt K, Engel GS. (*submitted and in review*) 2016

2.1 Abstract

Phytochromes are red/far-red photoreceptors that are widely distributed in plants and prokaryotes. Ultrafast photo-isomerization of a double bond in a biliverdin cofactor or other linear tetrapyrrole drives their photoactivity, but their photodynamics are only partially understood. Multi-exponential dynamics were observed in previous ultrafast spectroscopic studies and were attributed to heterogeneous populations of the pigment-protein complex. In this work, 2DES was applied to study dynamics of the bacteriophytochromes RpBphP2 and PaBphB. Two-dimensional photon echo spectroscopy (2DES) can simultaneously resolve inhomogeneity in ensembles and fast dynamics by correlating pump wavelength with the emitted signal wavelength. The distribution of absorption and emission energies within the same state indicates an ensemble of heterogeneous protein environments that are spectroscopically distinct. However, the lifetimes of the dynamics are uniform across the ensemble, suggesting a homogeneous dynamic model for the initial photo-dynamics of isomerization.

2.2 Introduction

Phytochromes are red/far-red photoreceptors in plants, fungi and prokaryotes that regulate a wide variety of physiological processes[1-3]. For example, the homodimeric bacteriophytochrome denoted RpBphP2 (P2) regulates the expression of photosynthetic light harvesting LH4 complexes in *Rhodoseudomonas palustris*[4]. The photochemistry of P2 is mediated by a Z-to-E isomerization of the C_{15}=C_{16} double bond of its linear tetrapyrrole cofactor, biliverdin-IXα (BV) [5, 6]. Details of the isomerization are not fully understood. Bacteriophytochromes interconvert between two spectrally distinct states, the P_r state with a red absorption peak around 700 nm and the P_{fr} state with a far-red absorption peak around 750 nm (Scheme 1). In P2, the dark state is P_r. The first step in the light-dependent $P_r \rightarrow P_{fr}$ transformation takes place in tens to hundreds of picoseconds with the formation of a Lumi-R intermediate state[6]. The subsequent Lumi-R$\rightarrow P_{fr}$ transformation involves rearrangement of the protein matrix that can take up to hundreds of milliseconds[7, 8], which modifies the activity of a covalently-attached kinase effector domain and initiates signaling to down-stream components. Reverse photochemistry of $P_{fr} \rightarrow P_r$ in P2 and similar bacteriophytochromes can occur thermally or by absorption of a second photon of far-red light proceeding through a Lumi-F intermediate[9]. Since the $P_r \rightarrow P_{fr}$ and $P_{fr} \rightarrow P_r$ reactions each require one photon and are completely separate, the $P_{fr} \rightarrow P_r$ reaction need not be the reverse of the $P_r \rightarrow P_{fr}$ reaction.

Reaction dynamics of the P_r →Lumi-R transformation have been examined by various spectroscopic methods, including pump-probe spectroscopies[10-15], femtosecond stimulated Raman spectroscopy[16] and picosecond time-resolved fluorescence spectroscopy[5, 17]. Multi-exponential decays were commonly observed[10-15, 18], with component lifetimes spanning four orders of magnitude (0.1-0.7 ps, 2-6 ps, 20-70 ps, 120-400 ps). The timescale of the initial

double bond isomerization was recently associated with a 30 ps component in a cyanobacteriophytochrome (Cph1Δ2)[19], significantly longer than that of isomerizations in rhodopsin, bacteriorhodopsin and photoactive yellow protein (0.2-3 ps) [20-22]. Detailed analysis of the multi-exponential decays is required to understand such slower dynamics. The multi-exponential decays are sometimes interpreted as a collection of separate populations relaxing through parallel pathways of intermediates[15, 23], but other studies have proposed a homogeneous explanation in which a single population relaxes through sequential intermediates[11, 16]. It is experimentally difficult to determine the origin of multi-exponential behavior because heterogeneous populations cannot be resolved by conventional spectroscopies. Hence, prior work has varied in the explanation for these dynamics. For example, 2007, van Thor et al. concluded that structural heterogeneity of the pigment-protein complex in Cph1 results in multiple populations relaxing through parallel pathways[15], but later revised the conclusion to include the possibility of the homogeneous model for the same protein in 2009[18]. Freer et al. attributed spectroscopic differences to chemical heterogeneity, or chemically distinct chromophores in cyanobacteriophytochrome Tlr0924[24]. However, the same research group later reported on dynamic heterogeneity in Cph1 that is dependent on the structure of the ground P_r state which cannot be explained by chemical heterogeneity[23]. Unlike many ultrafast spectroscopies employed in prior studies, 2DES resolves both the pump and probe axes and is therefore uniquely suited to resolve the debate over the homogeneity of relaxation in phytochromes.

The source of separate populations in the heterogeneous explanation is not entirely clear. In a protein environment it is common to see an array of diverse conformations, each with a slightly different electrostatic environment of the cofactor, giving rise to a range of transition

energies. The timescales of transformations between these conformations typically spans femtosecond to nanoseconds, but transition times between structurally very different conformations can take up to many seconds. In an ultrafast measurement, all of the processes that occur on a timescale longer than the duration of the experiment are effectively "frozen" and manifest as structural heterogeneity in the ensemble, associated with a range of populations and transition energies[25]. Therefore, we expect heterogeneity in the ground state, and indeed, such structural heterogeneity in the ground state is supported by single molecule fluorescence spectroscopy[26], resonance Raman spectroscopy[27], fluorescence line narrowing spectroscopy[28], 13C-1H HETCOR NMR[29] and pump-probe studies at multiple pumping wavelengths[23]. However, it remains unclear whether the spectroscopic variations due to structural heterogeneity result in qualitative differences in the subsequent photo-dynamic pathways[30, 31].

Two-dimensional electronic spectroscopy (2DES)[32, 33] can probe the photo-initiated dynamics on ultrafast timescales and display the dynamics in a series of time-resolved 2D correlation maps[34-37]. A review of 2DES and its applications by the Fleming group[32] is both understandable and eloquent. 2DES has been applied to study spectral diffusion[34, 38, 39], photosynthetic light-harvesting complexes[40-46], semiconducting nanocrystals[47-50], and atomic vapors[51-54]. Unlike traditional pump-probe experiments, 2DES correlates excitations at different energies with the fates of the excited states across the entire excitation window. Heterogeneity that is static on the timescale of the experiment is evident as populations that absorb slightly different wavelengths of light. Consequently, the inhomogeneously broadened spectroscopic feature in the 2DES map will appear elongated along the diagonal. Spectroscopic peaks can also be broadened by randomization due to the environment and ultrafast relaxation of

the chromophore and its environment. If these motions are fast on the time scale of the experiment, the peak will appear round and symmetric. More typically, the motions that would broaden the feature are slow compared to our experimental pulse lengths (15 fs) but fast compared to our longest waiting times (400 ps). Under these conditions, we see elongated features at short waiting times (e.g. T = 0 fs to T = 100 fs), but the features expand uniformly in both coordinates and appear as a round peak in 2DES data at longer waiting times (T = 400 ps). That is, 2DES separates broadening in the homogenous and inhomogeneous limits along distinct spectral axes and allows observation of the dynamics on the appropriate timescales between these two limits. The dynamics of subpopulations with transitions of different energies can thus be tracked separately. For clarity, we use the terms homogeneous and inhomogeneous broadening as they are used in ultrafast spectroscopy to describe spectroscopic features, but reserve heterogeneity and homogeneity to describe variations (or lack thereof) in conformations and transition energies. For example, a peak is initially inhomogeneously broadened in 2DES because of heterogeneity in the sample, but at longer times may appear homogeneously broadened as the system loses memory of its initial conformation.

In this work, we examine the dynamics of the photosensory core modules containing the PAS-GAF-PHY domains of two bacteriophytochromes with distinct ground states and photodynamics: RpBphP2 (P2) from Rhodopseudomonas palustris and PaBphP (Pa) from Pseudomonas aeroginosa[6, 55, 56]. Unlike the canonical bacteriophytochrome P2, Pa adopts the Pfr ground state in the dark and efficiently transforms to the P_r state upon activation with far-red light. The quite different photoconversions in these two core modules enables us to examine both P_r →Lumi-R and P_{fr}→Lumi-F transformations.

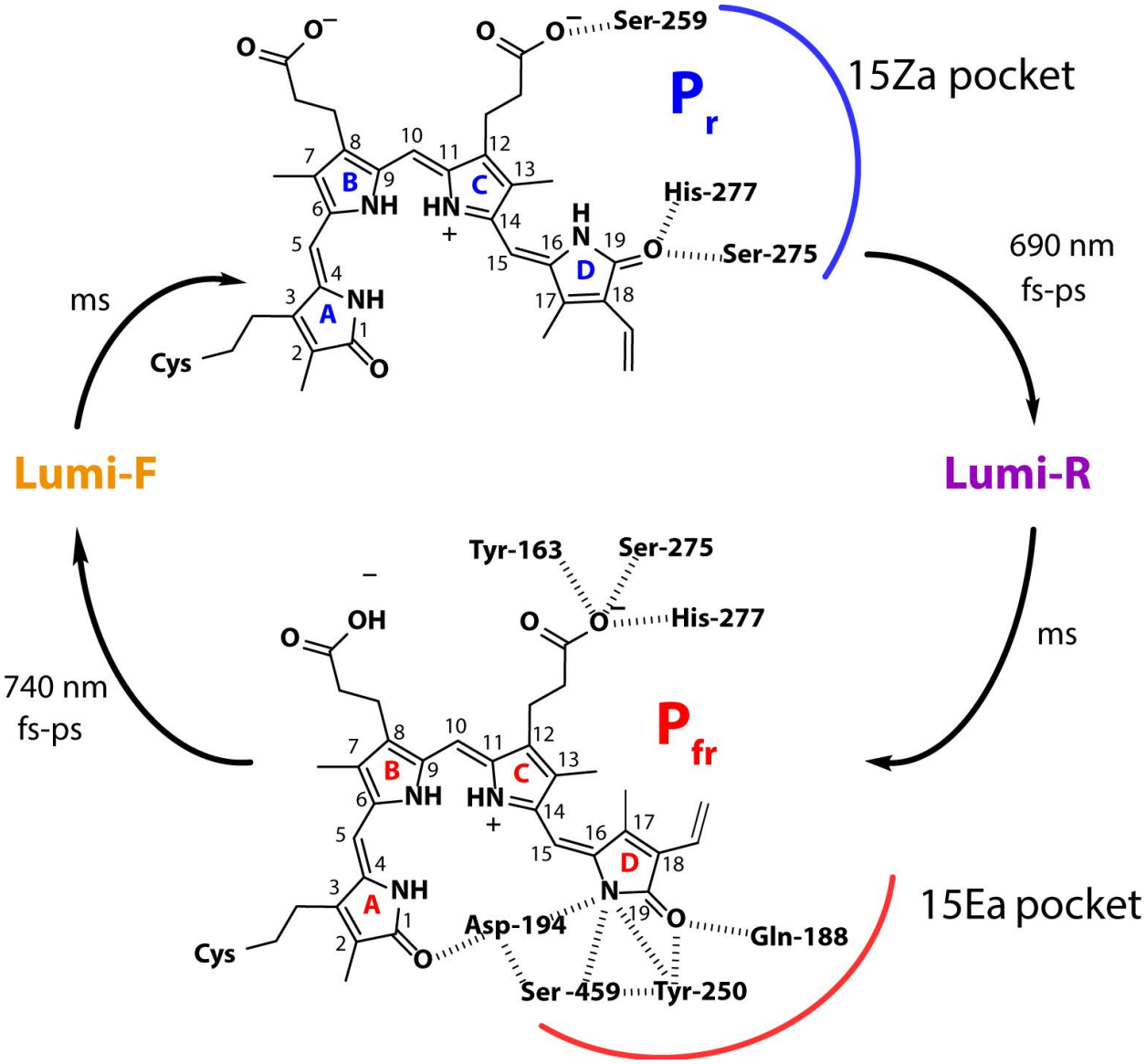

Scheme 2.1: The inter-conversion of biliverdin-IXα between the P_r (15Za) and P_{fr} (15Ea) states.

2.3 Methods

2.3.1 Spectroscopy

The experimental apparatus is described elsewhere[34-36]. A 5 kHz, 600 μJ pulse train centered at 800 nm from Coherent Legend Elite regenerative amplifier was focused into a 2m tube containing 1.5 atm of argon gas to generate ultra-broadband pulses spanning from 450 to

900 nm. The white light pulses were compressed by negatively chirped mirrors and a pulse shaper. The pulse duration was measured at the sample position to be ~6 fs by transient grating frequency resolved optical gating (TG-FROG). The beam was then directed into the 2DES apparatus described previously[57]. To avoid multi-exciton effects, an attenuated pulse energy of 15 nJ/pulse was used in the experiment. Rephasing 2DES data were collected over a range of coherence times from 0 to 90 fs in 1.5 fs increments and a range of waiting times (corresponding to the delay time in pump-probe spectroscopies) from -50 fs to 400 ps. Steps of 5 fs were used over the 0-700 fs range and logarithmically thereafter. We used separately collected transient absorption spectra to phase each 2D spectrum[37, 58]. The transient absorption spectra were collected with the same laser pulse as that in the 2DES experiment and the beam was attenuated to achieve a pump pulse of 50 nJ/pulse and probe pulse power of 0.4 nJ/pulse.

2.3.2 Sample Preparation

The photosensory core modules of the RpBphP2 and PaBphP bacteriophytochromes were co-expressed in *Escherichia coli* BL21 (DE3) with heme oxygenase (HO) for biliverdin synthesis. Vectors with PCR-amplified coding regions were constructed for HO, and the Pa and P2 photosensory core modules. Cells were aerobically cultured in 3 L LB + 100 μg/mL ampicillin + 50 μg/mL kanamycin to 0.6 OD at 600 nm in a 1 cm cuvette. Cells were then induced with 1mM isopropyl-β-D-thiogalactopyranoside (IPTG) and incubated with 0.5 mM δ-aminolevulinic acid to promote heme synthesis overnight (18 hours). Cells were harvested by centrifugation, lysed by sonication on ice for 30 minutes and incubated at 4 °C for 15 minutes with 200 μl of 20 mM biliverdin to ensure chromophore incorporation across the ensemble. The protein was purified on a Ni-NTA affinity column. The column was washed with 20 mM Tris buffer (pH 8) and 1M NaCl, then with sonication buffer. Protein was eluted with 20 mM Tris

buffer (pH 8), 50 mM NaCl and 300 mM imidazole and purity was monitored by absorption spectrum as shown in Fig. 2.1. The protein was then washed and concentrated on Amicon UltraCentrifugal Filters.

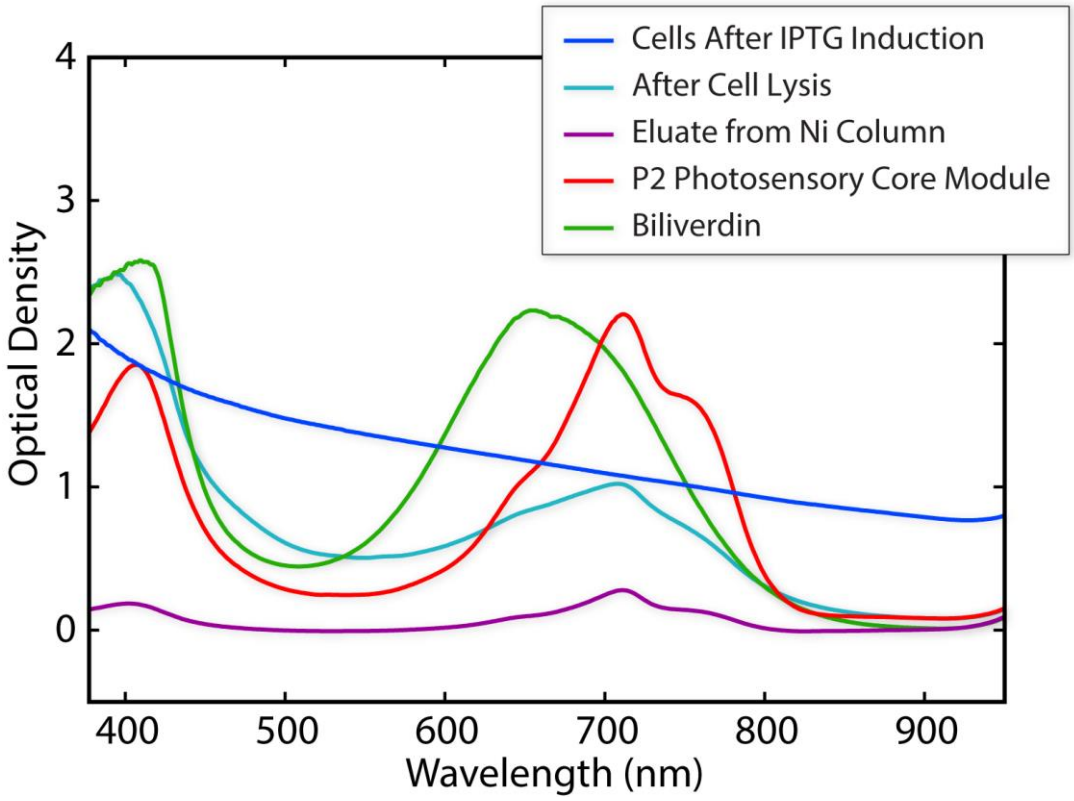

Figure 2.1: Absorption Spectra of the Purification of P2 Photosensory Core Module on a Ni-NTA affinity column. All absorption spectra were obtained in a 1 cm cuvette at room temperature (25 °C).

The protein solution was contained in a quartz flow cuvette with 200 μm path length. A peristaltic metering pump was used to flow fresh sample to the cuvette from an external reservoir with 3 mL sample volume. LED light of 690 nm or 740 nm was used to illuminate the external reservoir. The LED light total power was 20 mW for experiments on both Pa and P2. The samples had an absorbance at 700 nm of 0.2-0.3 O.D. in a path length of 200 μm.

2.4 Results and Discussion

2.4.1 P_r→Lumi-R Conversion of P2

As shown in Fig. 2.2, P2 adopts the P_r state in the dark, with an absorption peak at 709 nm and a vibronic shoulder at 647 nm. With continuous illumination at 690 nm, P2 partially converts to P_{fr} state, evident in the linear spectrum as a shoulder at 754 nm. Similar partial conversion with light activation at similar wavelengths is reported in the literature[4]. Partial conversion may arise from significant spectral overlap between P_{fr} and P_r states, leading to significant P_{fr}→ P_r back conversion under the LED light.

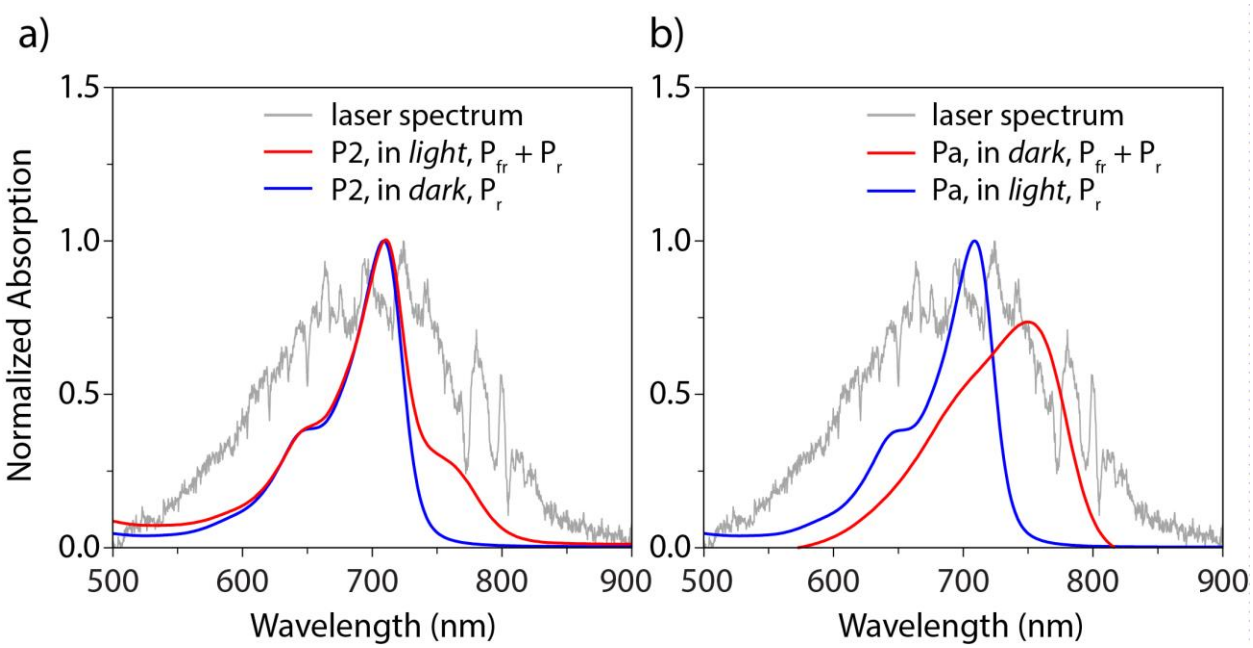

Figure 2.2: Absorption spectra of the P2 and Pa and the laser spectrum. (a) blue: P2 in dark, adopting the P_r state; red: P2 with illumination of 690 nm LED light, in a mixture of P_r and P_{fr} states; gray: laser spectrum. (b) blue: Pa with illumination of 740 nm LED light, adopting the P_r state; red: Pa in dark, in a mixture of P_r and P_{fr} states; gray: laser spectrum.

2DES data were acquired for P2 in the dark (P_r →Lumi-R conversion) for a series of waiting times. The end result is a series of 2D energy correlation maps each associated with a

different waiting time. As shown in Fig. 2.4a and b, positive signals on the 2D maps are associated with stimulated emission/ground state bleach, while negative signals are associated with excited state absorption. Together, these data illustrate how excited states evolve in time and reveal both relaxation and interconversion between different subensembles within the states[25].

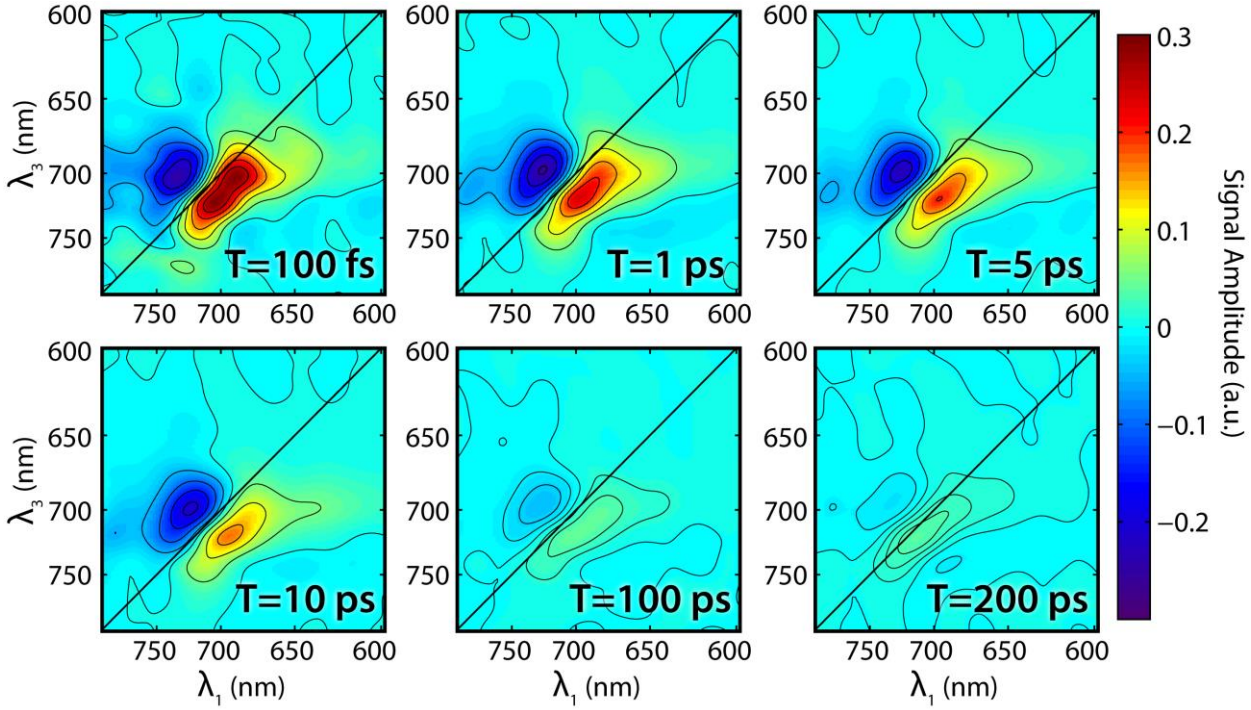

Figure 2.3: 2DES of P2 in the P_r state at long waiting times T= 100 fs, 1 ps, 5 ps, 10 ps, 100 ps, 200 ps. The signal has largely decayed by 100 ps, but the elongated inhomogeneous lineshape is persistent at long waiting times.

In rephasing 2DES data, homogeneous broadening widens the spectral line in both frequency axes on the 2DES map as time progresses. That is, the peak becomes rounder with time because there is less correlation with the initial state as the experiment progresses. In contrast, inhomogeneous broadening elongates the peak only along the diagonal because the photon echo eliminates inhomogeneous broadening in the anti-diagonal direction. In the case of

P2, the BV chromophore is embedded in an apo-protein environment. Although protein fluctuations homogeneously broaden the peak in the 2DES data, the solvation response to the BV excitation can be thought of as practically static because the time scale of our experiments is much faster than many protein rearrangements[25]. Ground state inhomogeneity manifests in the 2DES maps as a peak elongated along the diagonal, indicating a distribution of BV with slightly different initial transition energies that do not significantly change on the femtosecond to 400 picosecond time scale. The 2DES spectrum of P2 in the P_r state shows clear elongation along the diagonal at T=0 fs (Fig. 2.4a), consistent with ground state inhomogeneity. This elongation persists at longer waiting times (Fig. 2.3 and Fig. 2.4b).

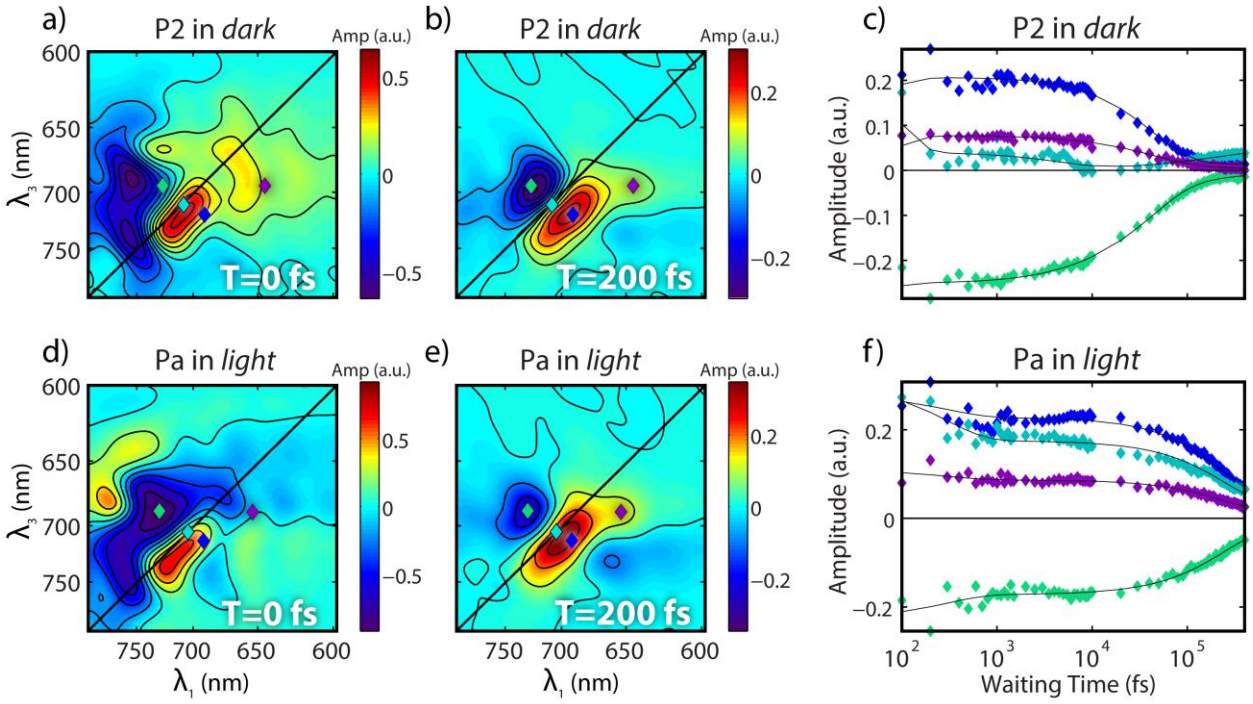

Figure 2.4: 2DES and dynamics of P2 in the P_r state at short times (a) at T = 0 fs; (b) at T = 200 fs; 2DES of the Pa in the P_r state (d) T = 0 fs; (e) T = 200 fs; Time traces of representative points marked by colored diamonds on the 2DES: (c) P2 in the P_r state and (f) Pa in the P_r state. The time trace data and their corresponding positions on the 2D maps are marked with the same color. Black lines are fittings of the data according to equation (1).

The intensities of the signal on the main diagonal showed oscillatory beating in waiting time with a periodicity of around 26 fs. This beating is consistent with a vibrational mode of 1253 cm^{-1}, which can be assigned to C-H rocking of the vinyl groups in BV (Fig. 2.5) [30]. The distribution of power intensity of the beating at 1253 cm^{-1} is shown in Fig. 2.5c. The distribution exhibits an elongated diagonal peak (Fig. 2.5c), consistent with vibrational motion on the ground state surface. The beating extends well beyond a 1 ps waiting time. A second beating frequency of 1158 cm^{-1} was also present, which occupies a region slightly above the diagonal in the 2D map. We attribute this beating signal to the same vibrational motion, but on the excited state surface.

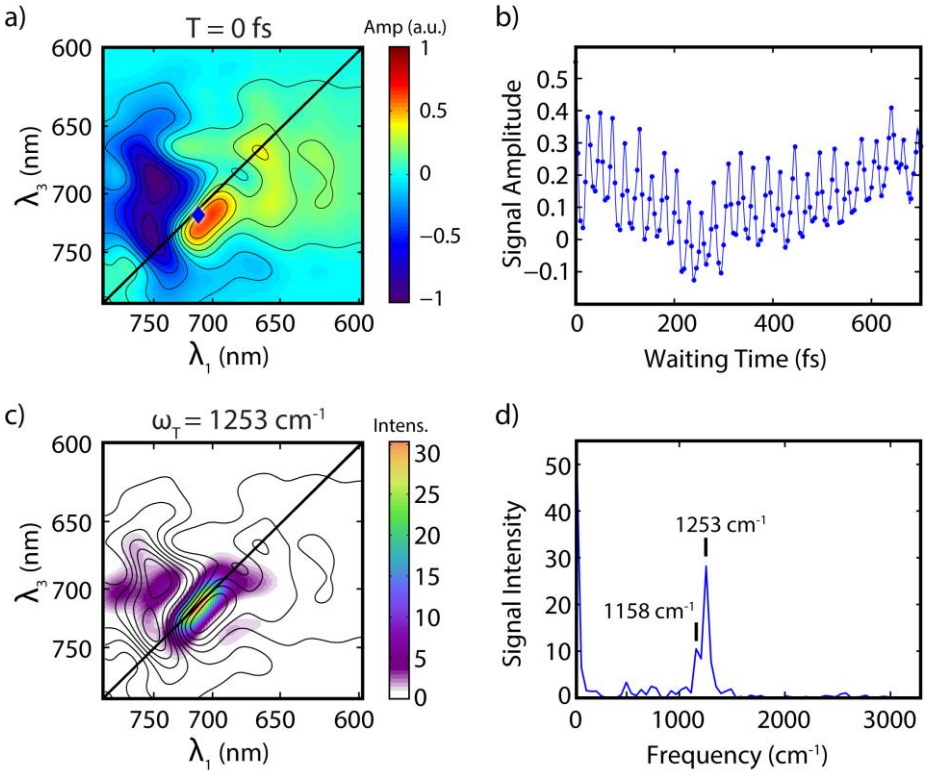

Figure 2.5: Beating signals of P2 in the $P_r \rightarrow$Lumi-R process. (a) 2DES map at T = 0 fs (b) Fourier interpolated time trace taken at λ_1=712 nm, λ_3=718 nm marked by the blue diamond on the 2DES plot. (c) Distribution map of the beating power at 1253 cm^{-1}. The color axis encodes the strength of the power spectrum at 1253 cm^{-1}. Contours of the 2DES at T = 0 fs are overlaid. (d) Fourier transform of the time trace in panel b, showing peaks at 1253 cm^{-1} and 1158 cm^{-1}.

The intensities of the spectra at longer waiting time (70 fs-400 ps) and larger time intervals (semi-log spacing) were fitted to a sum of three exponential decays (Fig. 2.4a-c). A global fitting was first carried out to give three global lifetimes and maps of three pre-exponential factors (A_1-A_3) together with a residual constant term A_4 as shown in equation 1:

$$y = A_1(\lambda_1, \lambda_3)e^{-\frac{t}{\tau_1}} + A_2(\lambda_1, \lambda_3)e^{-\frac{t}{\tau_2}} + A_3(\lambda_1, \lambda_3)e^{-\frac{t}{\tau_3}} + A_4(\lambda_1, \lambda_3) \quad (1)$$

The values of A_1-A_4 are dependent on both the excitation and emission wavelengths, and can be plotted as 2D maps. We refer to them as the Decay-Associated Spectra (DAS, Fig. 2.6a-d), analogous to Decay-Associated Difference Spectra (DADS) in pump-probe spectroscopy. The constant residue term A_4, is approximately equivalent to the 2DES at long waiting time, and represents the portion of the spectrum that remains after the decay of components A_1-A_3. Therefore, we associate it with the spectrum of the Lumi-R state. The spectrum of Lumi-R mainly contains a positive ground-state bleach signal overlaid with weak negative excited state absorption from its photogeneration. The lifetimes associated with A_1-A_3 from this global fitting are τ_1= 0.045 ps, τ_2=4.8 ps, τ_3=42 ps. The values of τ_2 and τ_3 are very similar to those reported by Kennis et al. from pump-probe spectroscopy (τ_1=0.4 ps, τ_2=4 ps, τ_3=43 ps, τ_4=170 ps)[5]. We attribute our lower value of τ_1 to our shorter pulse width, enabling us to detect early dynamics more accurately. Kennis et al. also identify a 170 ps component by both pump-probe and time-resolved fluorescence measurements. This component connects the excited state and ground state surfaces, and they attribute it to heterogeneity of the sample[5]. However, we did not observe such a component. If we add a fourth exponential component with lifetime constrained to be >100 ps in the fitting algorithm, we obtain τ_4=226 ps but its amplitude is negligible compared to those of the other three exponential components.

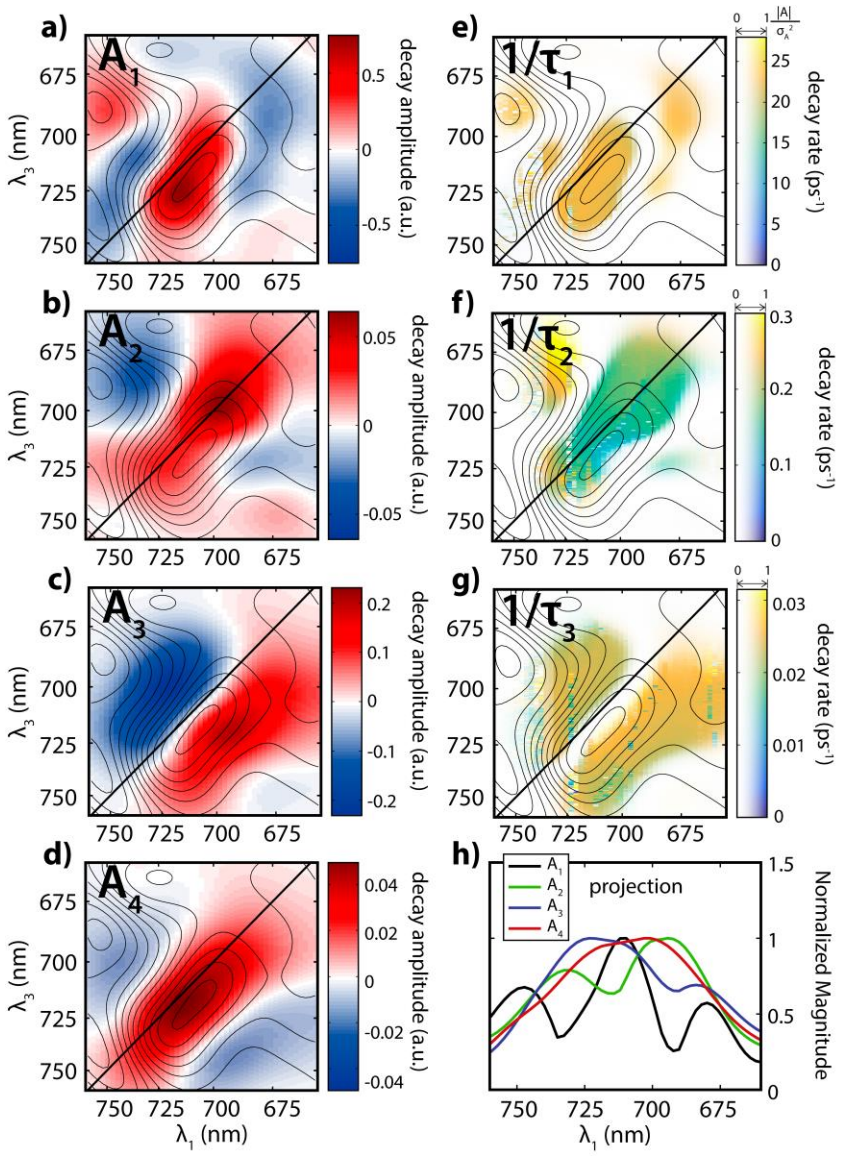

Figure 2.6: Decay Associated Spectra (DAS) support a homogeneous dynamic model for the P2 Pr→Lumi-R conversion (a-d) A_1-A_4 terms of Decay Associated Spectra (DAS) of P2 in the P_r state from global fitting to equation (1). The 2DES map at T = 0 fs is also overlaid for reference (contours in black in all panels). (e-g) Variations of the exponential decay rates $1/\tau_1$, $1/\tau_2$, and $1/\tau_3$ in ps^{-1}. Different rates are encoded by different colors in each panel as shown in the colorbars, and the drawing is also gated by DAS magnitude with a transparency map, so that the regions with smaller DAS magnitudes will show lighter on the figure, as shown by transparency axis on the colorbar. The transparency map is determined by the normalized magnitude of the DAS component divided by the variance of its fit. (h) Projection of the absolute value of the DAS to the $\lambda_1$axis (absorption or pump axis) to represent the excitation range of the observed signal. All four DAS components cover the same range of pump wavelengths. The dips in the projections arise from cancellation between positive and negative signals.

The existence of multiple lifetimes in the photodynamics of P2 can be explained by either a heterogeneous model or a homogeneous model. In the heterogeneous, components with different lifetimes are associated with different ground state sub-populations of the protein. That is, separate populations undergoing distinct decay pathways. In contrast, the homogeneous model assigns the multiple DAS components to sequential photodynamics of a single chemical component. With our 2DES DAS maps on hand, we can test these two models. If ground state heterogeneity exists, we expect inhomogeneous broadened peaks located across different pump wavelengths for each DAS component. In contrast, in the homogeneous model, the DAS components should occupy roughly the same region of the pump wavelengths. We have projected the absolute values of the DAS to the $\lambda_1$axes to represent the pumping range of each DAS. As shown in Fig. 2.6h, all the four DAS components possess a very similar pumping wavelength, consistent with a homogeneous model. The dips in the projections arise from the cancellation between positive and negative signals.

To further investigate possible heterogeneity within each DAS component, we allowed the lifetimes and amplitudes from the global fitting to be refined independently for each pixel on the 2DES map. This enables us to explore whether the fitted lifetimes vary across an inhomogeneously broadened peak. If so, this would indicate heterogeneity in the photodynamics. Such an individual refinement using the values of global fitting as starting points can be represented by equation 2:

$$y = A'_1(\lambda_1,\lambda_3)e^{-\frac{t}{\tau'_1(\lambda_1,\lambda_3)}} + A'_2(\lambda_1,\lambda_3)e^{-\frac{t}{\tau'_2(\lambda_1,\lambda_3)}} + A'_3(\lambda_1,\lambda_3)e^{-\frac{t}{\tau'_3(\lambda_1,\lambda_3)}} + A'_4(\lambda_1,\lambda_3) \quad (2)$$

The amplitude maps (DAS) for the individual fittings are very similar to that of the global fitting. When these maps are compared by subtraction, negligible residuals are obtained, confirming the robustness of the fitting algorithm. The fitting approach of equation (2) allows us to examine the

distribution of lifetimes across the map. As shown in Fig. 2.6e-g, the lifetimes from the individual fittings are plotted together with the contour line of the 2DES at T=0 fs. The lifetimes are expressed in decay rates ($1/\tau$) in ps^{-1} and encoded by color. The rates are also gated by the corresponding DAS amplitudes through an intensity (transparency) coding. For example, lifetimes in regions of negligible DAS intensities are shown in white. The $1/\tau_1$ and $1/\tau_3$ rates are found to distribute evenly across inhomogeneously broadened features on the 2D maps in Fig. 2.6. The $1/\tau_2$ component exhibits a rate that is 1.5 times faster in regions of excited absorption, indicating that the process of vibrational relaxation has a slightly different rate on the excited state surface. Nevertheless the variation of the rate constants across the map is small, and supports a homogeneous dynamic model. Finally, when we perform Singular Value Decomposition (SVD) on the data cube, two components are found, one dominant component with multiple exponential decays and one weak component with contributions only around 5% of the total amplitude and a lifetime of 0.1 ps.

These analyses by different routes all suggest that the system can be best modeled by a single population with homogeneous multi-exponential dynamics.

All possible models with three different decay components have been examined, and the Species Associated Spectra (SAS) corresponding to each model were constructed. Three possible models are identified. We prefer the model shown in Fig. 2.7, for its simplicity and adequacy in explaining all experimental observations. The other two candidate models are presented in Fig. 2.8.

In our proposed model, following excitation to the Franck-Condon region ($^{FC}P_r^*$), two stages of vibrational relaxation involving two independent nuclear coordinates lead to $^{rel}P_r^*$ with time constants of τ_1 and τ_2. This state then proceeds over a transition barrier resulting from

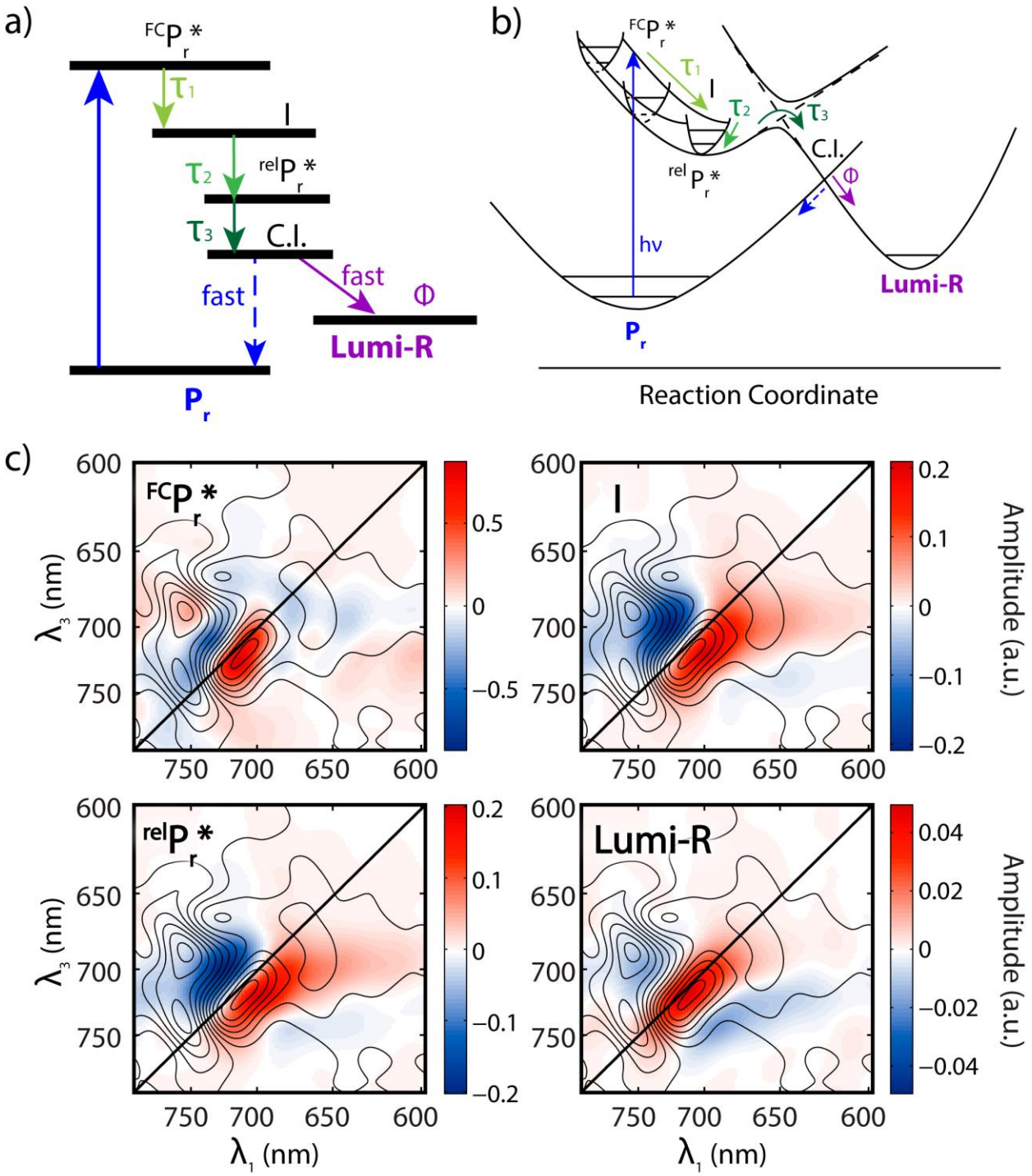

Figure 2.7: Proposed model of the P_r→Lumi-R conversion in P2 (a) the model to describe dynamics of the P2 in the P_r→Lumi-R transformation. (b) proposed reaction surface geometry. (c) SAS of the corresponding species.

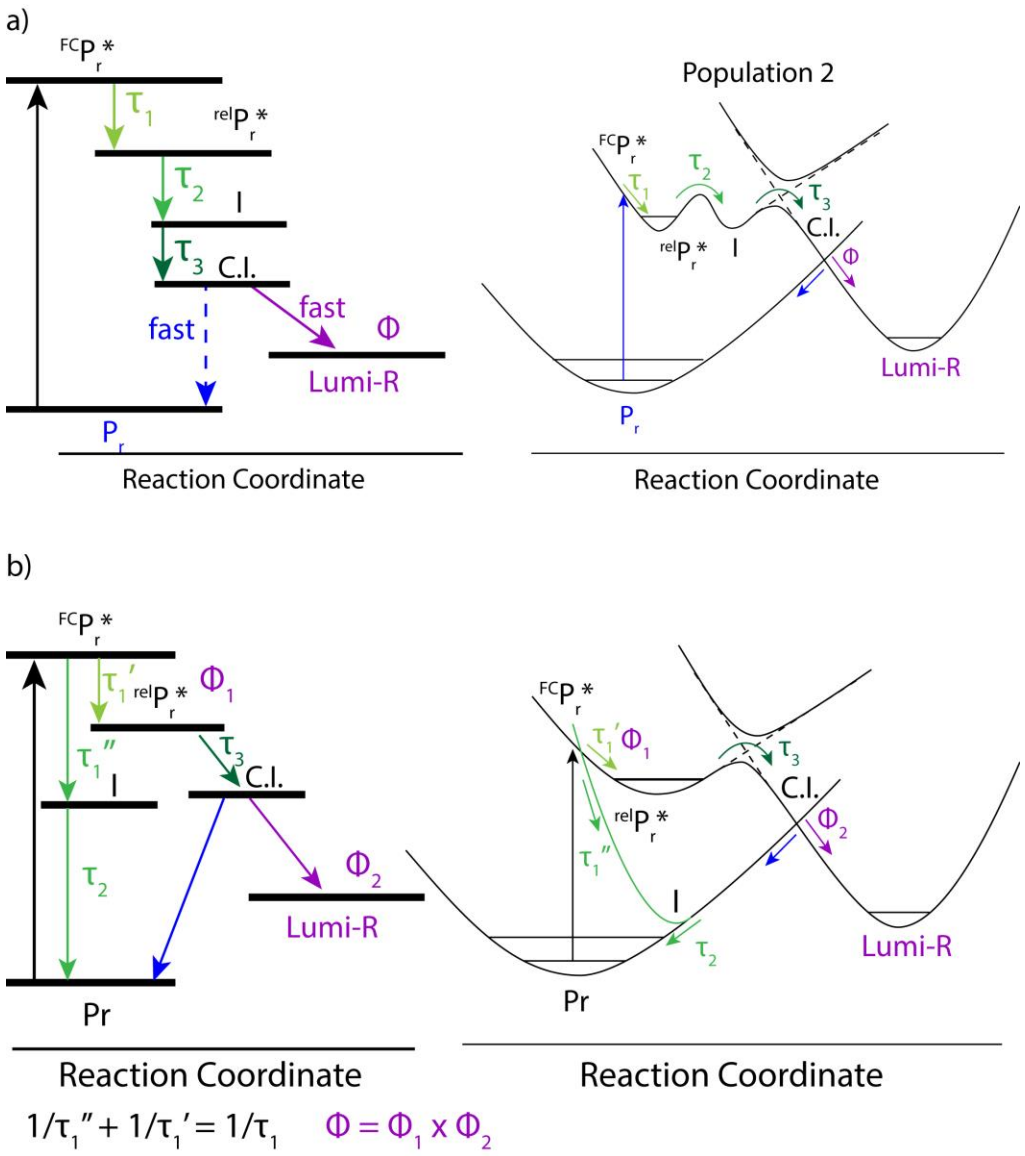

Figure 2.8: Two alternative models to describe dynamics of P2 in the $P_r \rightarrow$Lumi-R conversion.

avoided crossing between the P_r* excited state surface and the Lumi-R ground state surface, with typical time τ_3, and then proceeds to the Lumi-R product on the ground state surface. Before reaching the bottom of the Lumi-R state, a conical intersection (CI) between the Lumi-R ground state surface and the P_r ground state surface is encountered. The system either proceeds to the Lumi-R with a quantum efficiency of Φ or reverts to P_r at the CI.

2.4.2 P_r→Lumi-R conversion of Pa

As shown in Fig. 2.2b, Pa in dark adopts the P_{fr} form, with an absorption peak at 750 nm and a vibrational shoulder at 686 nm. Upon continuous illumination of an LED light at 740 nm, the Pa converts completely to the P_r state with an absorption peak at 700 nm (Fig. 2b). We first examined the P_r→Lumi-R conversion of Pa.

2DES was taken for Pa with continuous illumination of the LED light of 740 nm to populate its P_r state. As shown in Fig. 2.4d and e, similar to P2 in the 2DES, Pa in its P_r state gives an inhomogeneous broadened peak. The signals were also beating in waiting time, consistent with a vibrational mode of 1064 cm^{-1}. A map of the beating intensity at 1064 cm^{-1} exhibited an elongated diagonal peak and a separate peak in the excited state absorption region, indicating a similar vibrational frequency on the ground state and excited state surfaces. The time evolution dynamics of the spectra, however, is distinct from that of P2, as shown in Fig. 2.4. Similar global fitting was applied to obtain two time constants τ_1=0.31 ps and τ_2=251 ps. The pre-exponential amplitude maps (DAS) were again refined with the lifetime at individual spots on the 2D maps. The projected absolute values of the DAS on the $\lambda_1$axis again overlapped with each other, supporting a homogeneous model (Fig. 2.9f). Consistent with this hypothesis, SVD analysis also gives only one major component of the dynamic data. The shorter component $1/\tau_1$ shows different rates in different locations on the 2DES map, indicating different rate of vibrational relaxation on the ground state and excited state surfaces. The long component $1/\tau_2$, corresponding to the isomerization, is distributed much more evenly on the 2D-map, consistent with the homogeneous dynamic model (Fig. 2.9d-e). The τ_2 component of Pa is much slower than the corresponding component of P2, indicating a higher barrier before the conical intersection.

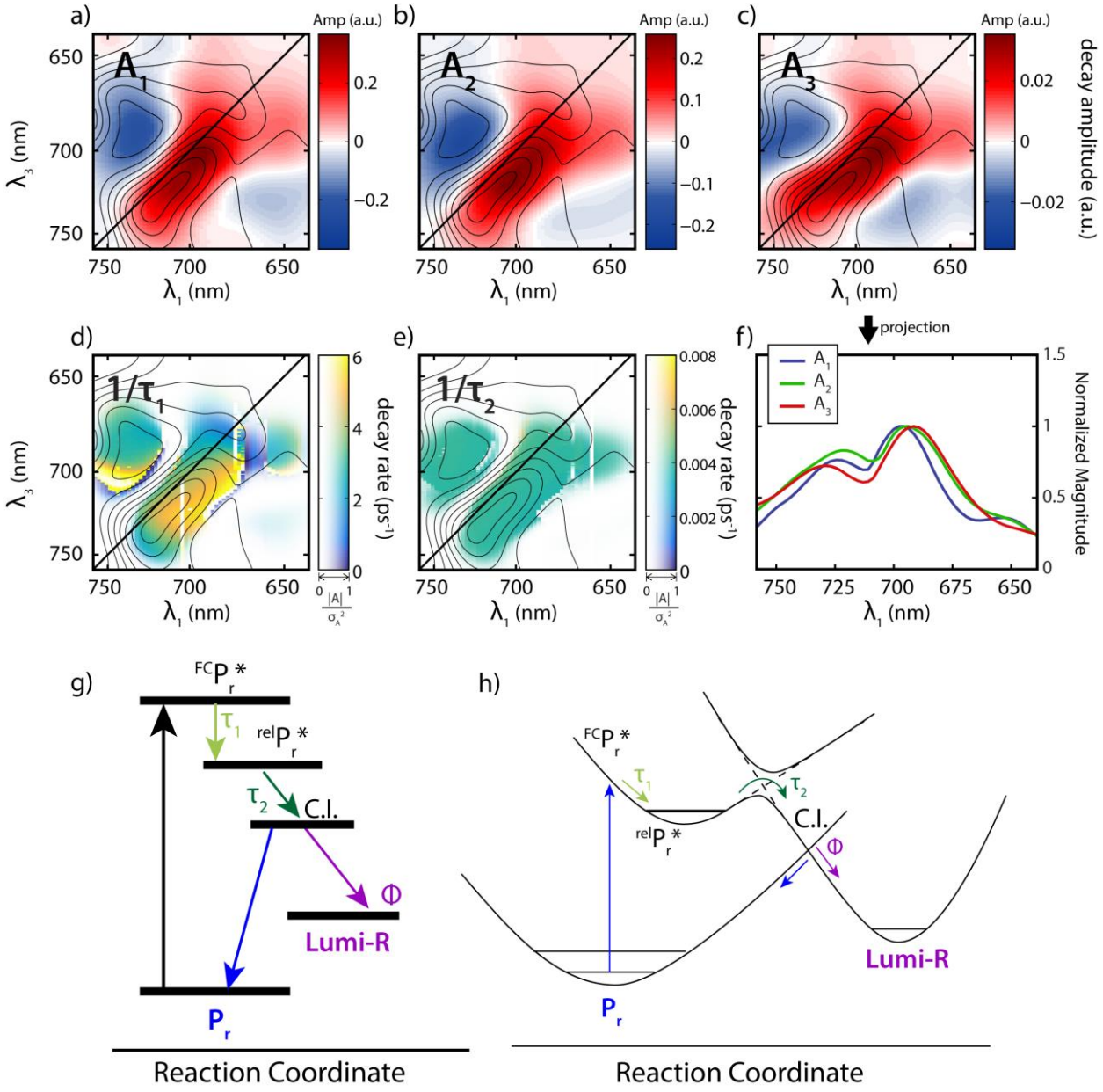

Figure 2.9: Dynamics of $P_r \rightarrow$Lumi-R conversion in Pa closely resemble P2. a-c)A_1-A_3 terms of the Decay Associated Difference Spectra (DADS) of the Pa in the P_r state from global fitting, as defined in equation 1. A contour of the 2DES map is also overlaid on the drawings. d-e) Distributions of the exponential decay rates $1/\tau_i$ (i=1-2) in ps^{-1}. Different rates are encoded by different colors as shown in the colorbars, and the drawing is also gated by the DADS intensities. f) Projection of the absolute value of the DADS to the $\lambda_1$axis (absorption axis) to represent the excitation range of the observed signal. Pa under light in the $P_r \rightarrow$Lumi-R conversion. g) A scheme showing a model to describe dynamics of the Pa in the $P_r \rightarrow$Lumi-R transformation. h) A scheme showing a proposed reaction surface geometry.

After an experimental analysis identical to that previously applied to P2, we propose a model very similar to that of P2 (Fig. 2.9g-h). The major difference between the $P_r \rightarrow$Lumi-R kinetic models of the P2 and the Pa is the substantially different barrier height before the CI, leading to very different rates of conversion.

2.4.3 $P_{fr} \rightarrow$Lumi-F conversion of P2

Under illumination at 690 nm, we can partially convert the P2 protein to the P_{fr} state (Fig. 2a). As the conversion is not complete, the illuminated sample is a mixture of the P_r and the P_{fr} states. When we performed 2DES on this sample, SVD analysis showed two major components for the dataset, consistent with a mixture of P_r and P_{fr} states. The 2D spectrum of the mixture clearly showed additional peaks at 740 nm, arising from the excitation wavelength of P_{fr}, distinct from that of the pure P_r state (Fig. 2.10). Direct global fitting 2DES dynamics of the mixture gives four lifetimes: τ_1= 0.27 ps, τ_2=5.8 ps, τ_3=39 ps, τ_4=151 ps. We tried to separate the P_{fr} component by subtracting a certain percentage of the P_r 2DES from the mixture spectrum, in which the percentage of the P_r form was refined as an independent parameter, and estimated to be 49%. The isolated P_{fr} component was fitted to three exponentials with τ_1= 0.97 ps, τ_2=2.0 ps, τ_3=50.5 ps. Since this spectrum separation algorithm is of limited effectiveness, due to numerous fitting parameters and significant spectral overlap between the P_{fr} and the P_r states, we did not pursue analysis in this direction any further.

The 2D beating spectrum is very different from that in the $P_r \rightarrow$Lumi-R conversion process (Fig. 2.11). A strong off-diagonal peak with excitation wavelength at >750 nm can be identified. This feature is associated with a broad peak in the ω_T domain centered at 1158 cm^{-1} with a FWHM of ~500 cm^{-1}, corresponding to a fast process of around 70 fs in the T domain. In agreement with this, the oscillating time trace in the T domain decays within 100 fs (Fig. 2.11b).

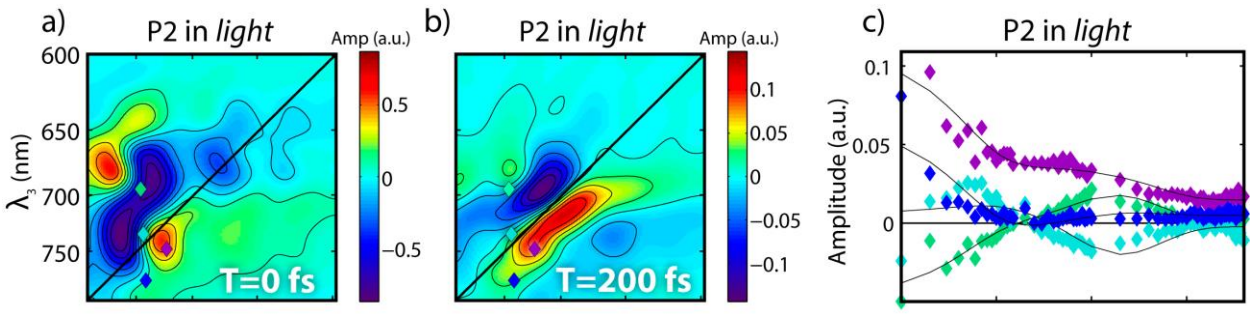

Figure 2.10: 2DES and dynamics of P2 in the mixture state of P_{fr} and P_r a) at T = 0 fs; b) at T = 200 fs; 2DES of the Pa in the mixture state of P_{fr} and P_r c) Time trace data and their corresponding positions on the 2D maps are marked with the same color. Black lines are fittings of the data.

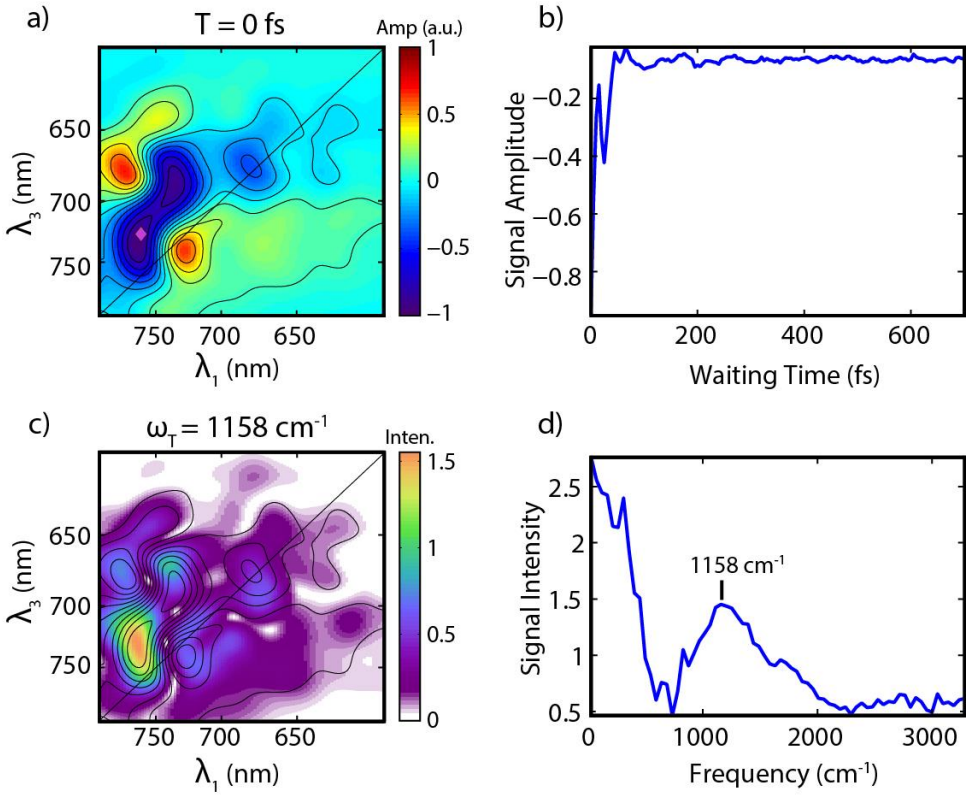

Figure 2.11: Beating signals of P2 in the mixed P_{fr} →Lumi-F and P_r→Lumi-R processes. (a) 2DES map at T = 0 fs with contours. (b) Time trace taken at λ_1=764 nm and λ_3=726 nm marked by the magenta diamond in panel a. The trace shows a beating signal with periodicity around 25 fs. (c) Distribution map of the beating power. The color axis encodes power spectrum intensity at 1158 cm^{-1}. Black contours of the 2DES at T = 0 fs are overlaid on the figure. (d) Fourier transform of the time trace in panel b, showing a broad peak centered at 1158 cm^{-1}, possibly associated with the Vinyl C-H rocking vibrational modes.

2.4.4 P_{fr}→Lumi-F conversion of Pa

The solution of the Pa protein in the dark at room temperature probably contains a fraction of the P_r state, as indicated by its broad absorption spectrum (Fig. 2b). Indeed, a related mutant Q188L even showed mixed P_r/ P_{fr} states in the crystal structure.[6, 55] The SVD analysis of its 2DES also showed two major components. Direct global fitting of the 2DES dynamics gives three lifetimes: τ_1= 0.18 ps, τ_2=3.0 ps, τ_3=244 ps. The third component τ_3=244 ps is very similar to the τ2 component from the P_r→Lumi-R conversion fitting. We analyzed the spectrum after Fourier transforming in the T domain, which showed similar off-diagonal features to those in the P2 P_{fr} →Lumi-F conversion at excitation wavelength of > 750 nm with abroad peak in the ω_T domain, indicating the fast dynamics.

2.5 Conclusion

The two bacteriophytochromes in this study show many similar characteristics, but their differences have the potential to elucidate the underlying principles. P2 and Pa both convert between P_r and P_{fr}, but adopt different conformations (Pr and Pfr respectively) in their dark states. P2 and Pa also demonstrate quite different relaxation rates in their various interconversions. Notably, the two bacteriophytochromes possess different local hydrogen bonding between ring D of the biliverdin (BV) and the surrounding polar residues in the protein pockets, which may account for the differences in rates[55]. Two sets of residues around BV are important—the “15Ea pocket” and the “15Za pocket” (Scheme 1). Ring D of BV in the P_{fr} form resides in the “15Ea pocket”, forming hydrogen bonds with the Asp-194, Tyr-250, Ser-459, and Gln-188 residues [4, 6, 55, 56]. Such interactions stabilized Pa in the P_{fr} dark state. In comparison, P2 has a mixture of polar and non-polar residues in the corresponding three

positions (Tyr, Leu and Phe). The ring D resides in the "15Za pocket" in the P_r form, interacting with a conservative His-277 residue and an additional polar residues Ser-259 and Ser-275 for Pa [4, 5]. This interaction slowed down the Pa dynamics of $P_r \rightarrow$Lumi-R (42 ps for P2, 251 ps for Pa).

The $P_{fr} \rightarrow$Lumi-F photo-dynamics are generally faster than those of the $P_r \rightarrow$Lumi-R process. The Fourier transforms over the T domain help isolate the oscillation signal from the $P_{fr} \rightarrow$Lumi-F process with excitation wavelength >750 nm. The broad peak in the ω_T domain arises from the ultrafast decay (<100 fs) of this oscillation. Such fast decoherence may be related to a CI on the $P_{fr} \rightarrow$Lumi-F pathway[9, 59]. A proposed scheme is shown in Fig. 2.12 in which the initial P_{fr} state is excited to the vibronic excited state manifold, followed by fast leaking through a CI between the P_{fr} excited state surface and the Lumi-F ground state surface.

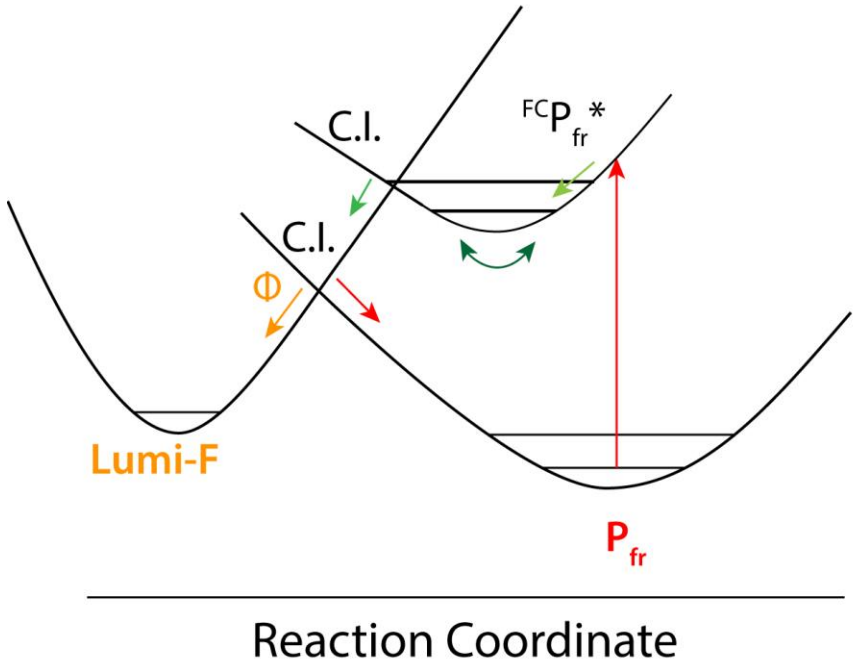

Figure 2.12: A proposed scheme showing the photodynamics of $P_{fr} \rightarrow$Lumi-F conversion

The $P_r \rightarrow P_{fr}$ and $P_{fr} \rightarrow P_r$ interconversions in phytochromes are initiated by ultrafast photo-induced isomerization of the chromophore[5, 6]. Previous spectroscopic studies of the isomerization have observed multi-exponential decays, and have attributed these dynamics to the existence of ground state heterogeneity across the ensemble[10-15, 18]. In this work, we leverage the two-dimensional resolution in 2DES to address whether ground state heterogeneity is indeed the origin of the functionally distinct relaxation pathways, as previously suggested. In 2DES, ground state heterogeneity is directly evident as an elongation of signal along the diagonal. Indeed, with lineshape analysis and global fitting, we were able to confirm the existence of this heterogeneity in the data (Fig 2). We could then ask whether complexes with different transition energies (e.g. on the blue side of the elongated peak versus the red side) follow the same dynamics. In this manner, we separately analyze subensembles such as the red and blue edges of ground state heterogeneity, and compare results. Across the entire inhomogeneously elongated peak, we see strikingly similar dynamics. That is, despite the presence of ground state heterogeneity, we observe the same multi-exponential decays (Fig. 2.6). This observation supports a model in which the multi-exponential terms describe evolution on the excited state surface rather than distinct subpopulations following different pathways. Regardless of the transition energy to the initial excited state, the ensemble is functionally homogeneous.

Because we observe no difference in the dynamics arising from ground state heterogeneity, we propose a model with just one component (of $P_r \rightarrow$Lumi-R relaxation and isomerization of the biliverdin cofactor that includes a transition barrier between the Franck-Condon region and the CI degeneracy. This barrier accounts for multi-exponential dynamics as well as the relatively slow CI isomerization compared to rhodopsin or photoactive yellow

protein. This model applies to both P2 and Pa, though the relaxation rate constants differ between the two proteins. We attribute the different rates of the dynamics between P2 and Pa to the number and strength of hydrogen bonds between the ring D of BV and the residues in the 15Za pocket of the proteins. We now have a clearer understanding of the relationship between the tetrapyrrole cofactor and its apo-protein as they influence ultrafast isomerization dynamics. Future work is needed to establish the generality of these findings across the broader phytochrome family of proteins.

2.6 Acknowledgments

The authors thank the DARPA QuBE program (N66001-10-1-4060), AFSOR (FA9550-10-1-0028), and the DoD Vannevar Bush Fellow Program (N00014-15-1-0048) the Camille and Henry Dreyfus Foundation, the Searle Foundation and NIH grant EY024363 (to K.M. and X.Y.) for supporting the work in this publication. M.L.F. was supported in part by the National Institute of Biomedical Imaging And Bioengineering of the National Institutes of Health under Award Number T32-EB009412.

2.7 References

[1] W.L. Butler, K.H. Norris, H.W. Siegelman, S.B. Hendricks, Detection, Assay, and Preliminary Purification of the Pigment Controlling Photoresponsive Development of Plants, Proceedings of the National Academy of Sciences of the United States of America 45 (1959) 1703-1708.

[2] M.S. Davis, A. Forman, J. Fajer, Ligated chlorophyll cation radicals: Their function in photosystem II of plant photosynthesis, Proceedings of the National Academy of Sciences of the United States of America 76 (1979) 4170-4174.

[3] J. Hughes, T. Lamparter, F. Mittmann, E. Hartmann, W. Gartner, A. Wilde, T. Borner, A prokaryotic phytochrome, Nature 386 (1997) 663-663.

[4] X. Yang, E.A. Stojkovic, J. Kuk, K. Moffatt, Crystal structure of the chromophore binding domain of an unusual bacteriophytochrome, RpBphP3, reveals residues that modulate photoconversion, Proceedings of the National Academy of Sciences of the United States of America 104 (2007) 12571-12576.

[5] K.C. Toh, E.A. Stojković, I.H.M. van Stokkum, K. Moffat, J.T.M. Kennis, Proton-transfer and hydrogen-bond interactions determine fluorescence quantum yield and photochemical efficiency of bacteriophytochrome, Proceedings of the National Academy of Sciences 107 (2010) 9170-9175.

[6] X.J. Yang, J. Kuk, K. Moffat, Conformational differences between the Pfr and Pr states in Pseudomonas aeruginosa bacteriophytochrome, Proceedings of the National Academy of Sciences of the United States of America 106 (2009) 15639-15644.

[7] N.C. Rockwell, Y.S. Su, J.C. Lagarias, Phytochrome structure and signaling mechanisms, Annu Rev Plant Biol 57 (2006) 837-858.

[8] C. Bongards, W. Gartner, The Role of the Chromophore in the Biological Photoreceptor Phytochrome: An Approach Using Chemically Synthesized Tetrapyrroles, Accounts Chem Res 43 (2010) 485-495.

[9] M. Bischoff, G. Hermann, S. Rentsch, D. Strehlow, Ultrashort processes of native phytochrome: Femtosecond kinetics of the far-red-absorbing form Pfr, J Phys Chem A 102 (1998) 4399-4404.

[10] A.E. Fitzpatrick, C.N. Lincoln, L.J.G.W. van Wilderen, J.J. van Thor, Pump–Dump–Probe and Pump–Repump–Probe Ultrafast Spectroscopy Resolves Cross Section of an Early Ground State Intermediate and Stimulated Emission in the Photoreactions of the Pr Ground State of the Cyanobacterial Phytochrome Cph1, The Journal of Physical Chemistry B 116 (2011) 1077-1088.

[11] K. Heyne, J. Herbst, D. Stehlik, B. Esteban, T. Lamparter, J. Hughes, R. Diller, Ultrafast Dynamics of Phytochrome from the Cyanobacterium Synechocystis, Reconstituted with Phycocyanobilin and Phycoerythrobilin, Biophysical Journal 82 (2002) 1004-1016.

[12] P.W. Kim, L.H. Freer, N.C. Rockwell, S.S. Martin, J.C. Lagarias, D.S. Larsen, Femtosecond Photodynamics of the Red/Green Cyanobacteriochrome NpR6012g4 from Nostoc punctiforme. 1. Forward Dynamics, Biochemistry 51 (2011) 608-618.

[13] P.W. Kim, L.H. Freer, N.C. Rockwell, S.S. Martin, J.C. Lagarias, D.S. Larsen, Second-Chance Forward Isomerization Dynamics of the Red/Green Cyanobacteriochrome NpR6012g4 from Nostoc punctiforme, Journal of the American Chemical Society 134 (2011) 130-133.

[14] P.W. Kim, N.C. Rockwell, L.H. Freer, C.-W. Chang, S.S. Martin, J.C. Lagarias, D.S. Larsen, Unraveling the Primary Isomerization Dynamics in Cyanobacterial Phytochrome Cph1 with Multipulse Manipulations, The Journal of Physical Chemistry Letters 4 (2013) 2605-2609.

[15] J.J. van Thor, K.L. Ronayne, M. Towrie, Formation of the Early Photoproduct Lumi-R of Cyanobacterial Phytochrome Cph1 Observed by Ultrafast Mid-Infrared Spectroscopy, Journal of the American Chemical Society 129 (2007) 126-132.

[16] J. Dasgupta, R.R. Frontiera, K.C. Taylor, J.C. Lagarias, R.A. Mathies, Ultrafast excited-state isomerization in phytochrome revealed by femtosecond stimulated Raman spectroscopy, Proceedings of the National Academy of Sciences 106 (2009) 1784-1789.

[17] K.C. Toh, E.A. Stojkovic, I.H.M. van Stokkum, K. Moffat, J.T.M. Kennis, Fluorescence quantum yield and photochemistry of bacteriophytochrome constructs, Physical Chemistry Chemical Physics 13 (2011) 11985-11997.

[18] L.J.G.W. van Wilderen, I.P. Clark, M. Towrie, J.J. van Thor, Mid-Infrared Picosecond Pump−Dump−Probe and Pump−Repump-Probe Experiments to Resolve a Ground-State Intermediate in Cyanobacterial Phytochrome Cph1, The Journal of Physical Chemistry B 113 (2009) 16354-16364.

[19] Y. Yang, M. Linke, T. von Haimberger, J. Hahn, R. Matute, L. González, P. Schmieder, K. Heyne, Real-Time Tracking of Phytochrome's Orientational Changes During Pr Photoisomerization, Journal of the American Chemical Society 134 (2012) 1408-1411.

[20] E.E. Grintsevich, I.E. Adzerikho, A.G. Mrochek, D.I. Metelitza, Polydisulfides of substituted phenols as effective protectors of peroxidase against inactivation by ultrasonic cavitation, Biochemistry. Biokhimiia 66 (2001) 740-746.

[21] M.E. Vanbrederode, T. Gensch, W.D. Hoff, K.J. Hellingwerf, S.E. Braslavsky, Photoinduced Volume Change and Energy-Storage Associated with the Early Transformations of the Photoactive Yellow Protein from Ectothiorhodospira-Halophila, Biophysical Journal 68 (1995) 1101-1109.

[22] K. Pande, C.D.M. Hutchison, G. Groenhof, A. Aquila, J.S. Robinson, J. Tenboer, S. Basu, S. Boutet, D.P. DePonte, M.N. Liang, T.A. White, N.A. Zatsepin, O. Yefanov, D. Morozov, D. Oberthuer, C. Gati, G. Subramanian, D. James, Y. Zhao, J. Koralek, J. Brayshaw, C. Kupitz, C. Conrad, S. Roy-Chowdhury, J.D. Coe, M. Metz, P.L. Xavier, T.D. Grant, J.E. Koglin, G. Ketawala, R. Fromme, V. Srajer, R. Henning, J.C.H. Spence, A. Ourmazd, P. Schwander, U. Weierstall, M. Frank, P. Fromme, A. Barty, H.N. Chapman, K. Moffat, J.J. van Thor, M. Schmidt, Femtosecond structural dynamics drives the trans/cis isomerization in photoactive yellow protein, Science 352 (2016) 725-729.

[23] P.W. Kim, N.C. Rockwell, S.S. Martin, J.C. Lagarias, D.S. Larsen, Dynamic Inhomogeneity in the Photodynamics of Cyanobacterial Phytochrome Cph1, Biochemistry 53 (2014) 2818-2826.

[24] L.H. Freer, P.W. Kim, S.C. Corley, N.C. Rockwell, L. Zhao, A.J. Thibert, J.C. Lagarias, D.S. Larsen, Chemical Inhomogeneity in the Ultrafast Dynamics of the DXCF Cyanobacteriochrome Tlr0924, The Journal of Physical Chemistry B 116 (2012) 10571-10581.

[25] X.J. Jordanides, M.J. Lang, X.Y. Song, G.R. Fleming, Solvation dynamics in protein environments studied by photon echo spectroscopy, Journal of Physical Chemistry B 103 (1999) 7995-8005.

[26] J.B. Nieder, M. Brecht, R. Bittl, Dynamic Intracomplex Heterogeneity of Phytochrome, Journal of the American Chemical Society 131 (2009) 69-+.

[27] D. von Stetten, M. Günther, P. Scheerer, D.H. Murgida, M.A. Mroginski, N. Krauß, T. Lamparter, J. Zhang, D.M. Anstrom, R.D. Vierstra, K.T. Forest, P. Hildebrandt, Chromophore Heterogeneity and Photoconversion in Phytochrome Crystals and Solution Studied by Resonance Raman Spectroscopy, Angewandte Chemie International Edition 47 (2008) 4753-4755.

[28] J.B. Nieder, E.A. Stojković, K. Moffat, K.T. Forest, T. Lamparter, R. Bittl, J.T.M. Kennis, Pigment–Protein Interactions in Phytochromes Probed by Fluorescence Line Narrowing Spectroscopy, The Journal of Physical Chemistry B 117 (2013) 14940-14950.

[29] C. Song, G. Psakis, C. Lang, J. Mailliet, W. Gartner, J. Hughes, J. Matysik, Two ground state isoforms and a chromophore D-ring photoflip triggering extensive intramolecular changes in a canonical phytochrome, Proceedings of the National Academy of Sciences of the United States of America 108 (2011) 3842-3847.

[30] K.M. Spillane, J. Dasgupta, J.C. Lagarias, R.A. Mathies, Homogeneity of Phytochrome Cph1 Vibronic Absorption Revealed by Resonance Raman Intensity Analysis, Journal of the American Chemical Society 131 (2009) 13946-13948.

[31] Katelyn M. Spillane, J. Dasgupta, Richard A. Mathies, Conformational Homogeneity and Excited-State Isomerization Dynamics of the Bilin Chromophore in Phytochrome Cph1 from Resonance Raman Intensities, Biophysical Journal 102 (2012) 709-717.

[32] M.H. Cho, T. Brixner, I. Stiopkin, H. Vaswani, G.R. Fleming, Two dimensional electronic spectroscopy of molecular complexes, J Chin Chem Soc-Taip 53 (2006) 15-24.

[33] B. AM, T. DB, S. GD, Crossing disciplines - A view on two-dimensional optical spectroscopy, Ann. Phys. (Berlin) 526 (2013) 31-49.

[34] J.D. Hybl, A.A. Ferro, D.M. Jonas, Two-dimensional Fourier transform electronic spectroscopy, J Chem Phys 115 (2001) 6606-6622.

[35] D.M. Jonas, Two-dimensional femtosecond spectroscopy, Annu Rev Phys Chem 54 (2003) 425-463.

[36] M.L. Cowan, J.P. Ogilvie, R.J.D. Miller, Two-dimensional spectroscopy using diffractive optics based phased-locked photon echoes, Chemical Physics Letters 386 (2004) 184-189.

[37] T. Brixner, T. Mancal, I.V. Stiopkin, G.R. Fleming, Phase-stabilized two-dimensional electronic spectroscopy, J Chem Phys 121 (2004) 4221-4236.

[38] K.L. Wells, Z. Zhang, J.R. Rouxel, H.-S. Tan, Measuring the Spectral Diffusion of Chlorophyll a Using Two-Dimensional Electronic Spectroscopy, Journal of Physical Chemistry B 117 (2013) 2294-2299.

[39] J.D. Hybl, A. Yu, D.A. Farrow, D.M. Jonas, Polar solvation dynamics in the femtosecond evolution of two-dimensional Fourier transform spectra, J Phys Chem A 106 (2002) 7651-7654.

[40] T. Brixner, J. Stenger, H.M. Vaswani, M. Cho, R.E. Blankenship, G.R. Fleming, Two-dimensional spectroscopy of electronic couplings in photosynthesis, Nature 434 (2005) 625-628.

[41] E.L. Read, G.S. Engel, T.R. Calhoun, T. Mancal, T.K. Ahn, R.E. Blankenship, G.R. Fleming, Cross-peak-specific two-dimensional electronic spectroscopy, Proceedings of the National Academy of Sciences of the United States of America 104 (2007) 14203-14208.

[42] U. Selig, C.-F. Schleussner, M. Foerster, F. Langhojer, P. Nuernberger, T. Brixner, Coherent two-dimensional ultraviolet spectroscopy in fully noncollinear geometry, Optics Letters 35 (2010) 4178-4180.

[43] G.S. Schlau-Cohen, A. Ishizaki, G.R. Fleming, Two-dimensional electronic spectroscopy and photosynthesis: Fundamentals and applications to photosynthetic light-harvesting, Chemical Physics 386 (2011) 1-22.

[44] N.S. Ginsberg, J.A. Davis, M. Ballottari, Y.-C. Cheng, R. Bassi, G.R. Fleming, Solving structure in the CP29 light harvesting complex with polarization-phased 2D electronic spectroscopy, Proceedings of the National Academy of Sciences of the United States of America 108 (2011) 3848-3853.

[45] E. Harel, G.S. Engel, Quantum coherence spectroscopy reveals complex dynamics in bacterial light-harvesting complex 2 (LH2), Proceedings of the National Academy of Sciences of the United States of America 109 (2012) 706-711.

[46] E.E. Ostroumov, R.M. Mulvaney, R.J. Cogdell, G.D. Scholes, Broadband 2D Electronic Spectroscopy Reveals a Carotenoid Dark State in Purple Bacteria, Science 340 (2013) 52-56.

[47] D.B. Turner, Y. Hassan, G.D. Scholes, Exciton Superposition States in CdSe Nanocrystals Measured Using Broadband Two-Dimensional Electronic Spectroscopy, Nano Lett 12 (2012) 880-886.

[48] G.B. Griffin, S. Ithurria, D.S. Dolzhnikov, A. Linkin, D.V. Talapin, G.S. Engel, Two-dimensional electronic spectroscopy of CdSe nanoparticles at very low pulse power, J Chem Phys 138 (2013).

[49] C.Y. Wong, G.D. Scholes, Biexcitonic Fine Structure of CdSe Nanocrystals Probed by Polarization-Dependent Two-Dimensional Photon Echo Spectroscopy, J Phys Chem A 115 (2011) 3797-3806.

[50] G. Moody, R. Singh, H. Li, I.A. Akimov, M. Bayer, D. Reuter, A.D. Wieck, A.S. Bracker, D. Gammon, S.T. Cundiff, Influence of confinement on biexciton binding in semiconductor quantum dot ensembles measured with two-dimensional spectroscopy, Physical Review B 87 (2013).

[51] P.F. Tian, D. Keusters, Y. Suzaki, W.S. Warren, Femtosecond phase-coherent two-dimensional spectroscopy, Science 300 (2003) 1553-1555.

[52] X. Dai, A.D. Bristow, D. Karaiskaj, S.T. Cundiff, Two-dimensional Fourier-transform spectroscopy of potassium vapor, Physical Review A 82 (2010).

[53] P.F. Tekavec, G.A. Lott, A.H. Marcus, Fluorescence-detected two-dimensional electronic coherence spectroscopy by acousto-optic phase modulation, J Chem Phys 127 (2007).

[54] H. Li, A.D. Bristow, M.E. Siemens, G. Moody, S.T. Cundiff, Unraveling quantum pathways using optical 3D Fourier-transform spectroscopy, Nature Communications 4 (2013).

[55] X. Yang, J. Kuk, K. Moffat, Crystal structure of Pseudomonas aeruginosa bacteriophytochrome: photoconversion and signal transduction, Proceedings of the National Academy of Sciences of the United States of America 105 (2008) 14715-14720.

[56] X. Yang, Z. Ren, J. Kuk, K. Moffat, Temperature-scan cryocrystallography reveals reaction intermediates in bacteriophytochrome, Nature 479 (2011) 428-432.

[57] H. Zheng, J.R. Caram, P.D. Dahlberg, B.S. Rolczynski, S. Viswanathan, D.S. Dolzhnikov, A. Khadivi, D.V. Talapin, G.S. Engel, Dispersion-free continuum two-dimensional electronic spectrometer, Appl Opt 53 (2014) 1909-1917.

[58] V.P. Singh, A.F. Fidler, B.S. Rolczynski, G.S. Engel, Independent phasing of rephasing and non-rephasing 2D electronic spectra, J Chem Phys 139 (2013).

[59] P.W. Kim, L.H. Freer, N.C. Rockwell, S.S. Martin, J.C. Lagarias, D.S. Larsen, Femtosecond Photodynamics of the Red/Green Cyanobacteriochrome NpR6012g4 from Nostoc punctiforme. 2. Reverse Dynamics, Biochemistry 51 (2011) 619-630.

Chapter 3:

Characterization of a Synthetic Light Harvesting Complex

3.1 Introduction

Light harvesting complexes, like Light Harvesting complex 2 (LH2) in *Rhodobacter sphaeroides,* have more than a dozen chromophores and the machinery often has a very congested absorption spectrum and changes from simply being in a protein environment are difficult to distinguish from coupling and energy transfer symptoms[1]. Are the chromophores interacting more with each other or the protein? Researchers have tackled this obstacle by either taking measurements of the free bacteriochlorophyll in solution as a control or by theoretical calculations of the protein contribution to the spectroscopic properties, but satisfying answers have not yet been found[2-4]. Here, we evaluate a synthetic light-harvesting complex modeled after LH2 and similar light harvesting complexes.

Light harvesting is a popular topic in present day society because solar energy is often looked to as the future primary source of energy and electricity, and as such, light harvesting has been extensively covered in the literature[1, 5-8]. It is currently accepted that light harvesting requires strong light absorbing chromophores that are strongly coupled to one another in fixed relative position to one another. In nature, light harvesting avoids the Förster energy transfer regime between neighboring chromophores although Förster transfer does dominate transfer between excitons within and between neighboring proteins, indicating the importance of strong coupling between chromophores[1]. Thermal fluctuations and vibrational motion is necessary for

energy transfer between excitonic states and complexes, but too much noise, and the system loses its memory and order[9]. Although biology is hot and wet relative to many systems chemists think about, two conditions that often indicate a high degree of randomness and fluctuations in the system, proteins are able to overcome this and provide a scaffold with low dynamic disorder on the time scales of energy transfer. If we are going to be able to design robust technologies in the future, it is vital that we understand how the protein is able to provide the necessary core conditions for light harvesting and ultrafast energy transfer despite constant fluctuations and disorder. It is still debated whether a protein scaffold with coupled chromophores is enough to mimic nature or is there a further principle left to uncover. Here, we address this question by investigating an artificial light harvesting system and compare its photophysical properties to light harvesting in nature.

The most logical way to discover whether we understand the design principles is to try to recreate light harvesting behavior. Recently, an artificial light-harvesting complex has been constructed out of Tobacco Mosaic Virus (TMV) capsid proteins[10-12]. TMV virus capsids are self-assembling protein structures that are typically, long cylinders in which the TMV genome is packed. The capsid protein is a peptide made of two main α-helices, and capsid monomers are stacked next to each other in a highly ordered spiral to create this cylinder. By altering the assembly conditions, it is possible to favor different geometries, and in the case of the TMV-based light-harvesting complex, the result is two stacked discs of capsid monomers (Fig. 3.1a). By introducing point mutations at the location of interest (Fig. 3.1b), chromophores can be selectively attached to the discs and the combination of every monomer attached to a chromophore results in a ring of chromophores reminiscent of the LH2 rings of bacteriochlorophyll (Fig. 3.1d). This TMV based system also provides the unique opportunity to

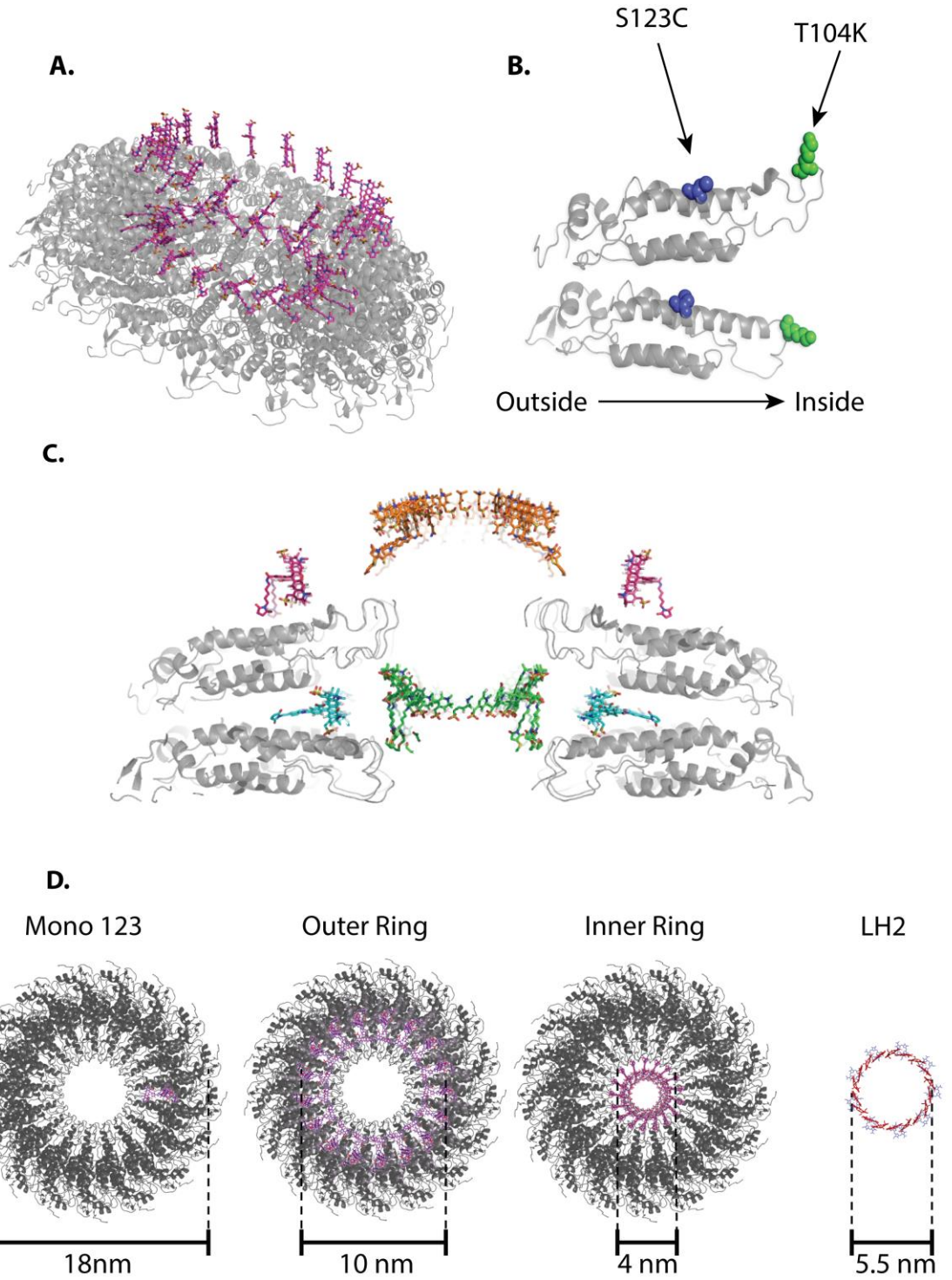

Figure 3.1: Structure of the TMV-based synthetic light-harvesting complex. (a) Side view of Outer Ring. (b) View of a monomer unit of the TMV protein. Blue highlights the position of Inner Ring chromophore attachment and green highlights the position of Outer Ring chromophore attachment. (c) Side slice view showing both Inner Ring and Outer Ring chromophores. (d) Diameter of chromophore rings as they compare with the bacteriochlorophyll ring in LH2 from *R. sphaeroides* (right).

investigate the behavior of a single chromophore attached to the protein rather than coupled to its neighbors in the ring. The artificial light-harvesting proteins provide a platform to investigate whether the protein acting as merely a scaffold is sufficient to recreate photosynthetic machinery. To this end, we examine TMV-based light harvesting complexes with Alexa Fluor 594 chromophores attached at the 123 residues (Outer Ring), 104 residues (Inner Ring), and a complex with only one chromophore attached at the 123 position of one monomer within the disc (Mono Ring) as well as free Alexa Fluor 594 (no protein) in solution. The Mono Ring was chosen to separately analyze the influence of the protein and the effects of coupling to other chromophores, while comparing the Outer and Inner Ring should provide insight on the strength of coupling because the two complexes both have 17 chromophores arranged in a ring, but the Inner Ring has a much smaller radius and therefore, should have stronger coupling between chromophores.

3.2 Results and Discussion

3.2.1 Absorption Spectra of the Light Harvesting Complexes

In photosynthetic light harvesting systems, the absorption spectra of the complexes do not usually match the absorption of the free, uncoupled chromophore in solution. For example, the chromophores in LH2 from *R. sphaeroides* are entirely bacteriochlorophylls—18 in the B850 spectral feature and 9 in the B800 feature shown in Figure 3.2a, but neither feature's absorption peak resembles bacteriochlorophyll in solution (Fig. 3.2a). The two primary factors that contribute to a spectral lineshape and absorption shifts are environment and coupling[13]. That is, the environment inside an LH2 complex looks very different than small solvent molecules surrounding the chromophore. This environment is composed of protein sidechains that each

have specific electronic properties that can slightly change the resonant optical transitions of the bacteriochlorophyll. Alternatively, strong coupling between many chromophores can significantly shift or alter an absorption spectrum depending on the strength of coupling. When two states close in energy are strongly coupled, the Coulombic interaction splits the states into a high energy and a low energy state[14]. Usually, one of these transitions is only weakly allowed due to orientation of chromophore dipoles and so coupling reveals itself in the absorption spectrum as either a red-shift or a blue-shift of the absorption maximum. In contrast to light harvesting complexes from purple bacteria, the absorption spectra of the TMV-modified light harvesting complexes do not show significant changes from the absorption spectrum of its chromophore, Alexa Fluor 594 nm, in solution (Fig. 3.2b). There are small shifts and differences between the TMV-based samples, but nothing on the order of bacteriochlorophyll and LH2. This is the first indication that this synthetic light harvesting system is not spectroscopically or functionally identical to wild type complexes like LH2.

The synthetic light harvesting system is constructed in such a way that allows us to analyze the properties of the Mono Ring, where only one chromophore is attached to the protein disc scaffold. This is useful because we can easily identify inhomogeneous broadening in the absorption peak without a 2D spectral lineshape analysis. The Mono Ring absorption profile is significantly broader than the free chromophore (Fig. 3.2c). This is expected in a protein environment, as discussed in chapter 2, and is confirmation of the current understanding of inhomogeneously broadened peaks due to protein heterogeneity[15]. More importantly, we can compare the spectra of the Outer Ring and Inner Ring to the Mono Ring instead of the free Alexa Fluor, allowing us to have a more accurate baseline to quantify coupling in the two TMV-light

harvesting systems since the Mono Ring is the same chromophore, uncoupled, in the same immediate environment.

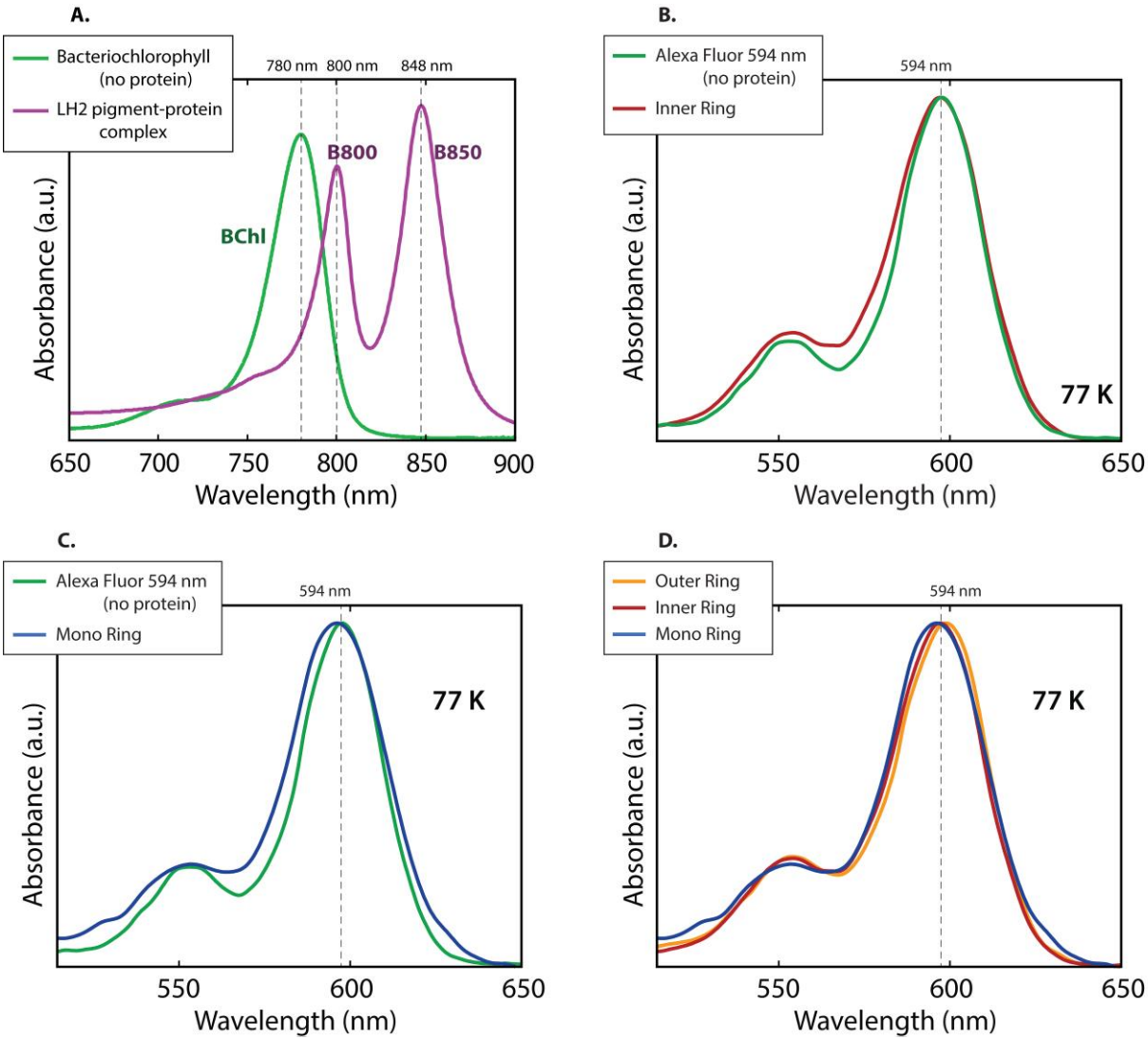

Figure 3.2: Comparison of absorption spectra of LH2 and the TMV based light harvesting systems with their free chromophores. (a) Absorption spectra of LH2 and free bacteriochlorophyll are significantly different. (b) Absorption of the Inner Ring and free Alexa Fluor show very little difference. (c) The Mono Ring absorption is broader than the free chromophore due to static disorder. (d) Outer Ring, Inner Ring, and Mono Ring show very little difference besides some small narrowing with the Outer Ring.

In absorption spectra of J-aggregates and other highly coupled systems, there is a well-documented effect on the absorption spectrum called "exchange narrowing" in which the linewidth narrows as the coupling between chromophores increases in strength[16]. When chromophores are strongly coupled, the system excitonic states and the molecular excited states start to diverge. Instead, excitonic states are linear combinations of the individual molecular excited states and as coupling strength increases, the excitonic states are delocalized over more and more molecules. As the delocalization length, or number of molecules contributing to the excitonic state increase, random fluctuations to each excited state contribute less and less to the excitonic state, thereby decreasing its inhomogeneous broadening. Formally, the line broadening function, which describes the contributions that broaden absorption lineshapes is defined by

$$g_{j,j}(t) = \int_0^t d\tau_2 \int_0^{\tau_2} d\tau_1 \, \langle \delta\Omega_j(\tau_1)\delta\Omega_j(0)\rangle$$

Where $\langle \delta\Omega_j(\tau_1)\ \delta\Omega_j(0)\rangle$ represents the excited state frequency fluctuations of the excitonic state. The fluctuation term can be simplified to $C(\tau_1)/N_j$ where $C(\tau_1)$ is the correlation function for a singly excited monomer and N_j is the delocalization length, by assuming an independent and homogeneous bath[16]. Therefore, the line broadening function for the excitonic state can be simplified to

$$g_{j,j}(t) = \frac{1}{N_j} g_0(t)$$

Where $g_0(t)$ is the line broadening function of the singly excited single molecule in the same environment. With this effect in mind, the absorption spectra in Figure 3.2d do not show us a system with highly coupled Alexa Fluor molecules. While the Outer Ring and Inner Ring

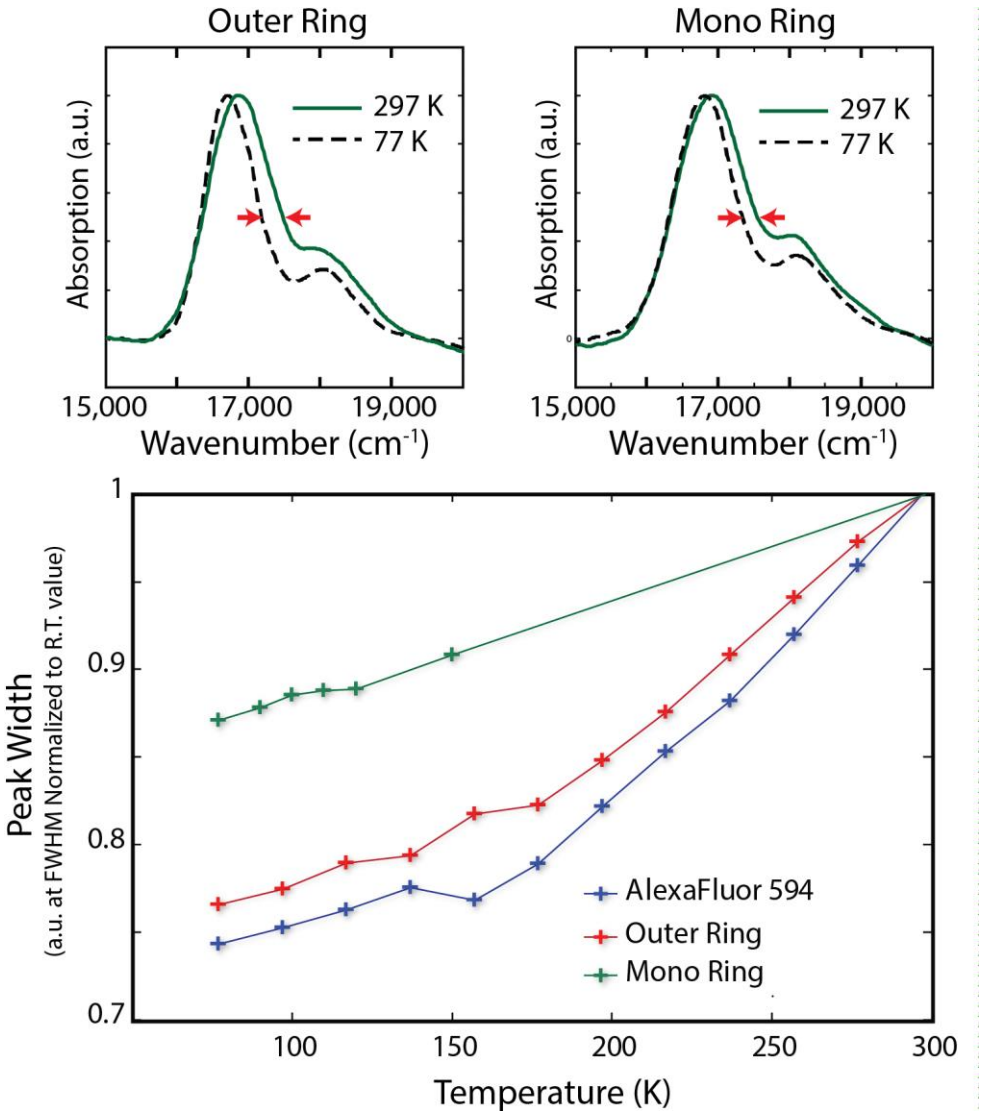

Figure 3.3: Narrowing of Outer Ring with decreasing temperature when compared to narrowing of the Mono Ring indicates exchange narrowing due to coupling.

complexes do show a small amount of narrowing relative to the Mono Ring, it is not sufficiently strong enough to overcome the inhomogeneous broadening due to a protein environment. However, at cryogenic temperatures, there is a noticeable difference between of the Outer Ring absorption spectrum tracks closer to the free Alexa Fluor in solution than the single Alexa Fluor attached to the TMV protein disc (Mono Ring), revealing just enough coupling between adjacent

chromophores in the Outer Ring complex to overcome the significant inhomogeneous broadening due to placing the chromophores in a protein environment. Exchange narrowing is not usually described as a temperature dependent effect. The narrowing is expected to change with coupling strength, so the data in Figure 3.3 need further explanation. The most likely explanation is that thermal effects overwhelm the coupling strength. In section 1.3.2 of this dissertation, the regimes of energy transfer were discussed. If the temperature dependence of exchange narrowing is in fact a result of thermal fluctuations, coupling strength should be less than coupling to the environment. Therefore, the TMV based light harvesting systems described in this chapter would be categorized in the Förster resonance energy transfer regime and not coherent resonance energy transfer as in many photosynthetic complexes.

In order to better understand how these chromophores are interacting, we need to quantify the coupling and inhomogeneity in the system. To this effect, we employ a simple lineshape model based on a description of eosin, another fluorescein derived chromophore, in Lang et al.'s model[17]. This model allows us to use the same dynamic disorder lineshape function for each sample, while altering the inhomogeneous broadening and coupling constant between neighboring chromophores, but limits us to the regime where the dipole approximation is valid, so we recognize it will not be useful in describing the Inner Ring's behavior and therefore do not attempt to do so. The model employed in this work defines the coupling to the bath through a spectral density function, $\rho(\omega)$, which quantifies the strength of coupling as a function of wavelength of bath modes[15, 17]. Fast relaxation components are modeled as a decaying function in the spectral density, while strong vibrational coupling is modeled as a harmonic oscillator and appears as a peak centered on the single mode in the spectral density[18]. The spectral density is integrated over all frequencies and over time to generate the

lineshape function. That is, the lineshape function is related to the correlation function for the transition by

$$C(t) = \int_0^\infty \rho(\omega) \coth\left(\frac{\hbar\omega}{2k_B T}\right) \omega^2 \cos \omega t \, d\omega + i \int_0^\infty \rho(\omega) \, \omega^2 \sin \omega t \, d\omega \qquad (1)$$

and the correlation function is related to the lineshape function by

$$g(t) = \int_0^t \int_0^{t_2} C(t_1) \, dt_1 dt_2 \qquad (2)$$

The response function is then calculated from the lineshape function[16] by

$$\phi_{BA}(t) = \frac{i}{\hbar} \Theta(t) B_{ge} A_{eg} \exp\left(-g(t) - i\omega_{eg} t\right) \qquad (3)$$

in which B_{ge} and A_{eg} are transition dipole strengths, determining the amount of absorption, $\Theta(t)$ is the heavyside step function, and ω_{eg} is the coherence contribution from the transition site energy.

The lineshape model for Alexa Fluor 594 is based on the Fleming eosin model[17], and many of the internal vibrational modes are assumed to be similar. Importantly, a very strongly coupled vibrational mode at 1300 cm^{-1} is included to represent the shoulder seen in the absorption spectra assigned to the large ring "breathing" modes. Temperature dependence is included in the model in calculating the dynamic disorder contributions to the lineshape. Any inhomogeneity in the system is modeled as variation in site energy and is independent of temperature. To model the Mono Ring absorption, 60 cm^{-1} of uncertainty in site energy is added to simulate the heterogeneity of protein environment. The Outer Ring was modeled using a 17 by 17 Hamiltonian matrix with nearest neighbor and second neighbor coupling constants. Nearest neighbor coupling was calculated by dipole-dipole approximation coupling to be 30.1 cm^{-1} while

second neighbor coupling was allowed to vary to a final value of 0.4 cm^{-1}. Since second neighbor coupling was weak, all other coupling constants are assumed to be zero. The Inner Ring chromophores were too close together for the approximation to remain valid and therefore, the results did not capture the experimental data.

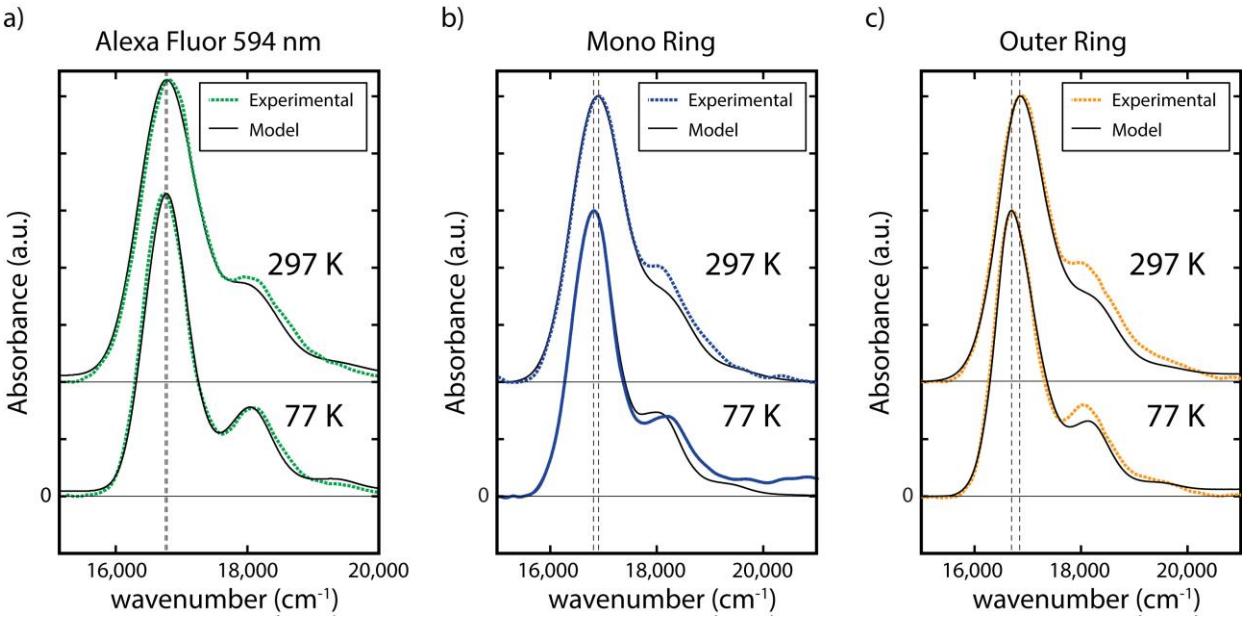

Figure 3.4: Lineshape model and experimental absorption data for free chromophore, the Mono Ring and the Outer Ring samples.

The results of this lineshape model help explain the lack of change in the width of each absorption spectrum. Although Figure 3.2 shows that the Outer Ring and free Alexa Fluor have remarkably similar widths, the Mono Ring reveals that there is in fact exchange narrowing occurring due to the 30 cm^{-1} nearest neighbor coupling in the Outer Ring sample (Fig. 3.4). That is, the Mono Ring sample is homogeneously broadened relative to free chromophore in solution, and the Outer Ring is modeled with the same degree of homogeneous broadening, but the resulting line width is approximately the same as free chromophore. Interestingly, the amount of broadening due to the static disorder from the protein scaffold is almost exactly canceled by the

exchange narrowing due to coupling in the Outer Ring sample. This is again, more evidence that we are in the FRET regime of energy transfer. The only feature that the model fails to capture is the behavior of the vibrational shoulder. The strength of coupling to the 1300 cm^{-1} vibrational mode is allowed to vary in the Alexa Fluor model, but the result of the fit, 109 cm^{-1}, is considered constant across all three samples. However, the strength of the shoulder in the model is significantly weaker than the shoulder in the Outer Ring experimental data. This discrepancy will be revisited in the analysis and discussion of the 2DES data.

3.2.2 2DES of Outer Ring and Alexa Fluor 594 as a Control

2DES data were acquired of the Outer Ring sample and the free Alexa Fluor 594 (no protein) and representative spectra are shown in Fig. 3.5. The Mono Ring and Inner Ring data are not shown due to weak signal. As the Mono Ring has only one chromophore instead of seventeen in each TMV layer, it is difficult to concentrate the protein to a high enough O.D. without causing aggregation. The 2DES data reveal differences in the decay behavior of both samples (Fig. 3.6). Notably, the Outer Ring decays significantly faster than free chromophore in solution (τ = 325 fs for the Outer Ring and τ = 590 fs for the free chromophore) indicating that there is an additional pathway available to the coupled system besides fluorescence and the non-radiative decay of the free chromophore. This could be energy transfer to a trap state or a radiationless internal conversion that is only available in a multi-chromophore coupled system.

As anticipated, the 2D spectra of the Outer Ring (Fig. 3.5b) shows an elongated peak along the diagonal when compared to the rounder peak in free Alexa Fluor (Fig. 3.5a). As discussed previously, this lineshape is a result of micro-conformational heterogeneity that is static on the time scale of this experiment, which would include most atomic rearrangement. The tiny differences in conformation result in a range of transition energies distributed around the

mean which gives rise to an elongated peak. Additionally, slightly more excited state absorption appears in the Outer Ring sample, indicating chromophore coupling.

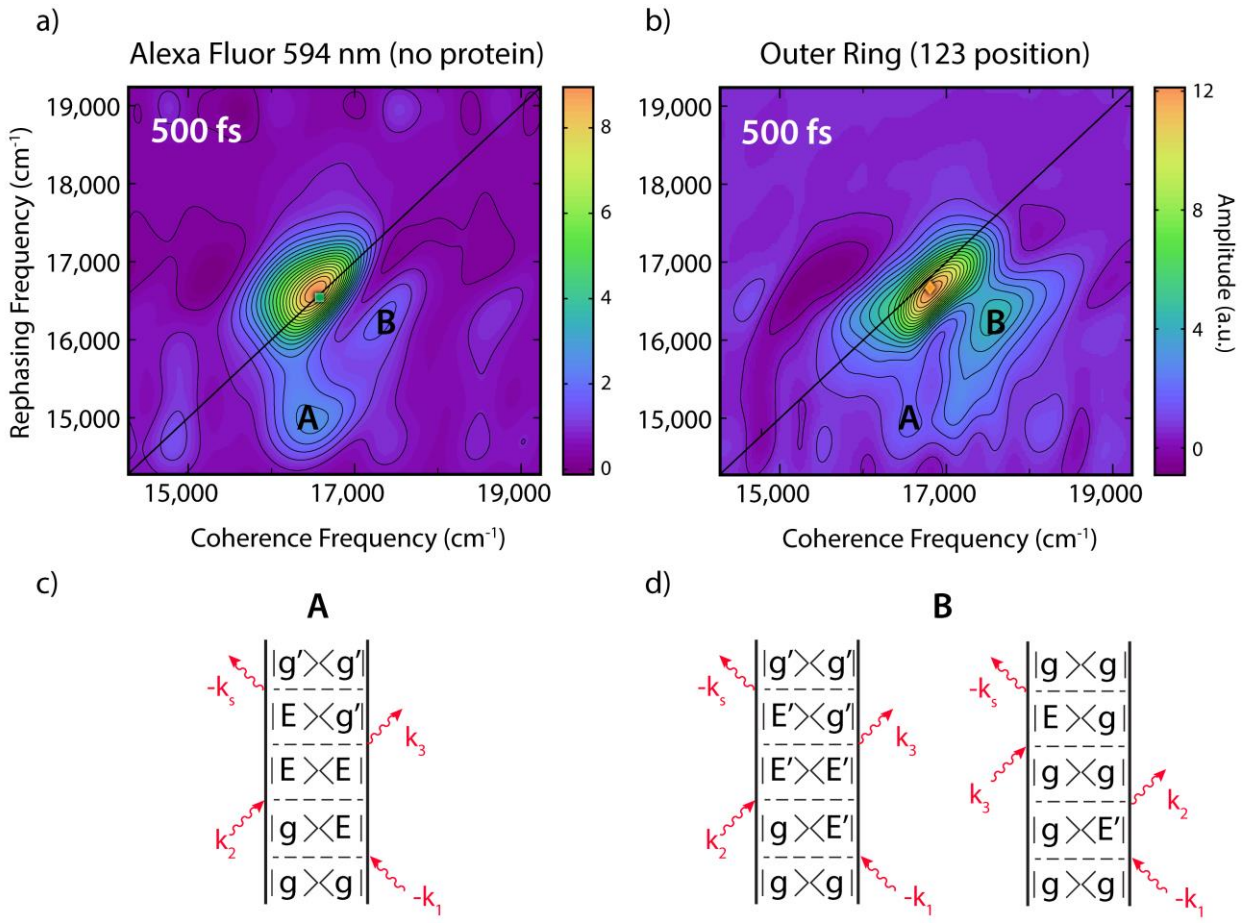

Figure 3.5 Excited state vibrations observed in the Outer Ring 2DES. (a) Representative 2DES of free Alexa Fluor 594 at T=500 fs. (b) Representative 2DES of the TMV-based light harvesting complex, the Outer Ring at T=500 fs. (c) Feynman diagram for static pathway that contributes to vibrational peak A. (d) Feynman diagram for static pathways that contribute to vibrational peak B. In both panel (c) and (d), excited vibrational states are indicated with an apostrophe (g', E').

The most significant difference between the chromophore and light harvesting complex 2D spectra is the relative strength of the shoulder peak (Fig. 3.5). In the lineshape model of the absorption spectra (Fig. 3.4), the model failed to capture the strength of the vibrational shoulder on both the Mono Ring and the Outer Ring, though much more significantly in the Outer Ring

which indicates it is a result of chromophore coupling. That could just be an artifact of uncertainty in the baseline, but in light of the 2DES data, it is likely significant. These 2DES data provide insight into the increased vibrational shoulder. Strongly coupled vibrational modes give rise to a series of peaks around the main diagonal peak in a 2D spectrum[18]. Each of these vibrational peaks results from a different subset of the possible interactions that reveal a strong vibrational coupling. In Fig. 3.5c-d, the static (no coherence or beating) pathways for the two vibrational peaks visible in the free chromophore and Outer Ring 2D spectra are given in Feynman diagram format. Notably, in these two vibrational peaks, static contributions from vibrations on the *excited state* only appear in peak B. The strength of peak B in the Outer Ring spectrum relative to the Alexa Fluor spectrum indicates that we are seeing vibrations on the excited state only when chromophore coupling is present. This is likely a symptom of energy transfer, but more investigation is needed to reach certainty.

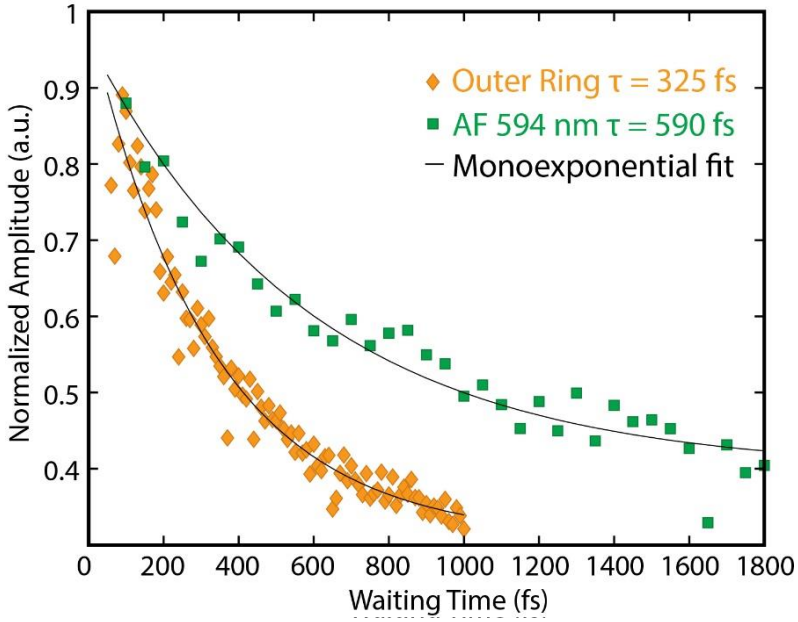

Figure 3.6: The coupled Outer Ring sample decays faster than free Alexa Fluor in solution. Both data sets are taken from the matching diamond or square indicated in the 2D spectra in Fig. 3.5 and are fit to a monoexponential plus offset.

3.3 Conclusion

The design principles of light harvesting complexes will guide future energy research and engineering and are therefore vital to understand. In this work, we test if a protein scaffold and proximal chromophores are sufficient to recreate efficient light harvesting by examining a synthetic complex based on TMV capsid proteins and covalently attached Alexa Fluor 594 nm molecules. Although the absorption spectra of the TMV-based light harvesting systems are not significantly different than the free chromophore in solution, lineshape modeling and 2DES data reveal there are excited state interactions. The lineshape model revealed that the system exhibits exchange narrowing which indicates chromophore coupling, and 2DES reveal strong excited state vibrations only for the coupled system, not the free chromophore, indicating that the coupled chromophores are interacting through their excited states. This is promising evidence of energy transfer and delocalized excitations, two necessary components of photosynthetic light harvesting. The strength of coupling is calculated to be 30.1 cm^{-1}. The coupling, in addition to the parity of exchange narrowing due to coupling and inhomogeneous broadening indicate the Outer Ring synthetic light harvesting system is operating in the incoherent regime of Förster resonance energy transfer rather than coherent resonance energy transfer as in the light harvesting complex of *R. sphaeroides*. These results indicate that the TMV based system is capable of light harvesting, but additional design principles are necessary to recreate light harvesting behavior from nature.

Figure 3.1 presents a series of views of the TMV-Alexa Fluor light-harvesting complex that help explain this lack of light harvesting behavior. The bound chromophores in these complexes exist in two distinct rings. One is buried between the discs of protein, but the other is practically floating on top and is much more exposed to solvent and much less motion restricted

than bacteriochlorophylls in photosynthetic light harvesting systems. The lack of physical confines of the chromophores mean that the relative orientation and distance between chromophores is not constant and has the potential to be subject to much larger fluctuations than in LH2, for example. The dipole approximation and the resulting calculation for nearest neighbor coupling used in the lineshape model is determined for only one orientation of chromophore, and therefore, cannot capture the effective coupling of chromophores constantly in motion. In this way, the synthetic complex is not capable of being fine-tuned in the way that photosynthetic complexes are because a single orientation and distance cannot be set. Therefore, further investigation is needed to determine if the protein does more than restrict motion of chromophores relative to one another or if the primary sequence level control of the electronic environment of each chromophore is relevant to light-harvesting.

3.4 Methods

3.4.1 Sample Preparation

Labeled TMV discs are expressed, modified and assembled as describes in Ref [10] using maleimide-functionalized Alexa Fluor 594 nm as the chromophore label.

3.4.2 Spectroscopy

Protein samples were mixed in a 3:2 ratio of glycerol to protein in buffer to a final O.D. of 0.05 for the Mono Ring and 0.3 for all other samples in a silanized quartz cell with a 200 μm path length. A reservoir cryostat from Oxford Instruments with liquid nitrogen was used to control the temperature from 77 K to 297 K. Continuum 2DES data[19] was acquired as described in Ref

[19] Outer Ring data waiting times range from 50 to 1000 fs in 5 fs steps, while the free Alexa Fluor data is from 100 to 1800 in 50 fs steps. Both data sets are acquired with coherence times from -50 to 100 fs in 1 fs steps.

3.5 Acknowledgements

This work was completed by M.L.F. with Drs. Daniel Finley, Justin Caram, Matthew Francis, and Greg Engel.

3.6 References

[1] R.E. Blankenship, Molecular mechanisms of photosynthesis, Second edition. ed., Wiley/Blackwell, Chichester, West Sussex, 2014.

[2] K.A. Fransted, J.R. Caram, D. Hayes, G.S. Engel, Two-Dimensional Electronic Spectroscopy of Bacteriochlorophyll a in Solution: Elucidating the Coherence Dynamics of the Fenna-Matthews-Olson Complex Using its Chromophore as a Control, J Chem Phys 127 (2012) 125101.

[3] M.C. Chang, A.J. Cross, G.R. Fleming, Internal dynamics and overall motion of lysozyme studied by fluorescence depolarization of the eosin lysozyme complex, J Biomol Struct Dyn 1 (1983) 299-318.

[4] M. Cho, G.R. Fleming, The integrated photon echo and solvation dynamics. II. Peak shifts and two-dimensional photon echo of a coupled chromophore system, J Chem Phys 123 (2005) 114506.

[5] D.C. Arnett, C.C. Moser, P.L. Dutton, N.F. Scherer, The first events in photosynthesis: Electronic coupling and energy transfer dynamics in the photosynthetic reaction center from Rhodobacter sphaeroides, J Phys Chem B 103 (1999) 2014-2032.

[6] G.S. Engel, T.R. Calhoun, E.L. Read, T.K. Ahn, T. Mancal, Y.C. Cheng, R.E. Blankenship, G.R. Fleming, Evidence for wavelike energy transfer through quantum coherence in photosynthetic systems, Nature 446 (2007) 782-786.

[7] E. Harel, G.S. Engel, Quantum coherence spectroscopy reveals complex dynamics in bacterial light-harvesting complex 2 (LH2), Proceedings of the National Academy of Sciences of the United States of America 109 (2012) 706-711.

[8] X.J. Jordanides, G.D. Scholes, G.R. Fleming, The mechanism of energy transfer in the bacterial photosynthetic reaction center, J Phys Chem B 105 (2001) 1652-1669.

[9] J. Prior, A.W. Chin, S.F. Huelga, M.B. Plenio, Efficient simulation of strong system-environment interactions, Phys Rev Lett 105 (2010) 050404.

[10] R.A. Miller, N. Stephanopoulos, J.M. McFarland, A.S. Rosko, P.L. Geissler, M.B. Francis, Impact of assembly state on the defect tolerance of TMV-based light harvesting arrays, J Am Chem Soc 132 (2010) 6068-6074.

[11] R.A. Miller, A.D. Presley, M.B. Francis, Self-assembling light-harvesting systems from synthetically modified tobacco mosaic virus coat proteins, J Am Chem Soc 129 (2007) 3104-3109.

[12] Y.Z. Ma, R.A. Miller, G.R. Fleming, M.B. Francis, Energy transfer dynamics in light-harvesting assemblies templated by the tobacco mosaic virus coat protein, J Phys Chem B 112 (2008) 6887-6892.

[13] X.J. Jordanides, M.J. Lang, X.Y. Song, G.R. Fleming, Solvation dynamics in protein environments studied by photon echo spectroscopy, J Phys Chem B 103 (1999) 7995-8005.

[14] D.J. Griffiths, Introduction to electrodynamics, 3rd ed., Prentice Hall, Upper Saddle River, N.J., 1999.

[15] G.R. Fleming, M.H. Cho, Chromophore-solvent dynamics, Annu Rev Phys Chem 47 (1996) 109-134.

[16] M. Cho, Two-Dimensional Optical Spectroscopy, CRC Press, Boca Raton, FL, 2009.

[17] M.J. Lang, X.J. Jordanides, X. Song, G.R. Fleming, Aqueous solvation dynamics studied by photon echo spectroscopy, J Chem Phys 110 (1999) 5884-5892.

[18] J.R. Caram, A.F. Fidler, G.S. Engel, Excited and ground state vibrational dynamics revealed by two-dimensional electronic spectroscopy, J Chem Phys 137 (2012) 024507.

[19] H. Zheng, J.R. Caram, P.D. Dahlberg, B.S. Rolczynski, S. Viswanathan, D.S. Dolzhnikov, A. Khadivi, D.V. Talapin, G.S. Engel, Dispersion-free continuum two-dimensional electronic spectrometer, Appl Opt 53 (2014) 1909-1917.

Chapter 4:

Mutations to *R. sphaeroides* Reaction Center Perturb Energy Levels and Vibronic Coupling but Not Observed Energy Transfer Rates

Adapted with permission from Flanagan ML, Long PD, Dahlberg PD, Rolczynski BS, Massey SC, Engel GS. J. *Mutations to* R. sphaeroides *Reaction Center Perturb Energy Levels and Vibronic Coupling but Not Observed Energy Transfer Rates*. J Phys Chem A (2016).

4.1 Abstract

The bacterial reaction center is capable of both efficiently collecting and quickly transferring energy within the complex; therefore the reaction center serves as a convenient model for both energy transfer and charge separation. To spectroscopically probe the interactions between the electronic excited states on the chromophores and their intricate relationship with vibrational motions in their environment, we examine coherences between the excited states. Here, we investigate this question by introducing a series of point mutations within 12 Å of the special pair of bacteriochlorophylls in the *Rhodobacter sphaeroides* reaction center. Using two-dimensional spectroscopy, we find that the timescales of energy transfer dynamics remain unperturbed by these mutations. However, within these spectra, we detect changes in the mixed vibrational-electronic coherences in these reaction centers. Our results indicate that resonance between bacteriochlorophyll vibrational modes and excitonic energy gaps promote electronic coherences and support current vibronic models of photosynthetic energy transfer.

4.2 Introduction

Photosynthetic organisms collect light with pigment-protein complexes and then funnel the energy to a reaction center for charge separation prior to downstream biochemistry that stores it in chemical form. This energy transfer can be extraordinarily fast and efficient, but it still is not fully understood.[1-5] Many studies have excited coherences between electronic and vibronic states and observed that such coherences can persist on the timescales of energy transfer, suggesting that coherent relaxation mechanisms may be important for energy transfer. It has been suggested that the protein creates a local environment protecting chromophores and coherences from external environmental fluctuations.[6, 7] Alternatively, the dynamics may be properties of the chromophores as the electronic states interact with vibrational motions of the chromophores themselves[8]. Bacteriochlorophylls are distinctive chromophores with multiple strong transition dipoles, established solvatochromatic dependence on their environment, and a complicated vibrational structure.[9, 10] Does the robustness of energy transfer come from the protein environment or is it intrinsic to the chromophore? To address this question, we first perturb the protein environment on the amino acid level, and then we specifically consider ramifications on the nearby chromophores. We present cryogenic two-dimensional electronic spectroscopy (2DES)[11-13] data for several mutants of the reaction center (RC) from *Rhodobacter sphaeroides*. Two amino acids near the special pair pocket are mutated to charged residues, and the cryogenic temperature narrows features so they are distinguishable. We present and analyze the resulting dynamics and coherences present in these complexes.

The connection between coherences and energy transfer is not yet fully understood. In 2DES, coherences have both electronic and vibrational origins[6, 8, 14-28]. For the sake of clarity, we will use the term vibronic to refer to any mixing between electronic and vibrational

degrees of freedom. At the most fundamental level, observed coherences report on how the electronic system interacts with the surrounding environment. The coherence lifetime indicates how well memory is preserved in the system. It is unclear how sensitive light harvesting dynamics to a specific amino acid sequence.[16, 29] Coherences act as a tool to characterize the changes to the environment due to these mutations. They allow us to correlate changes in the system-bath interactions to changes in transport dynamics.

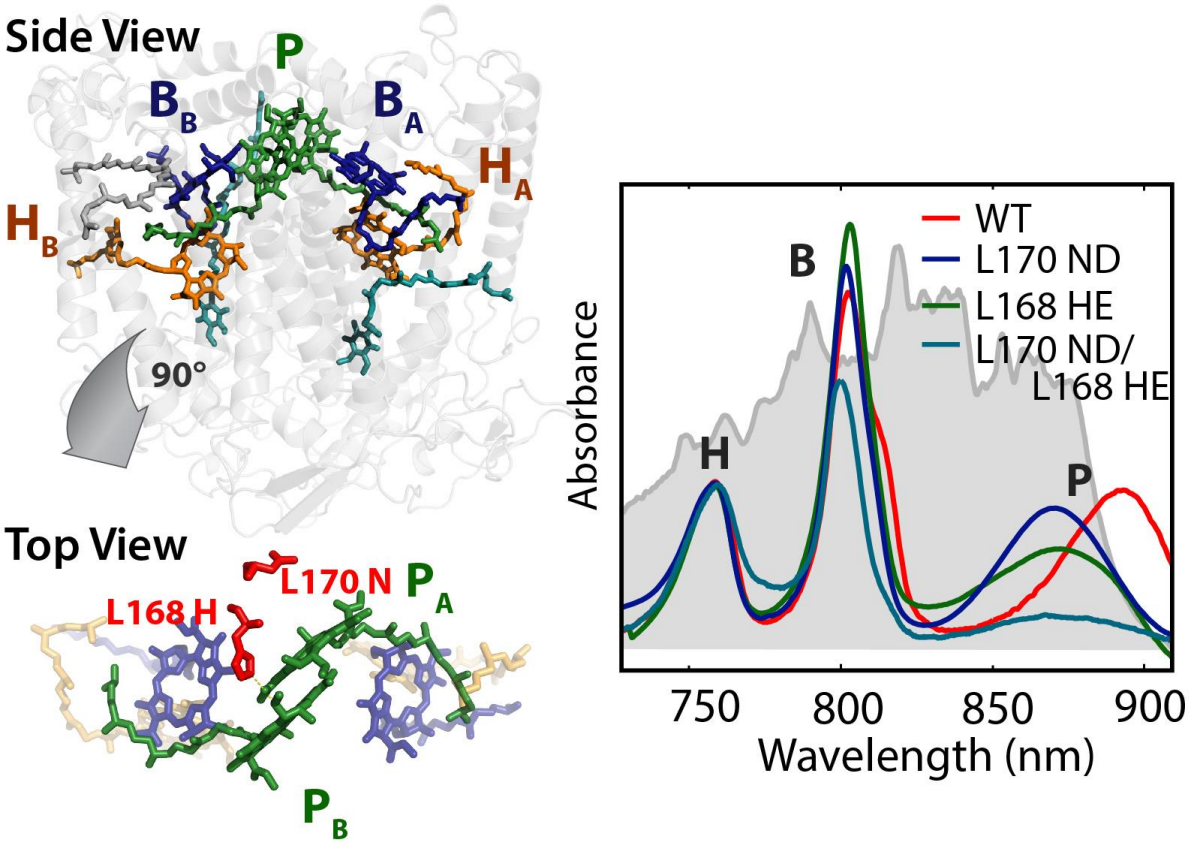

Figure 4.1: The *R. sphaeroides* Reaction Center complex mutants' structure and absorption spectra. The protein backbone contains the chromophores inside the matrix. With our bandwidth (gray shading), we can access the Q_y transitions of the two bacteriochlorophyll bands, B and P, and the bacteriopheophytin band, H. The absorption spectra of the wild type (WT) and three mutants (L170ND, L168HE, L170ND/L168HE) are shown. The mutations around the tightly coupled special pair (P) blue-shift the P feature.

In this work, we employ the RC as a model for energy transfer in a photosynthetic system. However, the RC exists *in vivo* primarily as the charge separation complex. We chose this complex because, in contrast to many light harvesting antenna complexes that have congested spectra involving many chromophores, the reaction center exhibits three well-separated absorption peaks in the far-red and near-IR electromagnetic spectrum termed P, B, and H (Figure 4.1). Energy transfer among these spectral bands has been well-studied.[2-4, 9] In this work, we alter the immediate environment around the special pair by amino acid point mutations. If the energy transfer and coupling between the chromophores depend on the amino acid contribution to the bath, we expect to see changes in rates or coupling to the environment with these mutations. We then further investigate the resonance between vibrational and electronic transitions to understand the design principles of solar light harvesting.

4.3 Methods

4.3.1 Sample Preparation

The wild-type and mutant reaction centers were poly-histidine-tagged and isolated from *R. sphaeroides* according to established protocols.[30] Cells were grown semi-aerobically at 31˚C, lysed by sonication, solubilized in 0.1% LDAO and purified with a Ni-NTA resin column, with a final buffer of 10 mM Tris, 0.1% LDAO, and 10 mM NaCl at pH 7.0. The sample was mixed to 50% glycerol, with a final OD of 0.3 at 800 nm in a 0.2 mm silanized quartz cell and quickly cooled to 77 K with an Oxford Instruments liquid nitrogen cryostat. Immediately before freezing, ~100 mM sodium ascorbate was added to all samples.

4.3.2 Spectroscopy

Two-dimensional electronic spectroscopy was performed as described in previous publications.[31, 32] Three beams are focused on a common point on the sample producing a signal in the phase-matched direction $k_s = -k_1 + k_2 + k_3$. For each 2D spectrum, the first time interval, the coherence time, is scanned from -0 to 200 fs at 4 fs intervals acquiring only the rephasing Feymann pathways. Waiting times were scanned from -100 to 1000 fs in 5 fs intervals. At the sample, each beam was 5-10 nJ/pulse, 8-12 fs in temporal length, and focused to a 90 μm beam-waist for all the experiments. A representative broadband laser spectrum is shown in Figure 4.1. All data is phased to separately acquired pump-probe data.[33] The broader bandwidth accesses more complete context for the observed dynamics. However, the broader bandwidth spectrum was achieved at cost to laser power stability (0.4% to 0.9% S.D./mean; 10 Hz), so replicate data for each sample with narrower bandwidth and more stable laser power (0.1-0.4% S.D./mean) is included to verify accuracy of our observations.

4.4 Results

4.4.1 Spectroscopy of Mutant Reaction Centers

The cryogenic linear absorption spectrum of each reaction center mutant is shown in Figure 4.1 with labeled P, B, and H peaks. Each spectrum in Figure 4.1 is normalized to the H peak because the bacteriopheophytins are least affected by our mutations. Each of the three peaks can be assigned principally to a pair of specific chromophores. The P, B, and H peaks are composed primarily of the special pair, accessory bacteriochlorophyll, and bacteriopheophytins respectively. These six chromophores are arranged in two nearly symmetric branches within the protein scaffold. Energy transfer occurs downhill in energy from H towards P.[9] The P and B peaks are each composed of two bacteriochlorophylls, yet the two bands absorb at different

frequencies. The strong coupling between the two closely spaced P chromophores creates strong excitonic mixing, and the geometry dictates that the lower energy band will carry the oscillator strength, giving rise to the strong red-shift of the P-band. The higher energy excitonic band of the special pair (P^+) absorbs weakly between 810-840 nm and appears as a slight shoulder on the B peak in the linear absorption spectrum.[3] Therefore, we attribute the differences in the intensity of the B peak in Figure 4.1 largely to changes in the P absorption due to mutation.

We study four reaction center variants: the wild type RC, RCs with one of two different point mutations, L170ND and L168HE, and a double mutant with both mutations. The L170ND mutation replaces an asparagine residue approximately 12 Å from the special pair with an aspartic acid. The L168HE mutation represents an even more drastic change, removing a hydrogen bond attaching the special pair to the protein. The special pair is where charge transfer in bacterial photosynthesis is initiated. These mutations are known to disrupt charge transfer in this complex and have been studied in this capacity previously[34]. In this work, the samples are in reduced conditions to minimize any long-lived charge transfer state and we investigate the effect of these perturbations on energy transfer and inter-pigment coupling. These mutations each blue-shift the P peak relative to the wild type (WT), but we do not see a significant red-shift of the P^+ band. The absorption spectrum of a chromophore tends to red-shift when its environment changes from solution to a protein cavity. The blue-shift in the mutants reveals a de-coupling of the special pair to the protein matrix[34] without significantly altering the coupling between the P chromophores. The broadening of the P absorption band, especially noticeable in the L168HE mutant and the double mutant, is consistent with an increase in heterogeneity across the ensemble implying that the special pair is somewhat destabilized without this hydrogen bond.

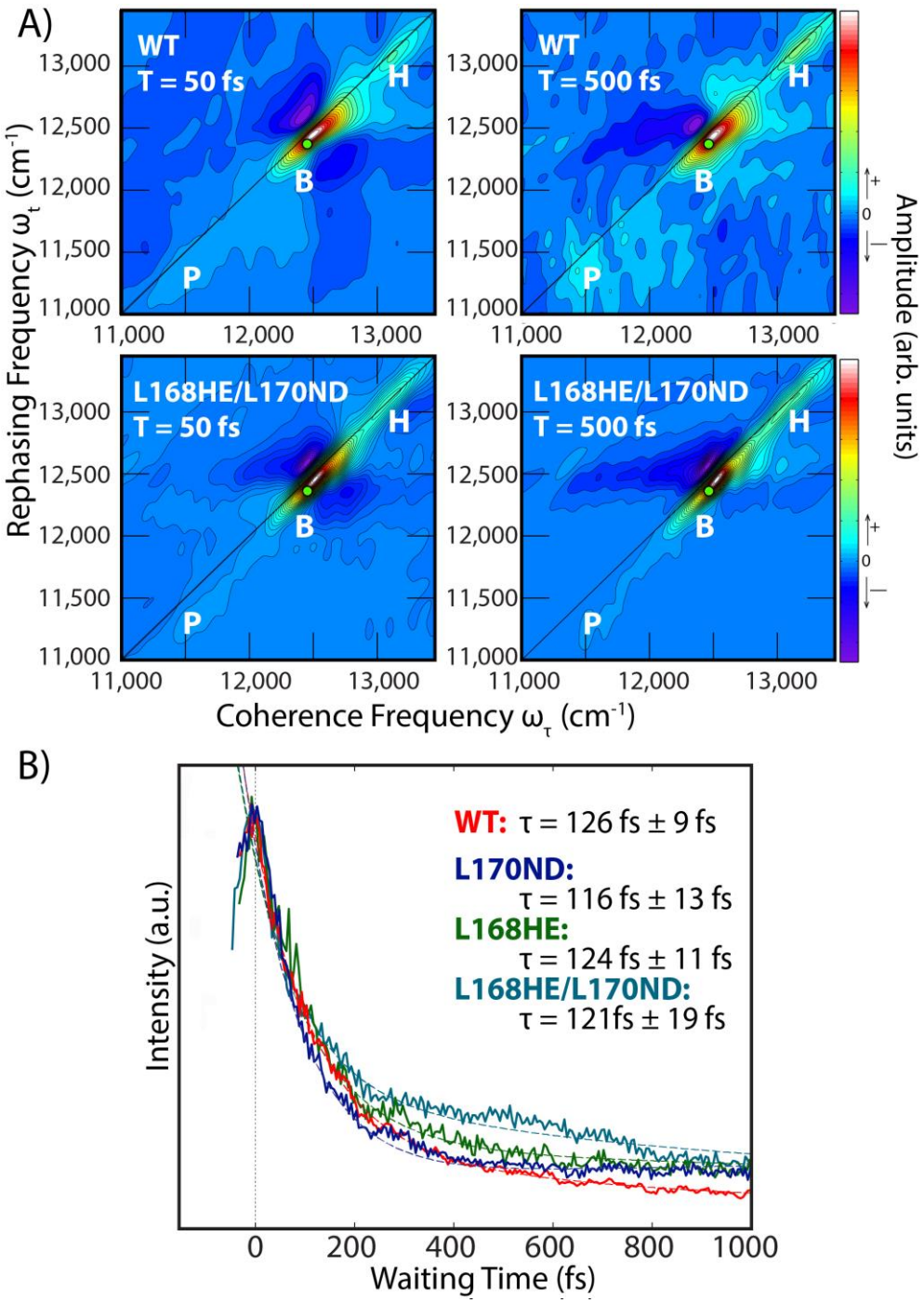

Figure 4.2: Rephasing 2DES and Dynamics of Mutant Reaction Centers**.** (a) Cryogenic rephasing 2D spectra of wild type and L168HE/L170ND mutant of the reaction center for waiting times T=50 fs and T=500 fs. The colormap for each spectrum is normalized to the maximum of that spectrum. The green circle marks the location the traces in panel b. (b) Waiting time traces of the B peak (green circle) for the WT and three mutants. Biexponential fits are shown as dashed lines for each waiting time trace. The dominant decay constant with one standard deviation is reported for each.

Representative broadband rephasing 2DES data for the WT and L170ND/L168HE double mutant at 77 K are shown in Figure 4.2a. Each spectrum is phased to pump-probe data and shows the real component of the data normalized to its own maximum. The laser bandwidth was sufficient to cover the majority of the P peak in the blue-shifted mutants, but only the red side of the band in the WT. In these spectra, the B and H peaks are apparent as diagonally elongated peaks. This diagonal elongation clearly illustrates inhomogeneous broadening of these bands.[35] Pigment-protein complexes tend to be inhomogeneously broadened because the protein environments are relatively static compared to the timescale of our measurements. The low amplitude P peak in the double mutant spectra is consistent with the weak transition in the linear absorption and the lower intensity on the red edge of the laser spectrum. The wild type spectrum shows the P feature is much rounder than the other peaks, which is consistent with the P state having the shortest lifetime.

4.4.2 Reaction Center Coherences

Several groups have reported coherences between the B and H excitons in the reaction center at both cryogenic and room temperatures.[6, 22, 36] However, the vibrational or electronic character of coherences across photosynthetic complexes is a subject of debate. Our data accesses the P exciton as well as the B and H, so we are able to compare coherence beating signals across a greater range of energies. In Figures 4.3, 4.4b, and 4.4c, we show the beating at the B/H and B/P crosspeaks (traces 1 and 3 respectively), as well as a location that is expected to be purely vibrational (trace 2). These are only representative traces. The entire data set is analyzed and the resultant beating maps of residual coherence signal are found in Figures 4.6 and 4.7. The traces are the residual of the signal in the waiting time domain after a double exponential fit is subtracted. Trace 2 shows a vibrational coherence associated with the accessory

bacteriochlorophylls at a known Raman mode, 730 cm^{-1}. Both traces 1 and 3 exhibit an expected vibrational mode, but also show an increase in amplitude with a fast decay. We believe that the short-time, high-amplitude signals that decay rapidly arise from a different source than the vibrational modes that persist at long times in agreement with previous studies on the reaction center and photosynthetic coherences[9, 17, 22, 24, 25]. Traces 1 and 3 both have two clear time components, a short time component and a long one. The large amplitude (3-5% of the signal) and fast decay in 100-200 fs in traces 1 and 3 are characteristic of electronic coherences, while the lower amplitude (1-2% of the signal) and long lifetime (greater than a picosecond) are characteristic of vibrational coherences. With spectroscopic data that includes excitation of more energetic vibrational modes, we can directly compare pure vibrational coherences and vibronic ones within the reaction center complex.

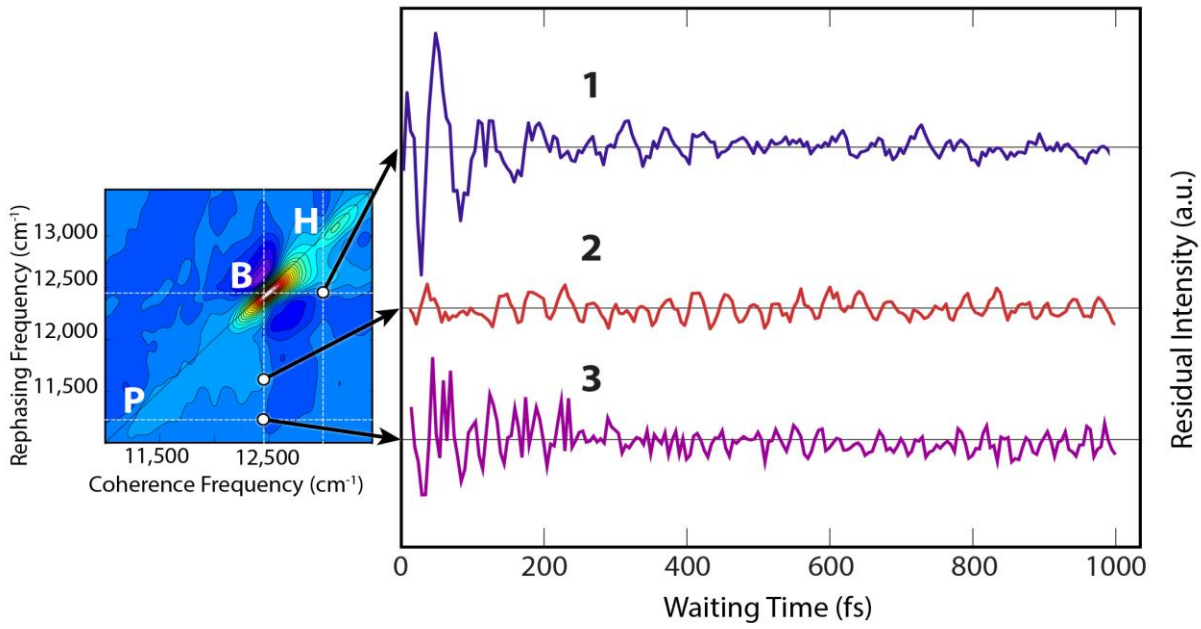

Figure 4.3: Coherence amplitude and decay rate enhancement at crosspeak locations. Three traces in waiting time are taken from the wild type 2D rephasing spectrum. Each trace is fit to a double exponential plus offset function and the residuals are shown above Exciton energies are highlighted with white dashed lines. Traces 1 and 3, which are located where an excitonic crosspeak would be, begin with a higher amplitude that quickly decays. Trace 2 is from a purely vibrational mode coupled to the B exciton. All residual traces are plotted to scale.

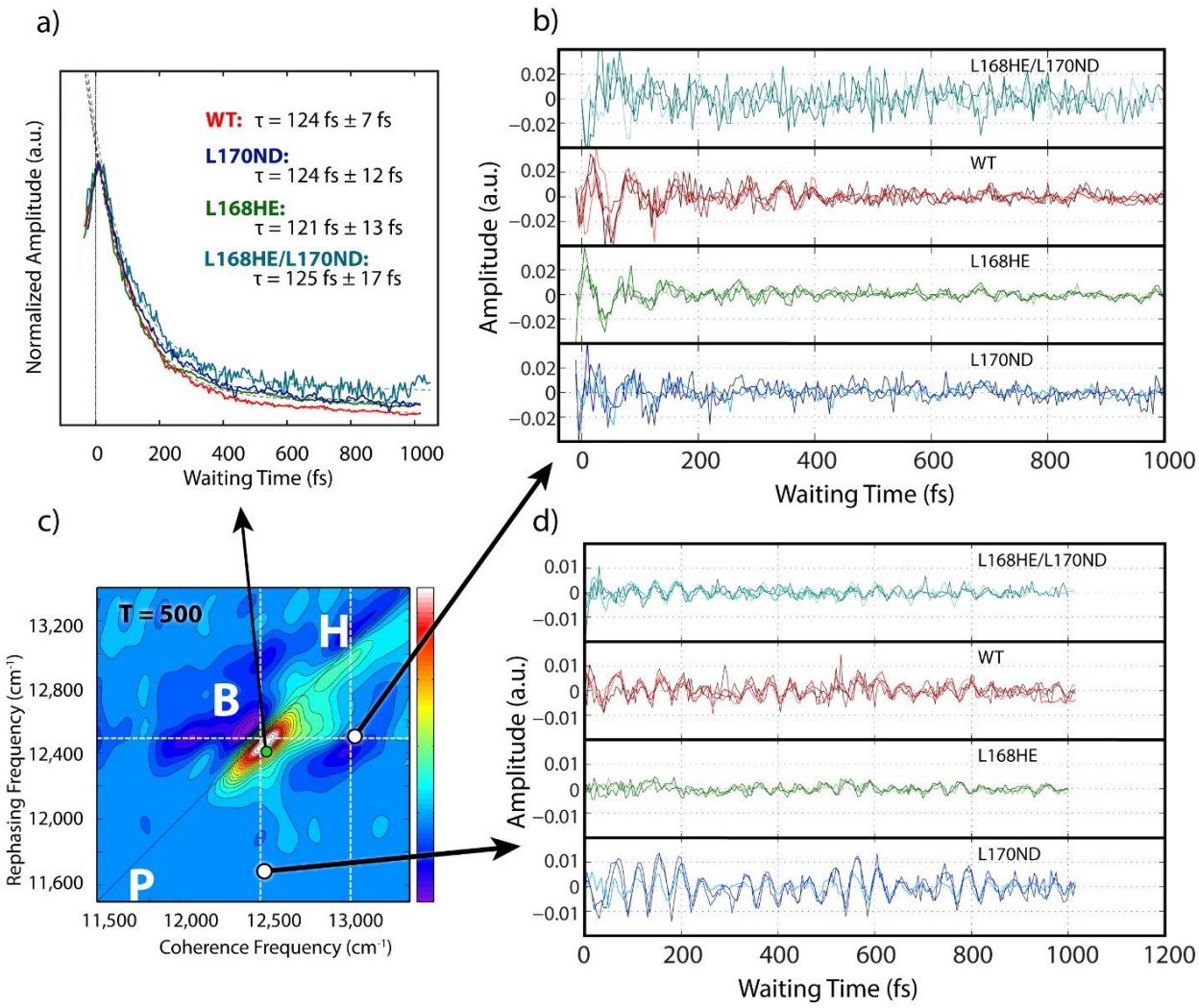

Figure 4.4: Dynamics and Coherences from narrow bandwidth laser spectrum. (a) Waiting time traces of the B peak (ω_τ = 12490 cm^{-1} and ω_t = 12470 cm^{-1}) for the WT and three mutants. The traces are the average of n=3 separate datasets. Biexponential fits are shown as dashed lines for each waiting time trace. The dominant decay constant with one standard deviation is reported for each. (c) 2DES spectrum at T=500 fs for the Wild Type reaction center with the narrow bandwidth excitation laser pulse. (b,d) Traces from the same locations as Figure 4.3 are shown for each RC sample. Each trace is fit to a double exponential plus offset function and the residuals are shown above. All residual traces are plotted to scale. Multiple traces are shown for each sample. These traces are from separate data sets taken on different days with different pulses. Traces from the B/H crosspeak location correlating to Trace 1 in Figure 4.3 are shown on the left. Traces correlating to Trace 2 in Figure 4.3 are shown on the right. This bandwidth did not extend far enough in the red to replicate Trace 3 in Figure 4.3.

4.5 Discussion

4.5.1 Energy Transfer Dynamics

Energy transfer between H, B, and P has been documented previously in the literature[2-4, 9]. Typically, energy transfer appears in a 2D spectrum as an off-diagonal crosspeak. Since the P peak has a relatively weak transition dipole and energy transfer from B to P is reported to be 115-200 fs,[3, 6, 37, 38] the crosspeak is barely visible above the noise as an elongated shoulder on the lower energy side of the B peak. Therefore, to look for differences in chromophore interactions, we need to extract the decay rates of the diagonal peaks in which the fast decay of B reveals population relaxation to P. A two-step global analysis was performed on the spectra in order to characterize the decay rates in the signal. In the first step each waiting time trace is fit to a double exponential with decay rates of 130 fs and 1000 fs plus an offset, based on rates reported in the literature[3]. In the second step we fit the decay rates, allowing for variation in the rates so we can compare mutant complexes to the wild type. The resulting decay rate spectra[39] are shown in Figure 4.5 and representative traces from one point (ω_τ = 12490 cm^{-1} and ω_t = 12470 cm^{-1}) on the B peak are shown in Figure 4.2b. The data show very similar decay constants centered around 125 fs across all four mutants and across the diagonal length of the peak, indicating that population transfer from B to P is robust and homogeneous. Since this decay constant closely matches previously reported values for B to P transfer, we attribute the short-time decay component to B to P transfers[3, 6, 37, 38].

The primary sequence modifications in the mutant proteins were designed to be disruptive. Both mutations are very close to the special pair and introduce distinct electrostatic environments. Therefore, the robustness of these results across samples is surprising. For these amino acid changes, the resulting decay rates are all within the margin of error of our

measurement. Energy transfer within this complex appears to be robust to mutation, and the protein scaffold is not delicately tuned to promote energy transfer. Interpreted through an evolutionary lens, this design makes sense: Biological systems are subject to constant perturbation and ideally, light-harvesting should be insensitive to common mutations and external influences[40]. We do not mean to say the protein has no impact on excited state dynamics, but only that these amino acid changes to environment do not manifest themselves as changes to transfer rates. The Fleming group reported similar results in transient absorption experiments of the reaction centers from *R. sphaeroides* and *Rb.capsulatus*[41]. The B-P energy gap is different in the two reaction centers, but surprisingly, the authors are unable to establish a significant change in the B-P transfer rate.

The observations are consistent with a few differing hypotheses. Either the protein environment has no effect on the excited state dynamics in this complex and the observed dynamics are simply uncoupled from the protein, or the dynamics do rely on some aspect of coupling to the environment but the complex is built to withstand this large primary sequence perturbation. Considering that a protein is a relatively static and structured solvation environment and that extensive experimental evidence exists for electronic-vibrational coupling in pigment-protein complexes, we believe the first explanation is unlikely. Rather, we postulate that the complex's efficiency is well buffered against environmental changes. This hypothesis is consistant with prior results for the FMO complex[29].

In 2012, Kreisbeck and Kramer investigated the effect of different spectral densities on dynamics in the FMO complex[17]. They found that the continuum component of the spectral density seems to greatly affect the dynamics; indeed, they only needed three explicit peaks in the function to reproduce FMO's behavior. This work suggests we can separate the bath into two

components: the overdamped protein environment and a few underdamped vibrational frequencies. Chin et al. in 2013, Tiwari, Peters, and Jonas in 2012, and Christensson et al. in 2012 have come to similar conclusions regarding the distinction between intrapigment vibrations and the protein environment. Bacteriochlorophyll has a complex vibrational structure that has been extensively studied, so we next look to see if the vibrational structure in the excited state-environment could help explain the persistence of fast and efficient transfer[10, 14, 42-44].

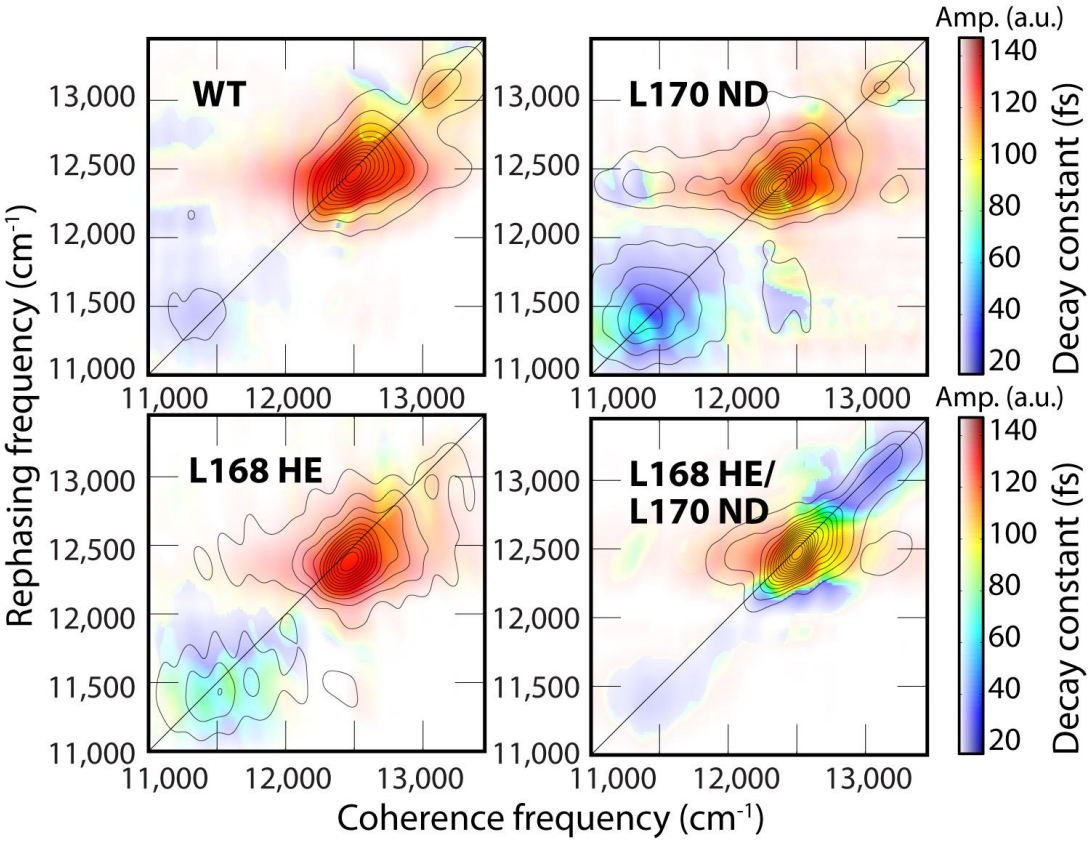

Figure 4.5: Decay Associated Spectra for wild type (WT) and mutant RCs. Each set of 2D data was subject to a biexponential global analysis. The waiting time trace for each pixel is fit to a function of the form $y = A_1 \exp\left(\frac{T}{130}\right) + A_2 \exp\left(\frac{T}{1000}\right) + A_3$. The resulting parameters are then used as inputs and the rate constants (initially 1/130 and 1/1000) are allowed to vary. The result is a short (under 140 fs) and a longer lifetime (greater than 800 fs). The shorter lifetime is plotted for each RC sample in this figure.

4.5.2 Vibrational Coupling

Recently, several groups have proposed vibronic models in which resonance and mixing between electronic energy gaps and vibrational modes are explicitly important in promoting the speed and efficiency of photosynthetic functions.[15, 18, 21, 22, 27, 45-49] The vibronic models propose some amount of mixing between the electronic and vibrational modes. If the vibrational contribution is included explicitly in the Hamiltonian, the result is a vibronic basis set defining states of the system. This can be used to explain energy differences and complicated excited state dynamics. Alternatively, the vibrational modes may be included as part of the bath. In this family of model, the vibration manifests as a peak in the spectral density function representing the bath, not the continuum. Both of these models are able to explain preserved and enhanced coherence signatures and energy transfer behavior, and they also depend on vibrational modes coupled to the electronic transition.

In Figure 4.3, we compare the residual beats from locations on the 2D map we expect to be pure vibrational coherences to residual beats from locations where an electronic coherence might occur (crosspeak locations). In each of the crosspeak residual traces, the frequency of the beat matched both the excitonic energy gap as well as the Raman mode expected at that location on the 2D map. However, at exciton crosspeak locations the signal has two clear time components; it has increased amplitude and decay times under 200 fs (Traces 1 and 3 in Figure 4.3 and 4.4b) and a component with a lifetime over 1000 fs. The long time component closely resembles purely vibrational signals seen in the data (Trace 2 in Figure 4.3 and 4.4d). This long lifetime suggests some amount of vibrational-electronic mixing is responsible for the nature of the quantum beats at crosspeak locations and enhancing the signal at this frequency. In both Tiwar i et al. and Chin et al. coherence enhancement and energy transport depend on the

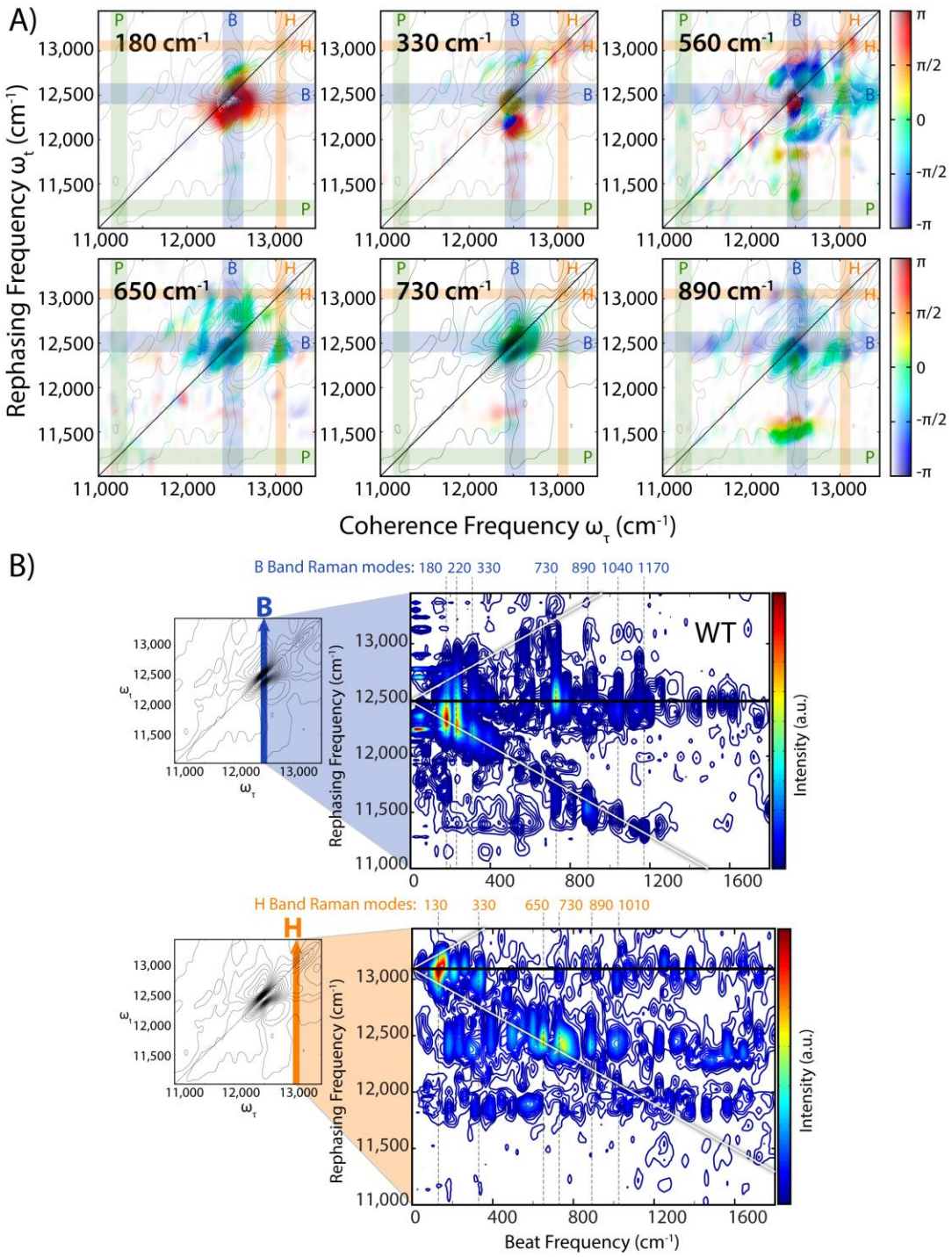

Figure 4.6: Power spectra reveal vibration-exciton coupling. A) The Fourier magnitude and phase for six frequencies are plotted on the 2D map. The color of the heatmap indicates phase in radians, while the intensity of the peak corresponds to magnitude. Contour lines from the 2D spectra are shown. The transparent bars highlight energies of the P, B, and H exciton energies. B) Power spectrum slices through rephasing frequencies at the B and H site energies for the wild type reaction center. The solid black line in each spectrum indicates the energy that the slice was taken, while the white lines represent expected vibrational peak locations.

existence of a dominant vibrational mode resonant with the electronic transition[25, 50]. Therefore, we interpret the observation of enhanced coherences in our data as indirect evidence of the importance of an underdamped, resonant vibration coupled to the electronic states involved in excitonic energy transport. The frequency, and dephasing time of these coherences depend on the environment, so we next use these coherences to investigate changes in the system-bath coupling when the protein is mutated.

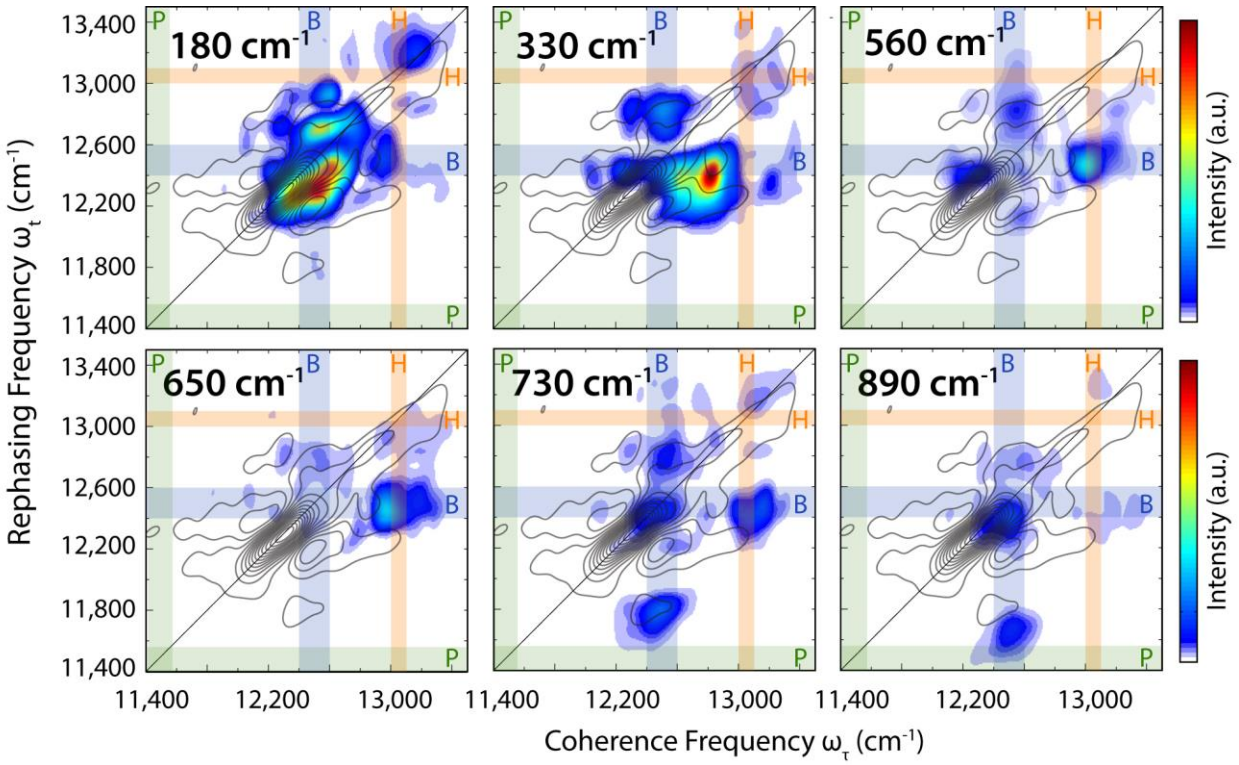

Figure 4.7: Beat Map for WT Reaction Center using narrow laser bandwidth. The power spectrum amplitudes for the six frequencies in Figure 4.6a are plotted on the rephasing 2D map for some of the observed modes. The transparent bars highlight energies of the P, B, and H exciton energies.

Resonance Raman studies have shown that the different chromophores within the reaction center have different Raman spectra.[2, 10] Bacteriochlorophyll and bacteriopheophytin have many vibrational modes below 1200 cm^{-1}, the range accessible by our broadband laser

pulse with excitation at 800 nm. Raman spectra from excitations of the B, P, and H bands show that some vibrational modes may be common to multiple excitons, but it is difficult to separate these modes to understand if they are delocalized modes or simply modes with similar frequency. Indeed, each waiting time trace through the spectrum shows signatures of many beating frequencies. The relative enhancement of beating signals from the various vibrational modes is markedly different depending on the immediate environment.[14] In the reaction center, the protein and the coupling provide very specific environments for the chromophores, so we expect the vibrations that couple to each exciton will not be identical. The vibrational spectrum within the 2DES spectra reveals which modes are enhanced in each exciton in this complex. Figure 4.6a presents the magnitude and phase of the known bacteriochlorophyll vibrational modes 180, 330, 560, 650, 730, and 890 cm^{-1} mapped across the 2D spectra.[7, 19, 42, 43, 51, 52] Contour lines from the 2D spectrum are overlaid on the maps for clarity. The 730 and 890 cm^{-1} modes show notable beating below the diagonal. In 2012, Butkus et al. theorize that vibrational crosspeaks should beat out of phase with the diagonal peak, while crosspeaks due to electronic coupling should be in phase with the diagonal peak. In experiments, many groups have reported phase shifts closer to $\pi/2$ radians in electronic coherences[6, 23, 24, 53]. Through this lens, the 730 cm^{-1} mode below the B exciton is vibrational, while the 890 cm^{-1} mode oscillates $\pi/2$ radians out of phase with the diagonal peak indicating electronic origins. The 730 cm^{-1} mode is clearly present on the H peak in addition to the B exciton. The 650 cm^{-1} mode also appears on the H exciton. The lower energy modes are stronger in intensity, consistent with Raman studies.[10, 42, 43] Consistent with previous reported data, the 180 cm^{-1} mode is the strongest in both bacteriochlorophylls and bacteriopheophytins. Additionally, the 890 cm^{-1} mode is stronger in the accessory bacteriochlorophylls and the 730 cm^{-1} in both the B and H excitons,

while the 650 cm^{-1} mode is assigned to the bacteriopheophytins. These data lead us to conclude that the long-lived vibrational oscillations are properties of the pigments themselves, and not of the protein structure, in agreement with previous experiments.

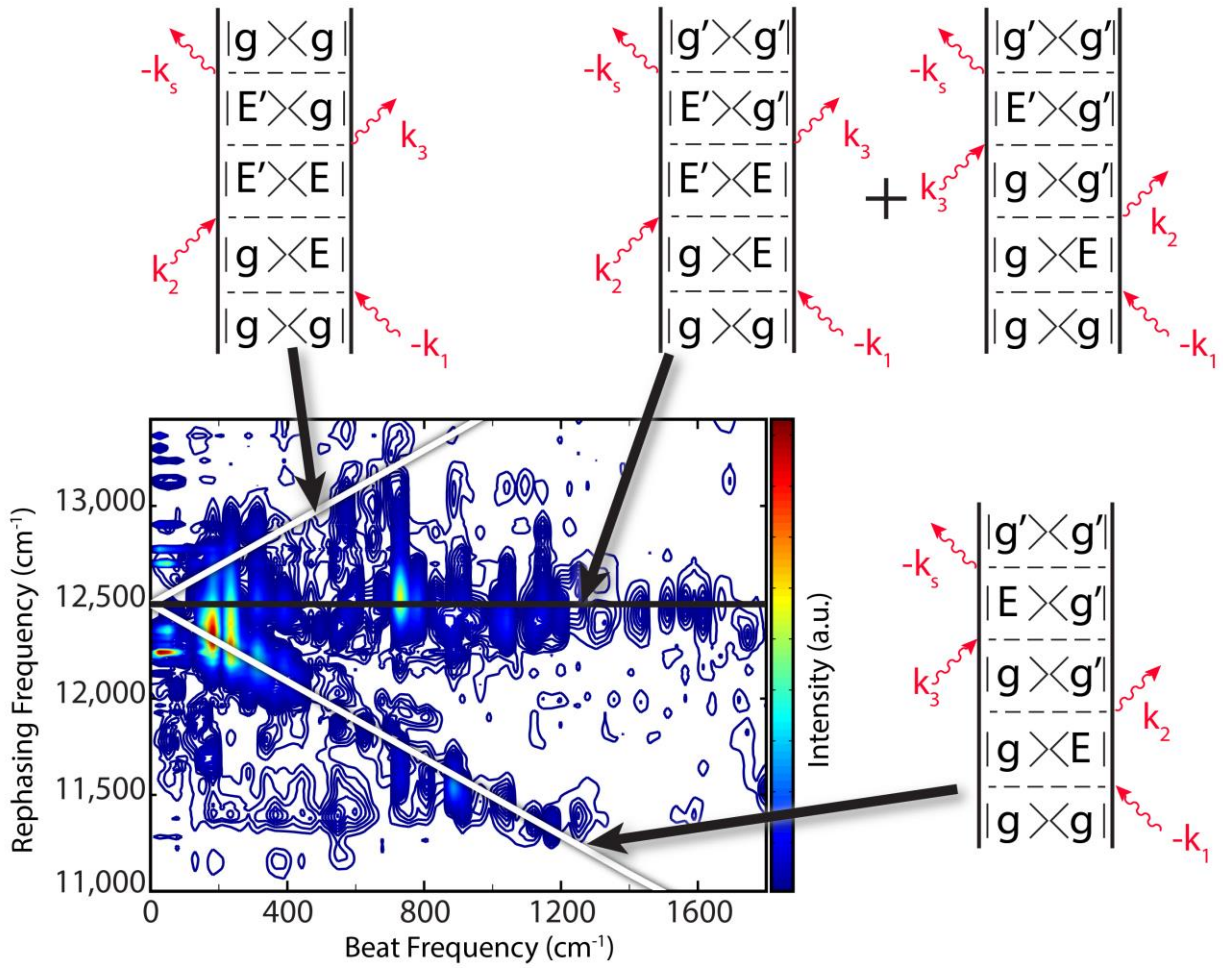

Figure 4.8: Feynman Diagrams associated with beating within 2D rephasing spectra of the Reaction Center. The WT power spectra of beating along the B band from Figure 4.6 is reproduced here for clarity. The Feynman pathways that describe peaks that fall on each line are shown for the black and white lines. In these, 'g' is the ground state, 'E' is an electronic excited state, and a prime, g' or E' indicates a hot vibrational state of energy ω on that electronic state.

In Figure 4.6b, the power spectra for vertical slices through the datasets are shown for both the H and B band. The top power spectrum slice at ω_τ=12,500 cm^{-1} (Figure 4.6b, top) corresponds to the frequency of the B band and the lower power spectrum corresponds to the H

band frequency, ω_τ=13,100 cm^{-1} (Figure 4.6b, lower). The solid black line through the power spectrum marks the rephasing frequency that equals the coherence frequency of the slice. In other words, data on the black line represents the power spectrum of the beating at the point where the slice crosses the main diagonal of the 2D spectrum. The solid white lines marks the region within the power spectrum where beating above/below the diagonal of the 2D spectrum matches the energy gap corresponding to the difference between the coherence and rephasing frequencies. For example, the 730 cm^{-1} beating feature below the diagonal peak in Figure 4.6a is the same as the contour peak at 730 cm^{-1}, 11,770 cm^{-1} on the white line in the B band power spectrum (Fig. 4.6b, upper). The dashed lines mark some of the expected modes from Cherepy et al. Resonance Raman studies.[42] In this spectrum, most of the prominent features fall on either the black or white lines.

While the beating occurs throughout the spectrum, previous work has shown that vibrational and vibronic coherences appear primarily on the main diagonal as well as above, below and to the right of the diagonal peak on a rephasing two-dimensional spectrum.[23, 54-58] As shown in Figure 4.8, the power spectrum of the beating at every point along the ω_τ=12,500 cm^{-1} (B band) slice shows beating arising from distinct rephasing Feynman diagrams. These diagrams assist in assigning beats to the ground and excited state surfaces as well as examining intensity patterns for signs of enhancement due to vibronic coupling. In fact, each Feynman pathway shown in Figure 4.8 contains exactly two transitions that involve a Franck-Condon factor leading to simple hypothesis that the transitions should be equally strong. Instead, we observed stronger beating on the white line than on the black line when the vibrational mode is coincident with an electronic energy gap. To clarify this observation, the power spectrum along

each on these lines is plotted in Figure 4.9 for the wild type and each mutant reaction center. In the wild type power spectra corresponding to the black line in Figure 4.8 (B exciton) shows a strong mode at 730 cm^{-1}, but any modes at 890, 1040, or 1180 cm^{-1} are indistinguishable from noise. However, the power spectra from the lower white line in Figure 4.8 (the crosspeak locations) shows clear peaks at 890, 1040 and 1170 cm^{-1}. The beating signatures can be affected

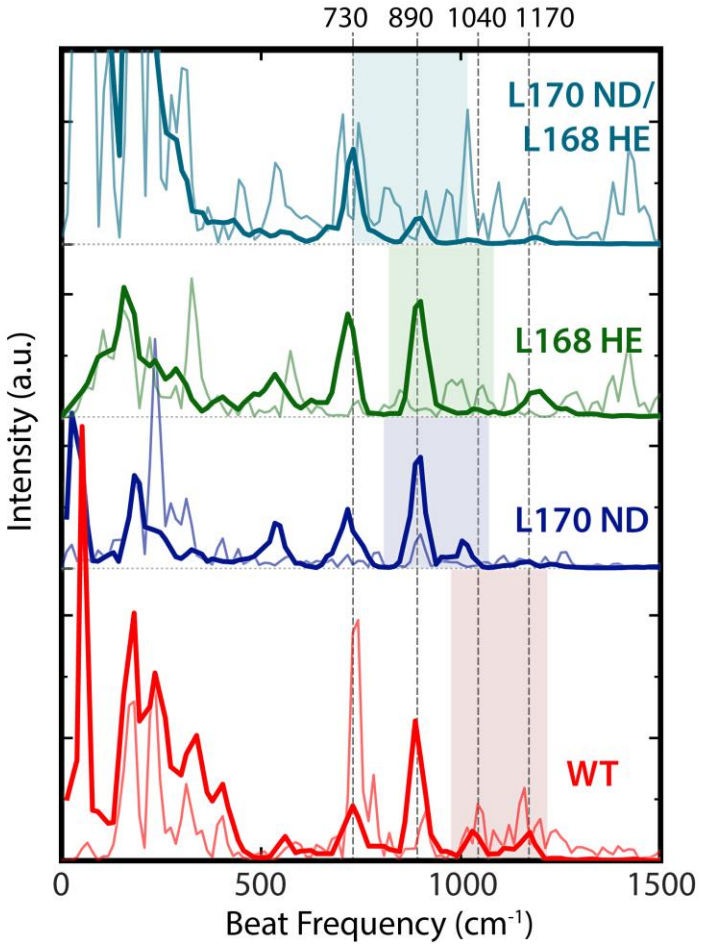

Figure 4.9: Power spectra of beating in mutant *R. sphaeroides* show changes in vibronic coupling with perturbations to P band transition energy. Two power spectrum slices are shown for each mutant reaction center. The fine lines show beating of the diagonal feature corresponding to the B exciton (equivalent to the horizontal black line in Fig 4.6). The thick lines are power spectra of beating below the B exciton where the beat frequency matches the gap between ω_τ and ω_t (equivalent to the lower diagonal white line in Fig 4.6). The shading illustrates the energy gap in each wild type or mutant reaction center.

by the laser excitation spectrum and compression[59]. The high-energy vibrational modes are more dependent on the laser power at the edges of the spectrum. These spectra all result from excitation of the B exciton, but excitation of the vibrational modes and detection on the white line in Figure 4.8 greatly depend on the red edge of the spectrum. Similar analysis for the mutant reaction centers is shown in Figure 4.10. Therefore, definitive assignment of the mechanism requires further measurements, but the coincidence between the Raman modes and the excitonic energy gaps along with the enhanced amplitude of beating modes coincident with excitonic cross peaks strongly suggests a vibronic origin over purely vibrational or electronic beats.

The power spectra for the mutant RCs shown in Figures 4.9 and 4.10 support the theory of vibrational and electronic state mixing as well, and offer an explanation for the lack of change in energy transfer between mutants. Each of the mutant samples has a blue-shifted P peak relative to the WT, and therefore, a different excitonic energy difference between B and P. These mutants have the same vibrational progression below the B diagonal peak, but the higher frequency modes, 1040 and 1170 cm^{-1} are weaker or missing, while the 730 and 890 cm^{-1} appears stronger in the power spectra. The power spectra follow the pattern set by the wild type; each of the peaks along the white line power spectrum that is resonant with the electronic transition is missing from the corresponding black line spectrum. However, the mutants do not have the 730 cm^{-1} peak in the black line spectrum that the wild type has, implying that the nature of the 730 cm^{-1} vibrations in the mutants is different than the wild type. This result is interesting because it supports the view that coherence and fast energy transfer do depend on the existence of a vibrational mode that is resonant with the electronic energy gap. Bacteriochlorophyll has enough strong vibrational modes at low energies that the electronic transitions coupled to different vibrations in the mutants than in the wild type.

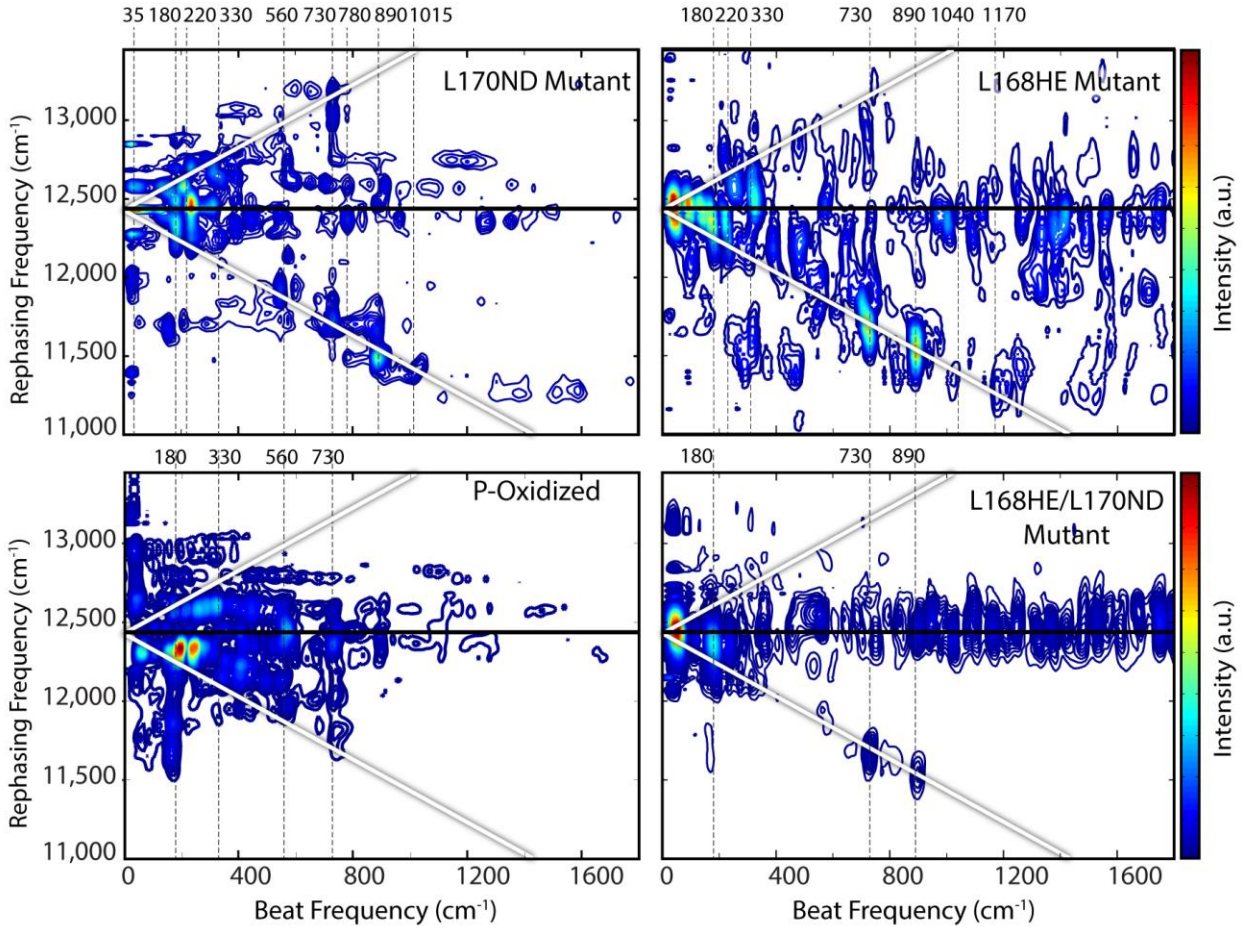

Figure 4.10: Full power spectra of beating in mutant *R. sphaeroides* show changes in vibronic coupling with perturbations to P band transition energy. Power spectrum slices along rephasing frequencies at the B band transitions (ω_τ=12,490 cm^{-1}) energies for each mutant and the P-oxidized reaction center. The solid black line in each spectrum indicates the energy that the slice was taken, while the white lines represent expected vibrational peak locations. The P-oxidized data was taken with the narrow bandwidth laser, so we can't detect the presence of any features on the red side (bottom) of the plot or vibrations at high energy such as the 1040 or 1170 cm-1 modes. The mutant spectra were all taken with the broad bandwidth. The mutant and P-oxidized RCs have the similar vibrational modes below the B band energy, but the higher frequency modes, 1040 and 1170 cm^{-1} are weaker or missing, while the 890 cm^{-1} appears stronger in the power spectra.

4.6 Conclusion

We perturbed the immediate environment around the special pair chromophores by point mutations to the protein in the vicinity. We do not observe significant changes in the time scales associated with B to P energy transfer with these perturbations though we do observe large spectral changes. Therefore, we conclude that the primary structure of the protein is not finely tuned to promote energy transfer in the reaction center; this observation does not run counter to the evolutionary pressure on this complex for charge separation rather than light harvesting. In this complex, the protein simply provides the environment that determines each chromophore's site energy and coupling to other chromophores. In other words, the protein determines the excitonic energy gaps. As long as there is a vibrational mode degenerate with this energy gap, coherences and vibronic mixing appears to be enhanced. For example, when bacteriochlorophyll had vibrations that matched the new B/P energy gap in the mutant RCs and vibronic mixing occurred with the 730 and 890 cm^{-1} modes instead of the 1040 and 1170 cm^{-1} modes. Because of the existence of a weak P+ state due to exciton Davydov splitting, often assigned to a 810 nm slight shoulder on the B peak absorption (Figure 1), it is also likely that energy transfer may occur through coupling to the P+ state and therefore, independent of the B-P energy gap. However, we prefer the model described in this work for its simplicity in conserving energy and because we observe changes in the strongly coupled vibrational modes as the B-P energy gap changes, an observation not explained by the B→ P+ energy pathway (Figure 6).

The mutants RCs explored in this study differ in one or two amino acids in close proximity to the special pair. The resulting dynamics prove to be robust to these mutations. Evolutionarily, this robustness could be an advantage since light harvesting would easily survive mutations to the genome. Alternatively, the evolutionary pressure on this complex is related to

charge separation rather than energy transfer so it remains possible that such finely tuned mechanisms are operative but simply not in this complex This persistence of B dynamics despite changes in the P exciton supports the notion that resonance between vibrational modes and excitonic energy differences is important in this fast energy transfer. The accessory bacteriochlorophylls exhibit a progression of strong vibrational modes from 730 to 1170 cm^{-1} meaning that it has the array of vibrational modes to resonate with a range of excitonic energy gaps. The chromophore itself is adaptable to changes in the exciton energies.

Bacteriochlorophyll on its own does not exhibit strong vibrational coherences in 2DES,[60] but in a protein it shows a distinctive vibrational structure. In this study, we show a very clear map of which vibrations are enhanced in the reaction center, consistent with resonance Raman data in the literature.[10, 42-44] This map strikingly emphasizes that vibrations appear in the same locations as exciton crosspeaks. A detailed analysis of the beats present on- and off-crosspeak locations reveals a fundamental difference in the nature of vibrational coherences when they coincide with an excitonic energy gap. At a crosspeak location, these coherences clearly exhibit both electronic and vibrational characteristics. This coincidence significantly supports the vibronic hypothesis that it is the resonance and mixing between the two modes that prolongs the coherences. It is both the protein's effect on the site energy of each exciton as well as inherent properties in bacteriochlorophyll that contribute to this robust phenomenon in the bacterial reaction center.

4.7 Viewing this work in the context of Electronic Coherences and Coherent Energy Transfer

Efforts to describe photosynthetic energy transfer in terms of Förster resonance energy transfer (in which coupling between electronic states of the chromophores is very weak) or in terms of Redfield relaxation theory (in which coupling between electronic states is very strong relative to coupling to the environment) have not succeeded in replicating the speed and efficiency of observed photosynthetic energy transfer[61-67]. Photosynthetic energy transfer occurs in a regime in which none of the energetic couplings vastly overwhelms the rest; rather, coupling between chromophores is roughly the same as site disorder and coupling to the bath and site disorder [64-66, 68]. Therefore, it has been difficult to develop a useful theory of how this energy transfer occurs and by what mechanism. Similar to most biological processes, photosynthetic energy transfer persists in a delicate balance. In this case, the balance can be described between inter-pigment coupling and exchange with the environment, or between electronic coherence and dephasing from fluctuations in the environment [62, 63]. It has been suggested that these pigment-protein complexes have evolved to exploit subtle quantum-mechanical effects to protect and enhance this careful balance, and that intra-complex energy transfer in governed by intermediate coherent resonance energy transfer in which energy migrates as a quantum random walk[6, 16, 37, 50, 62-66, 68].

In 2007, Engel et al. reported in *Nature* direct observation of long-lived electronic coherences using 2DES in the Fenna-Matthews-Olson (FMO) complex, a photosynthetic complex from *Chlorobium tepidum.*[16] Electronic coherences are expected in spectroscopies employing short and broadband laser pulses. However, these coherences were lasting hundreds rather than tens of femtoseconds, as had been predicted, and therefore, the coherences persist on

the same time scale as energy transfer. Engel et al. suggest that these electronic coherences are evidence of coherent, or wave-like energy transfer making this one of the first examples of experimental evidence of mid-regime coherent resonance energy transfer.[16] The important questions raised by this report are 1) are the quantum beating signals indeed due to long-lived electronic coherences? and 2) How are the electronic coherences preserved for such long timescales and protected from fluctuations in the environment? The first of these two questions has led to a heated debate over the origin of quantum beating in 2DES of photosynthetic complexes.

No theory can be generally accepted unless the experimental evidence can be verified and all other possible explanations can be ruled out. 2DES is useful for observing electronic coherences, but it is difficult to definitively distinguish between electronic coherences and vibrational coherences on the ground state. Ground state vibrational coherences are not evidence for coherent energy transfer, so accurate assignment is essential if coherences are to be viewed as evidence of wave-like energy transfer. Therefore, a lively debate over this distinction has followed the 2007 report in *Nature*.[5, 16, 68-71] Theoretical studies have made a few predictions for distinguishing the origin of quantum beating in 2DES data: 1. in general, electronic coherences are expected to be greater in initial amplitude and dephase in about one hundred femtoseconds, while vibrational coherences should have a smaller amplitude but persist for at least a picosecond. However, this very distinction is the one that the evidence in Engel et al. contradicts [72, 73]. 2. Electronic coherences, vibrational coherences on the ground state and vibrational coherences on the excited state all appear in specific, and predictable locations on the 2D map. These locations also differ predictably between rephasing signal and nonrephasing signal, so by analyzing the two signals separately and comparing the appearances of beatings,

one can infer the origin of coherences[50, 55, 74]. 3. Vibrational coherences should exist between dipoles in the same orientation while electronic coherences should vary in dipole orientation. Spectroscopists have exploited this by using pulses with opposite polarizations to select out purely electronic coherences [75]. 4. Vibrational coherences reveal vibrations that are also revealed in Resonance Raman spectroscopy. Therefore, a quantum beat at a frequency absent in the corresponding Raman spectrum can be excluded from being a ground state vibrational mode. However, chlorophylls have intricate vibrational structure and it is difficult to find a frequency that is entirely absent from the Raman spectrum.

Since 2007, electronic coherences have been reported in FMO, light harvesting complex 2 (LH2) and the reaction center (RC) from purple bacteria, light harvesting complex II (LHCII) in higher plants and algae, and small molecules, as well as equally as many arguments that said coherences are purely vibrational[6, 24, 36, 76-81]. 2DES polarization experiments and detailed analyses have begun to lead researchers to suggest that beating signals are often vibronic, or with mixed vibrational and electronic character to varying degrees[8, 12, 15, 18, 19, 26, 27, 47-49]. While this settled the debate between vibrational and electronic coherences, it did nothing to help explain the mechanism of coherent energy transfer [82].

The work presented in this chapter does not address the controversy as to the origin of coherences. In this study, we observe vibrational and vibronic coherences and use these signals to understand the interaction between electronic states and their environment instead of contribute to the debate over electronic coherences and their role in coherent energy transfer. That is, enhancement of amplitude and dephasing time of coherences report on the interaction between the electronic states and the environment [50, 82, 83]. We can use coherences as probes of the chromophore-environment interaction to lay out the effect of mutations on this

relationship. Originally, the experiment was designed hoping to answer the second question laid out above: How are the electronic coherences preserved for such long timescales and protected from fluctuations in the environment? The careful balance between inter-pigment coupling and bath fluctuations of photosynthetic energy transfer suggests some fine-tuning of the protein structure surrounding the chromophores. Thus, the series of mutations around the special pair of bacteriochlorophylls in this study was chosen in an attempt to break the coherences or energy transfer. Electronic coherence has been reported between the B and H excitons, and it was likely, the same would be evident between B and P when the laser bandwidth was increased to capture the P exciton[6, 36]. If the apo-protein is protecting and prolonging the electronic coherences for coherent energy transfer, mutating the correct amino acids responsible for this protection should result in a change in the observed beating pattern in 2DES. However, instead of observing strong electronic coherences, we were unable to definitively assign the enhancement of amplitude seen at crosspeaks to purely electronic origin. Instead, we used the available vibrational coherences to probe and understand the interaction between electronic states and its environment and the dependence on the primary protein structure.

4.8 Acknowledgments

We thank JoAnn Williams for providing the WT and mutant bacterial strains. The authors would also like to thank MRSEC (DMR 14-20709), the DARPA QuBE program (N66001-10-1-4060), AFSOR (FA9550-09-1-0117), the Camille and Henry Dreyfus Foundation, and the Searle Foundation for supporting the work in this publication. P.D.L. acknowledges support from the DOE-SCGF program. S.C.M. acknowledges support from the Department of Defense (DoD) through the National Defense Science & Engineering Graduate Fellowship (NDSEG) Program.

P.D.D. acknowledges support from the NSF-GFRP program, and M.L.F. and P.D.D. were supported by the National Institute of Biomedical Imaging And Bioengineering of the National Institutes of Health under Award Number T32-EB009412.

4.9 References

[1] H. van Amerongen, L. Valkunas, R. van Grondelle, Photosynthetic excitons, World Scientific, Singapore ; River Edge, N.J., 2000.

[2] D.C. Arnett, C.C. Moser, P.L. Dutton, N.F. Scherer, The First Events in Photosynthesis: Electronic Coupling and Energy Transfer Dynamics in the Photosynthetic Reaction Center from Rhodobacter sphaeroides, The Journal of Physical Chemistry B, 103 (1999) 2014-2032.

[3] X.J. Jordanides, G.D. Scholes, G.R. Fleming, The Mechanism of Energy Transfer in the Bacterial Photosynthetic Reaction Center, The Journal of Physical Chemistry B, 105 (2001) 1652-1669.

[4] D.Y. Parkinson, H. Lee, G.R. Fleming, Measuring Electronic Coupling in the Reaction Center of Purple Photosynthetic Bacteria by Two-Color, Three-Pulse Photon Echo Peak Shift Spectroscopy, The Journal of Physical Chemistry B, 111 (2007) 7449-7456.

[5] G.D. Scholes, G.R. Fleming, A. Olaya-Castro, R. van Grondelle, Lessons from nature about solar light harvesting, Nat Chem, 3 (2011) 763-774.

[6] H. Lee, Y.-C. Cheng, G.R. Fleming, Coherence Dynamics in Photosynthesis: Protein Protection of Excitonic Coherence, Science, 316 (2007) 1462-1465.

[7] D.B. Turner, R. Dinshaw, K.-K. Lee, M.S. Belsley, K.E. Wilk, P.M.G. Curmi, G.D. Scholes, Quantitative investigations of quantum coherence for a light-harvesting protein at conditions simulating photosynthesis, Physical Chemistry Chemical Physics, 14 (2012) 4857-4874.

[8] N. Christensson, H.F. Kauffmann, T. Pullerits, T. Mancal, Origin of Long-Lived Coherences in Light-Harvesting Complexes, J Phys Chem B, 116 (2012) 7449-7454.

[9] R.E. Blankenship, Molecular mechanisms of photosynthesis, Blackwell Science, Oxford ; Malden, MA, 2002.

[10] N.J. Cherepy, A.P. Shreve, L.J. Moore, S.G. Boxer, R.A. Mathies, Electronic and nuclear dynamics of the accessory bacteriochlorophylls in bacterial photosynthetic reaction centers from resonance Raman intensities, J Phys Chem B, 101 (1997) 3250-3260.

[11] T. Brixner, T. Mancal, I.V. Stiopkin, G.R. Fleming, Phase-stabilized two-dimensional electronic spectroscopy, The Journal of Chemical Physics, 121 (2004) 4221-4236.

[12] M.L. Cowan, J.P. Ogilvie, R.J.D. Miller, Two-dimensional spectroscopy using diffractive optics based phased-locked photon echoes, Chemical Physics Letters, 386 (2004) 184-189.

[13] J.D. Hybl, A.W. Albrecht, S.M.G. Faeder, D.M. Jonas, Two-dimensional electronic spectroscopy, Chemical Physics Letters, 297 (1998) 307-313.

[14] D.C. Arnett, T.-S. Yang, N.F. Scherer, Optical and Vibrational Coherence in Bacteriochlorophyll a, in: Time-Resolved Vib. Spectrosc., Proc. Int. Conf. TRVS, Los Alamos National Labs, Santa Fe, NM, 1997, pp. 131-135.

[15] A. Chenu, N. Christensson, H.F. Kauffmann, T. Mancal, Enhancement of Vibronic and Ground-State Vibrational Coherences in 2D Spectra of Photosynthetic Complexes, Sci Rep-Uk, 3 (2013) 2029.

[16] G.S. Engel, T.R. Calhoun, E.L. Read, T.-K. Ahn, T. Mancal, Y.-C. Cheng, R.E. Blankenship, G.R. Fleming, Evidence for wavelike energy transfer through quantum coherence in photosynthetic systems, Nature, 446 (2007) 782-786.

[17] C. Kreisbeck, T. Kramer, Long-Lived Electronic Coherence in Dissipative Exciton Dynamics of Light-Harvesting Complexes, J Phys Chem Lett, 3 (2012) 2828-2833.

[18] J. Lim, D. Palecek, F. Caycedo-Soler, C.N. Lincoln, J. Prior, H. von Berlepsch, S.F. Huelga, M.B. Plenio, D. Zigmantas, J. Hauer, Vibronic origin of long-lived coherence in an artificial molecular light harvester, Nat Commun, 6 (2015) 7755.

[19] F. Milota, V.I. Prokhorenko, T. Mancal, H. von Berlepsch, O. Bixner, H.F. Kauffmann, J. Hauer, Vibronic and Vibrational Coherences in Two-Dimensional Electronic Spectra of Supramolecular J-Aggregates, J Phys Chem A, 117 (2013) 6007-6014.

[20] M.B. Plenio, J. Almeida, S.F. Huelga, Origin of long-lived oscillations in 2D-spectra of a quantum vibronic model: Electronic versus vibrational coherence, J Chem Phys, 139 (2013) 235102.

[21] E. Romero, R. Augulis, V.I. Novoderezhkin, M. Ferretti, J. Thieme, D. Zigmantas, R. van Grondelle, Quantum coherence in photosynthesis for efficient solar-energy conversion, Nat Phys, 10 (2014) 677-683.

[22] I.S. Ryu, H. Dong, G.R. Fleming, Role of Electronic-Vibrational Mixing in Enhancing Vibrational Coherences in the Ground Electronic States of Photosynthetic Bacterial Reaction Center, J Phys Chem B, 118 (2014) 1381-1388.

[23] D.B. Turner, K.E. Wilk, P.M.G. Curmi, G.D. Scholes, Comparison of Electronic and Vibrational Coherence Measured by Two-Dimensional Electronic Spectroscopy, The Journal of Physical Chemistry Letters, 2 (2011) 1904-1911.

[24] V. Butkus, D. Zigmantas, L. Valkunas, D. Abramavicius, Vibrational vs. electronic coherences in 2D spectrum of molecular systems, Chemical Physics Letters, 545 (2012) 40-43.

[25] A.W. Chin, J. Prior, R. Rosenbach, F. Caycedo-Soler, S.F. Huelga, M.B. Plenio, The role of non-equilibrium vibrational structures in electronic coherence and recoherence in pigment-protein complexes, Nat Phys, 9 (2013) 113-118.

[26] V. Butkus, L. Valkunas, D. Abramavicius, Vibronic phenomena and exciton-vibrational interference in two-dimensional spectra of molecular aggregates, J Chem Phys, 140 (2014) 034306.

[27] F.D. Fuller, J. Pan, A. Gelzinis, V. Butkus, S.S. Senlik, D.E. Wilcox, C.F. Yocum, L. Valkunas, D. Abramavicius, J.P. Ogilvie, Vibronic coherence in oxygenic photosynthesis, Nat Chem, 6 (2014) 706-711.

[28] G. Panitchayangkoon, D. Hayes, K.A. Fransted, J.R. Caram, E. Harel, J.Z. Wen, R.E. Blankenship, G.S. Engel, Long-lived quantum coherence in photosynthetic complexes at physiological temperature, P Natl Acad Sci USA, 107 (2010) 12766-12770.

[29] D. Hayes, J. Wen, G. Panitchayangkoon, R.E. Blankenship, G.S. Engel, Robustness of electronic coherence in the Fenna–Matthews–Olson complex to vibronic and structural modifications, Faraday Discussions, 150 (2011) 459-469.

[30] J.O. Goldsmith, S.G. Boxer, Rapid isolation of bacterial photosynthetic reaction centers with an engineered poly-histidine tag, Biochimica et Biophysica Acta (BBA)-Bioenergetics, 1276 (1996) 171-175.

[31] H.B. Zheng, J.R. Caram, P.D. Dahlberg, B.S. Rolczynski, S. Viswanathan, D.S. Dolzhnikov, A. Khadivi, D.V. Talapin, G.S. Engel, Dispersion-free continuum two-dimensional electronic spectrometer, Appl Optics, 53 (2014) 1909-1917.

[32] J.R. Caram, H.B. Zheng, P.D. Dahlberg, B.S. Rolczynski, G.B. Griffin, D.S. Dolzhnikov, D.V. Talapin, G.S. Engel, Exploring size and state dynamics in CdSe quantum dots using two-dimensional electronic spectroscopy, J Chem Phys, 140 (2014) 084701.

[33] V.P. Singh, A.F. Fidler, B.S. Rolczynski, G.S. Engel, Independent phasing of rephasing and non-rephasing 2D electronic spectra, J Chem Phys, 139 (2013) 084201.

[34] J.C. Williams, A.L.M. Haffa, J.L. McCulley, N.W. Woodbury, J.P. Allen, Electrostatic Interactions between Charged Amino Acid Residues and the Bacteriochlorophyll Dimer in Reaction Centers from Rhodobacter sphaeroides†, Biochemistry, 40 (2001) 15403-15407.

[35] M.H. Cho, T. Brixner, I. Stiopkin, H. Vaswani, G.R. Fleming, Two dimensional electronic spectroscopy of molecular complexes, J Chin Chem Soc-Taip, 53 (2006) 15-24.

[36] S. Westenhoff, D. Paleček, P. Edlund, P. Smith, D. Zigmantas, Coherent Picosecond Exciton Dynamics in a Photosynthetic Reaction Center, Journal of the American Chemical Society, 134 (2012) 16484-16487.

[37] Y. Jia, D.M. Jonas, T. Joo, Y. Nagasawa, M.J. Lang, G.R. Fleming, Observation of Ultrafast Energy Transfer from the Accessory Bacteriochlorophylls to the Special Pair in Photosynthetic Reaction Centers, The Journal of Physical Chemistry, 99 (1995) 6263-6266.

[38] M.H. Vos, J. Breton, J.-L. Martin, Electronic Energy Transfer within the Hexamer Cofactor System of Bacterial Reaction Centers, The Journal of Physical Chemistry B, 101 (1997) 9820-9832.

[39] J.A. Myers, K.L.M. Lewis, F.D. Fuller, P.F. Tekavec, C.F. Yocum, J.P. Ogilvie, Two-Dimensional Electronic Spectroscopy of the D1-D2-cyt b559 Photosystem II Reaction Center Complex, J Phys Chem Lett, 1 (2010) 2774-2780.

[40] T. Kramer, C. Kreisbeck, Modelling excitonic-energy transfer in light-harvesting complexes, in: AIP Conference Proceedings, 2014.

[41] Y.W. Jia, D.M. Jonas, T.H. Joo, Y. Nagasawa, M.J. Lang, G.R. Fleming, Observation of Ultrafast Energy-Transfer from the Accessory Bacteriochlorophylls to the Special Pair in Photosynthetic Reaction Centers, J Phys Chem-Us, 99 (1995) 6263-6266.

[42] N.J. Cherepy, A.P. Shreve, L.J. Moore, S.G. Boxer, R.A. Mathies, Temperature Dependence of the Qy Resonance Raman Spectra of Bacteriochlorophylls, the Primary Electron Donor, and Bacteriopheophytins in the Bacterial Photosynthetic Reaction Center†, Biochemistry, 36 (1997) 8559-8566.

[43] N.J. Cherepy, A.P. Shreve, L.J. Moore, S. Franzen, S.G. Boxer, R.A. Mathies, Near-Infrared Resonance Raman-Spectroscopy of the Special Pair and the Accessory Bacteriochlorophylls in Photosynthetic Reaction Centers, J Phys Chem-Us, 98 (1994) 6023-6029.

[44] A.P. Shreve, N.J. Cherepy, S. Franzen, S.G. Boxer, R.A. Mathies, Rapid-Flow Resonance Raman-Spectroscopy of Bacterial Photosynthetic Reaction Centers, Faseb J, 6 (1992) 11207-11211.

[45] M. del Rey, A.W. Chin, S.F. Huelga, M.B. Plenio, Exploiting Structured Environments for Efficient Energy Transfer: The Phonon Antenna Mechanism, J Phys Chem Lett, 4 (2013) 903-907.

[46] Y. Sato, B. Doolittle, Influence of intra-pigment vibrations on dynamics of photosynthetic exciton, J Chem Phys, 141 (2014) 185102.

[47] V. Perlik, J. Seibt, L.J. Cranston, R.J. Cogdell, C.N. Lincoln, J. Savolainen, F. Sanda, T. Mancal, J. Hauer, Vibronic coupling explains the ultrafast carotenoid-to-bacteriochlorophyll energy transfer in natural and artificial light harvesters, J Chem Phys, 142 (2015) 212434.

[48] J.M. Womick, B. West, N.F. Scherer, A.M. Moran, Vibronic effects in the spectroscopy and dynamics of C-phycocyanin, J Phys B-at Mol Opt, 45 (2012) 154016.

[49] J.M. Womick, A.M. Moran, Vibronic Enhancement of Exciton Sizes and Energy Transport in Photosynthetic Complexes, J Phys Chem B, 115 (2011) 1347-1356.

[50] V. Tiwari, W.K. Peters, D.M. Jonas, Electronic resonance with anticorrelated pigment vibrations drives photosynthetic energy transfer outside the adiabatic framework, P Natl Acad Sci USA, 110 (2013) 1203-1208.

[51] J. Seibt, T. Pullerits, Beating Signals in 2D Spectroscopy: Electronic or Nuclear Coherences? Application to a Quantum Dot Model System, J Phys Chem C, 117 (2013) 18728-18737.

[52] J. Dostal, T. Mancal, F. Vacha, J. Psencik, D. Zigmantas, Unraveling the nature of coherent beatings in chlorosomes, J Chem Phys, 140 (2014) 115103.

[53] G. Panitchayangkoon, D.V. Voronine, D. Abramavicius, J.R. Caram, N.H.C. Lewis, S. Mukamel, G.S. Engel, Direct evidence of quantum transport in photosynthetic light-harvesting complexes, P Natl Acad Sci USA, 108 (2011) 20908-20912.

[54] P.E. Tekavec, J.A. Myers, K.L.M. Lewis, J.P. Ogilvie, Two-dimensional electronic spectroscopy with a continuum probe, Opt Lett, 34 (2009) 1390-1392.

[55] J.R. Caram, A.F. Fidler, G.S. Engel, Excited and ground state vibrational dynamics revealed by two-dimensional electronic spectroscopy, J Chem Phys, 137 (2012) 024507.

[56] S.S. Senlik, V.R. Policht, J.P. Ogilvie, Two-Color Nonlinear Spectroscopy for the Rapid Acquisition of Coherent Dynamics, J Phys Chem Lett, 6 (2015) 2413-2420.

[57] D. Egorova, M.F. Gelin, W. Domcke, Analysis of cross peaks in two-dimensional electronic photon-echo spectroscopy for simple models with vibrations and dissipation, J Chem Phys, 126 (2007) 074314.

[58] S.M.G. Faeder, D.M. Jonas, Two-dimensional electronic correlation and relaxation spectra: Theory and model calculations, J Phys Chem A, 103 (1999) 10489-10505.

[59] C.J. Bardeen, Q. Wang, C.V. Shank, Selective Excitation of Vibrational Wave-Packet Motion Using Chirped Pulses, Phys Rev Lett, 75 (1995) 3410-3413.

[60] K.A. Fransted, J.R. Caram, D. Hayes, G.S. Engel, Two-dimensional electronic spectroscopy of bacteriochlorophyll a in solution: Elucidating the coherence dynamics of the Fenna-Matthews-Olson complex using its chromophore as a control, J Chem Phys, 137 (2012) 125101.

[61] C.C. Jumper, J.M. Anna, A. Stradomska, J. Schins, M. Myahkostupov, V. Prusakova, D.G. Oblinsky, F.N. Castellano, J. Knoester, G.D. Scholes, Intramolecular radiationless transitions dominate exciton relaxation dynamics, Chemical Physics Letters, 599 (2014) 23-33.

[62] M.B. Plenio, S.F. Huelga, Dephasing-assisted transport: quantum networks and biomolecules, New J Phys, 10 (2008).

[63] P. Rebentrost, M. Mohseni, I. Kassal, S. Lloyd, A. Aspuru-Guzik, Environment-assisted quantum transport, New J Phys, 11 (2009).

[64] A. Ishizaki, T.R. Calhoun, G.S. Schlau-Cohen, G.R. Fleming, Quantum coherence and its interplay with protein environments in photosynthetic electronic energy transfer, Physical Chemistry Chemical Physics, 12 (2010) 7319-7337.

[65] A. Ishizaki, G.R. Fleming, Unified treatment of quantum coherent and incoherent hopping dynamics in electronic energy transfer: Reduced hierarchy equation approach, J Chem Phys, 130 (2009).

[66] A. Ishizaki, G.R. Fleming, On the adequacy of the Redfield equation and related approaches to the study of quantum dynamics in electronic energy transfer, J Chem Phys, 130 (2009).

[67] P. Nalbach, A. Ishizaki, G.R. Fleming, M. Thorwart, Iterative path-integral algorithm versus cumulant time-nonlocal master equation approach for dissipative biomolecular exciton transport, New J Phys, 13 (2011).

[68] A. Chenu, G.D. Scholes, Coherence in Energy Transfer and Photosynthesis, Annu Rev Phys Chem, 66 (2015) 69-96.

[69] R. Tempelaar, T.L.C. Jansen, J. Knoester, Vibrational Beatings Conceal Evidence of Electronic Coherence in the FMO Light-Harvesting Complex, J Phys Chem B, 118 (2014) 12865-12872.

[70] V. Tiwari, W.K. Peters, D.M. Jonas, ENERGY TRANSFER Vibronic coherence unveiled, Nat Chem, 6 (2014) 173-175.

[71] T. Mancal, N. Christensson, V. Lukes, F. Milota, O. Bixner, H.F. Kauffmann, J. Hauer, System-Dependent Signatures of Electronic and Vibrational Coherences in Electronic Two-Dimensional Spectra, J Phys Chem Lett, 3 (2012) 1497-1502.

[72] T. Brixner, J. Stenger, H.M. Vaswani, M. Cho, R.E. Blankenship, G.R. Fleming, Two-dimensional spectroscopy of electronic couplings in photosynthesis, Nature, 434 (2005) 625-628.

[73] S. Mukamel, Multidimensional femtosecond correlation spectroscopies of electronic and vibrational excitations, Annual Review of Physical Chemistry, 51 (2000) 691-729.

[74] Y.C. Cheng, G.R. Fleming, Coherence quantum beats in two-dimensional electronic spectroscopy, J Phys Chem A, 112 (2008) 4254-4260.

[75] E.L. Read, G.S. Engel, T.R. Calhoun, T. Mancal, T.K. Ahn, R.E. Blankenship, G.R. Fleming, Cross-peak-specific two-dimensional electronic spectroscopy, P Natl Acad Sci USA, 104 (2007) 14203-14208.

[76] A.F. Fidler, V.P. Singh, P.D. Long, P.D. Dahlberg, G.S. Engel, Probing energy transfer events in the light harvesting complex 2 (LH2) of Rhodobacter sphaeroides with two-dimensional spectroscopy, J Chem Phys, 139 (2013).

[77] A.F. Fidler, V.P. Singh, P.D. Long, P.D. Dahlberg, G.S. Engel, Time Scales of Coherent Dynamics in the Light-Harvesting Complex 2 (LH2) of Rhodobacter sphaeroides, J Phys Chem Lett, 4 (2013) 1404-1409.

[78] E. Harel, G.S. Engel, Quantum coherence spectroscopy reveals complex dynamics in bacterial light-harvesting complex 2 (LH2), P Natl Acad Sci USA, 109 (2012) 706-711.

[79] G.S. Schlau-Cohen, A. Ishizaki, T.R. Calhoun, N.S. Ginsberg, M. Ballottari, R. Bassi, G.R. Fleming, Elucidation of the timescales and origins of quantum electronic coherence in LHCII, Nat Chem, 4 (2012) 389-395.

[80] G.S. Schlau-Cohen, T.R. Calhoun, N.S. Ginsberg, E.L. Read, M. Ballottari, R. Bassi, R. van Grondelle, G.R. Fleming, Pathways of Energy Flow in LHCII from Two-Dimensional Electronic Spectroscopy, J Phys Chem B, 113 (2009) 15352-15363.

[81] D. Hayes, G.B. Griffin, G.S. Engel, Engineering Coherence Among Excited States in Synthetic Heterodimer Systems, Science, 340 (2013) 1431-1434.

[82] K.M. Pelzer, T. Can, S.K. Gray, D.K. Morr, G.S. Engel, Coherent Transport and Energy Flow Patterns in Photosynthesis under Incoherent Excitation, J Phys Chem B, 118 (2014) 2693-2702.

[83] K.M. Pelzer, A.F. Fidler, G.B. Griffin, S.K. Gray, G.S. Engel, The dependence of exciton transport efficiency on spatial patterns of correlation within the spectral bath, New J Phys, 15 (2013).

Chapter 5:

Proposed Directions for Future Research

5.1 Introduction: Understanding Photochemistry

The experimental efforts presented in this dissertation highlight the delicate balance at the heart of chemistry in biology. Biological processes are constantly working to overcome the entropic tendency towards equilibrium, and light sensing and harvesting are no exceptions to this rule. In bacteriophytochromes, the chromophore isomerization occurs fast enough to resist interruption by fluctuations but occurs with low enough frequency to not accidentally initiate cell signaling. Light harvesting in purple bacteria transports energy from absorption location to the reaction center also occurs reliably despite being situated in a noisy environment, and the evidence in chapter 4 of this dissertation indicates that the balance between delocalization and loss of energy to chromophore vibrations is essential to prevent trapping or complete loss. Indeed, this process is so delicately balanced that we are unable to replicate this behavior in synthetic protein-chromophore light harvesting systems, as described in chapter 3.

Capturing useful light energy and controlling efficient photochemical reactions are important goals that science must complete in order to prepare society for a post-fossil fuel world. The seemingly random nature of photochemistry has prevented its use in synthesis and large scale production, but proteins have learned to control these reactions and have done so for over a billion years. In order to avoid a future of inefficient trial-and-error, and to understand the ways in which proteins succeed in this task, we must understand both the photochemical process of the chromophore as well as the role of the protein on the structural and primary sequence level. The

work in this dissertation has worked to shed light on how the protein influences the reactions so that we can separate protein effects from the pure photochemistry in future research. However, our understanding of light harvesting, photochemistry, and excited state dynamics in biological systems are not complete and more work in necessary to fully isolate the core design principles. In this chapter, I will outline some directions for future research.

5.2 Bacteriorhodospin: Exploring Conical Intersections

The bacteriophytochrome study presented in chapter 2 of this dissertation demonstrates that the protein is capable of promoting the same excited state dynamics and the same branching ratio between trans and cis configurations regardless of the initial position within the ground state energy well. However, the question of how the protein is able to control decay through the conical intersection point is vital in understanding the design principles of the complex but is still unknown. To probe the fundamentals of conical intersection control in biology, I propose a series of 2DES experiments on mutations in bacteriorhodopsin, another pigment protein complex in which the pigment undergoes a conical intersection isomerization. 2DES is an ideal tool to observe conical intersections with because, as shown in chapters 2 and 4 of this dissertation, we can analyze each sub-ensemble independently and track the decaying wavepacket's path information. This way, we can detect small changes in the decay pathway of the excited retinal molecule. 2DES also allows us to track the strongly coupled vibrational frequencies through vibrational coherence at the same time. Additionally, bacteriorhodopsin is an ideal system with which to understand conical intersections because it can be easily isolated from its organism *Halobacter salinarum* and its characteristic isomerization has been extensively studied in the

literature. The time constants and important residues for its biological proton pump function have been previously studied, and there are therefore many mutation studies that can inform a choice of mutants for this study.

In *H. salinarum*, bacteriorhodopsin functions as an auxiliary source for a proton gradient to power ATP synthase. The protein pumps a proton across the membrane and against the gradient when the embedded retinal molecule isomerizes. The proton gradient is used to power ATP synthase, providing energy for the cell. The organism can grow chemotrophically without light energy, but in the presence of visible light, it synthesizes enough bacteriorhodopsin such that entire swaths of the cell membrane are littered with crystalline trimers of bacteriorhodopsin. These phases of the membrane are named "purple membrane" and when the cell is sheered and the cell membrane fragmented, purple membrane is easily separable by density from the rest of the membrane. That is, it is simple to study bacteriorhodopsin in its endogenous trimer structure in the membrane and as isolated monomers in detergents. Since the development of UVA-GRAPES allows us to perform 2DES with membrane lipids present, we have the ability to observe conical intersections in bacteriorhodopsin and in its endogenous trimeric structure[1]. All of the following proposed experiments can be performed in both membrane and detergent micelles.

Bacteriorhodopsin is a member of the rhodopsin family of proteins. These proteins are all photoreceptors, though their functions widely vary, and they are all small, transmembrane protein in which a retinal molecule is covalently bonded to a lysine residue on the seventh helix (Fig. 1). However, the isomerization varies between rhodopsin family proteins. Retinal has a long conjugated tail (Fig. 2) and in solution, each bond is likely to undergo an isomerization with some probability. However, once bound inside the apo-protein, one bond isomerization is

selected and occurs with an increased quantum yield when compared to retinal in solution. For example, mammalian rhodopsin is used in the eye for vision isomerizes from 11-*cis* to all-*trans*, while both proteorhodopsin, channelrhodopsin, and bacteriorhodopsin convert from all-*trans* to 13-*cis*. The isomerization of retinal is non-selective, meaning it isomerizes about the 9^{th}, 11^{th}, 13^{th}, and 15^{th} bonds[2]. In solution, the process occurs in a few picoseconds with a quantum yield of about 0.25 for each, but in bacteriorhodopsin, the isomerization is 100% selective for all-*trans* to 13-*cis* and occurs with a quantum yield of isomerization product of 0.65[2]. For bovine rhodopsin, it is closer to a quantum yield of 0.67 for 11-*cis* to all-*trans*[2].

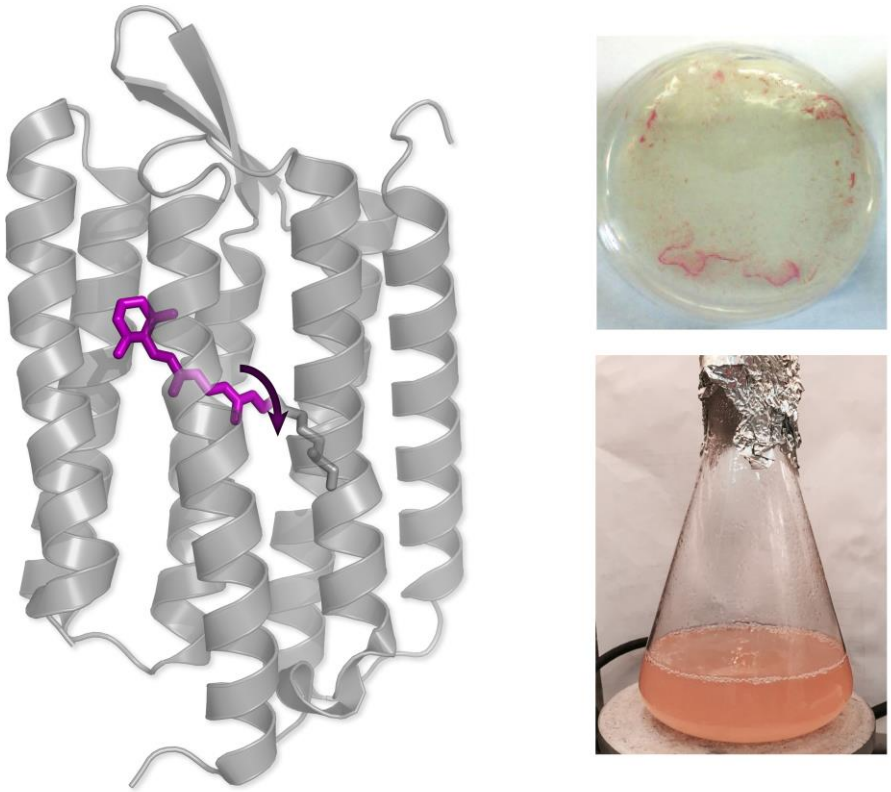

Figure 5.1: Structure of bacteriorhodopsin from *Halbacter salniarum*. (a) bacteriorhodopsin is a seven transmembrane helix protein with a covalently attached cofactor, retinal. Upon absorption of light, the 13^{th} carbon undergoes an isomerization from *trans* to *cis*. (b) Plate and liquid cultures of *H. salinarum* in the Engel lab. The pink color is from a combination of bacteriorhodopsin (purple) and sensory rhodopsins (red).

The theory of conical intersections defines the cone shape or the single degeneracy in two nuclear coordinates of the molecule in questions. These two coordinates, typically a stretch or rotation, span a "branching space" that defines the potential energy surfaces and intersection point. Therefore, identifying the important nuclear modes is the first step necessary to understanding this process in bacteriorhodopsin. In 2005, the Mathies group presented femtosecond stimulated raman spectroscopy (FSRS) data indicating that a 969 cm^{-1} hydrogen out of plane (HOOP) mode on the 11^{th} carbon and C_{11}=C_{12} torsion mode define the branching space in mammalian rhodopsin which undergoes an isomerization from 11-*cis* to all *trans*[3]. Additionally, in 2013, Liebel and Kukura report similar findings for bacteriorhodopsin. Using a new Raman technique, population assisted impulsive Raman spectroscopy (PAIRS), the authors

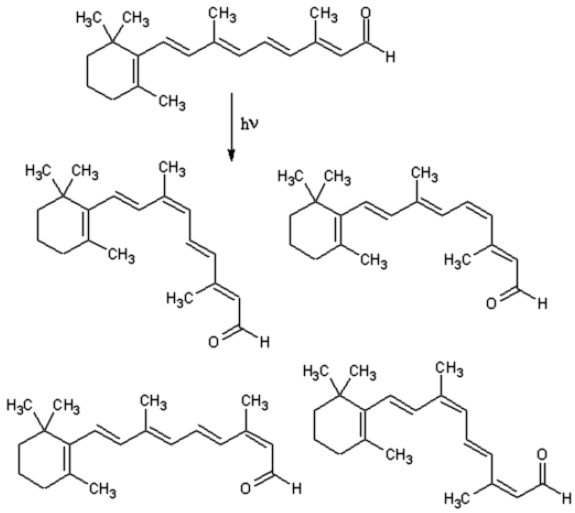

Figure 5.2: Retinal isomerizations in solution consist of 9-*cis*, 11-*cis*, 13-*cis*, and 9-*cis*-13-*cis*. Rhodopsin proteins control reactivity to select one isomerization process.

report that a 952 cm^{-1} HOOP mode and a low frequency 177 cm^{-1} torsional mode around the thirteenth carbon instead of the eleventh, however it is the symmetric C_{13}=C_{14} stretch around 1525 cm^{-1} that is displaced in the Franck-Condon region [4]. The striking agreement between these two studies in two different rhodopsin proteins implies that the two modes define the branching space of the visible retinal conical intersection, though it is unclear whether the stretch

or torsion define the reaction coordinate. In 2DES studies, we can observe which of these modes are strongly coupled to the decaying wavepacket and isolate the relevant modes.

5.2.1 Mutations that Perturb Isomer Control

Bacteriorhodopsin is capable of selecting which retinal isomer results after light absorption. Because this excited state decay occurs through a conical intersection that connect multiple product wells, we can infer that there is something about the nearby protein residues that are either sterically or electronically altering the branching space or wavepacket momentum such that the same isomer is produced every time. To determine how the protein is affecting this decay process, we need to study the electronic and vibrational differences between the wild type and relevant mutants. There are 11 residues within 6 Å of the C_{13} atom and are shown in Figure 3. Of these residues, a few have been studied with respect to their contribution to the proton pump function of bacteriorhodopsin. The proton translocation happens on a much slower process than the isomerization, so it is unlikely that the biological function plays a part in driving the isomerization. However, the mutants generated to study the proton translocation have been well characterized in the literature. Notably, the aspartic acid residue D85 and D212 have been extensively studied. The mutation D85N causes a red-shift and D85E cause a blue-shift in the absorption spectra, but both absorption are weaker under the same concentration and conditions when compared to the wild type[5-8]. However, D212 mutated to the same conservative residues, asparagine (N) and glutamic acid (E), give the opposite spectral shifts as D85, meaning D212N blue-shifts and D212E red-shifts the absorption peak.[7, 8] Importantly, the D212 mutations show a change in Raman spectra of the 1600 cm-1 modes, corresponding to C=C symmetric stretches.[5, 6] These mutants will all provide useful information about the subtle

effects of the protein, but none of the mutations disrupted or changed the isomerization product of the retinal molecule. Both aspartic acids are display their sidechains toward the protonated Schiff base covalently attaching the retinal to K216. Therefore, I propose that the first mutation study be on neighboring aromatic residues that are a little further from the Schiff base, namely, Y185 and W86, and to focus on more disruptive mutations than the D→N/E discussed above. However, it would be ideal to study mutations of all 11 residues. In this manner, a systematic study of the retinal pocket in bacteriorhodopsin will likely illuminate how the protein guides reactivity.

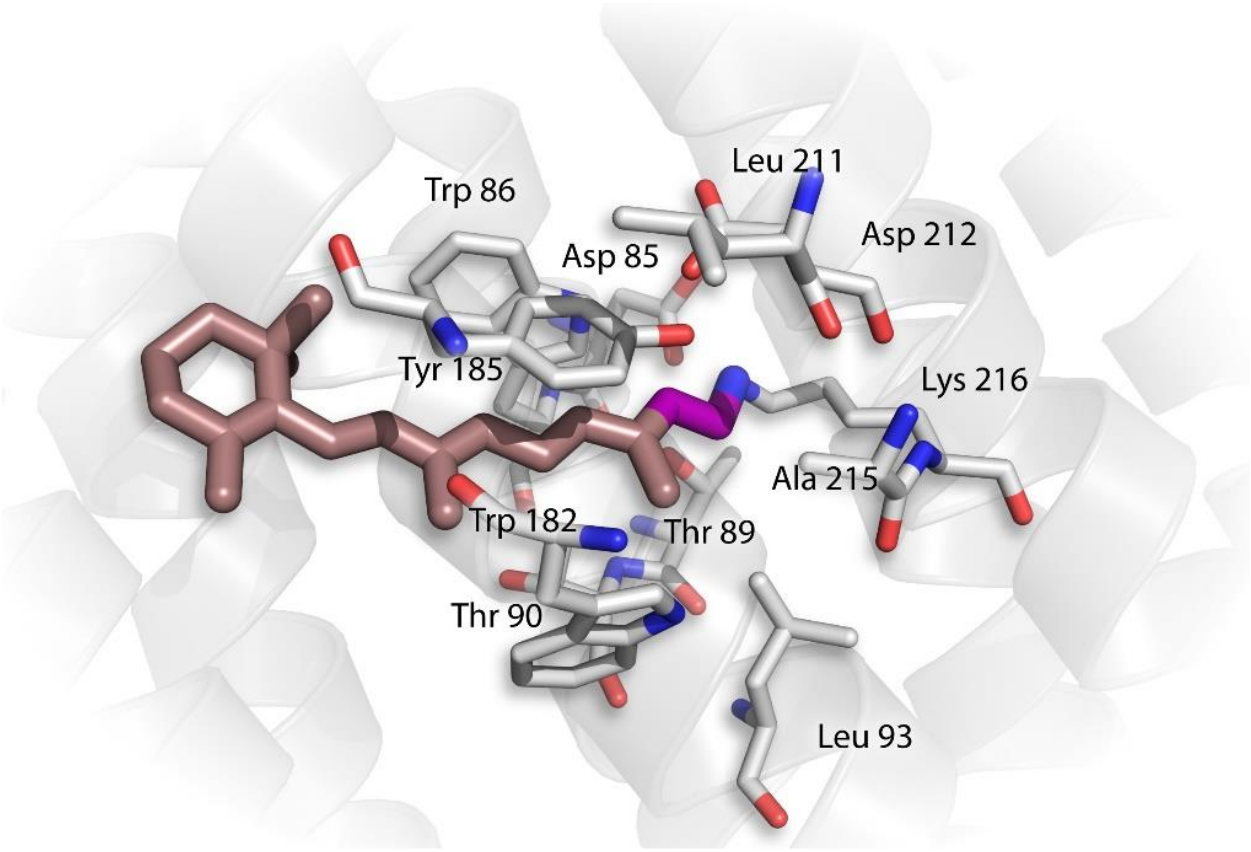

Figure 5.3: The eleven residues within 6 Å of the C_{13} atom of the retinal chromophore. Retinal is shown in salmon, while the C_{13} and C_{14} atoms are highlighted in magenta.

5.3 Nucleosomes: 2DES of Labeled Proteins to Probe Biology

In 1995, Polach and Widom discovered that the repeating unit of packaged chromatin, the nucleosome is in constant motion.[9] It is dynamically unwrapping and rewrapping the DNA strand around the core histone proteins. This finding shed light on the old question of how transcription factors and DNA binding proteins are able to find their targets within the tightly wound packaged chromatin.[10-12] The relationship between tightly ordered euchromatin and gene expression is fundamental to eukaryotic life. Since 1995, there have been publications expanding on this idea. Studies have found that DNA can unwrap halfway without losing their association to the histone core, and is able to rewrap itself. The contradiction inherent in this observation is vital to understanding gene expression in eukaryotes. Biochemists have been studying the dynamics of DNA wrapping in nucleosome with techniques from enzymatic digestion assays to fluorescence FRET measurements.[9, 11] However, the heterogeneity and correlation of motion in the system continues to elude researchers.

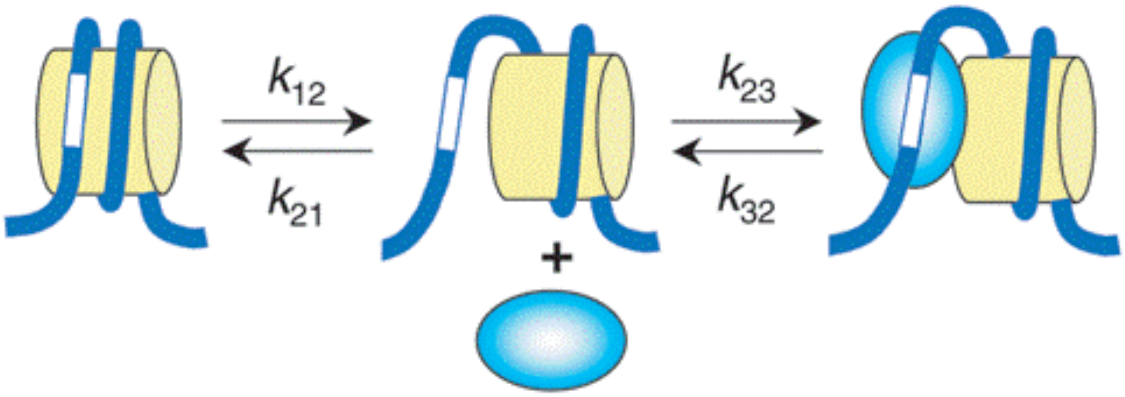

Figure 5.4: Scheme for transcription factor access to the DNA packaged into nucleosome. DNA unwraps due to random fluctuations with forward rate constant k_{12}, while transcription factors that bind to target DNA in the unwrapped portion, bind with rate constant k_{23}. This figure is reproduced with permission from Ref. 12

The work in this dissertation aims to build on our ability to characterize photophysics in protein environments. Chemists have been studying solvation dynamics, relaxation, and energy transfer between dyes for decades.[13-16] To spectroscopically answer remaining questions about nucleosome dynamics, I propose using 2DES to extract structural, conformational, heterogeneity, and coupling information from the same dye-labeled samples used in traditional FRET experiments. 2D spectroscopy can uncover correlations, couplings, and heterogeneity lost in traditional FRET experiments.

On the time scale of 2DES femtosecond to picosecond experiments, all large scale conformational motion of proteins and DNA are effectively frozen in place. That is, every sub-ensemble is frozen, and the distribution of conformations remains constant across the entire ensemble. 2DES can characterize the distribution of sub-ensembles while simultaneously measuring FRET rates between proximal chromophores FRET pairs. Additionally, by using well characterized FRET pairs in the experiment, 2DES can detect small changes in the solvation environment of each chromophore, providing more detailed insight into conformational information. The major hurdle in this experiment will be deciphering a likely congested spectra, but with proper controls and the multiple strategies employed in the Engel research group to untangle dense data, this is easily overcome[17-19].

The first set of experiments to be pursued in this direction should aim to characterize the endogenous dynamics of the mononucleosome in the absence of any larger chromatin structure or transcription factors competing with binding to the DNA fragments. Each of the standard histones that comprise the nucleosome core unit are already easily expressible in *E. coli* with histidine tags for easy purification,[20] and there exist a set of so-called “Widom 601” DNA sequences that have been developed to bind the histone core.[21] A series of experiments and

controls in which three chromophores are attached to the DNA at both ends and one in the center may uncover the symmetry, correlation, and frequency of fluctuations and unwrapping in the mononucleosome. When the nucleosome is completely wrapped, both ends of the double stranded DNA fragment will be in close proximity with each other and the center of the DNA fragment (Fig. 5). The three labels will all be strongly coupled in this conformation, and provide three distinct spectroscopic features to interact and to track with 2DES. To help assign signals to the proper conformations and sub-ensembles, a series of control experiments must accompany this experiment. Experiments of controls in solution and a nucleosome with one attached chromophore are necessary, but all combinations of two chromophores will add more useful information to understanding the resulting data.

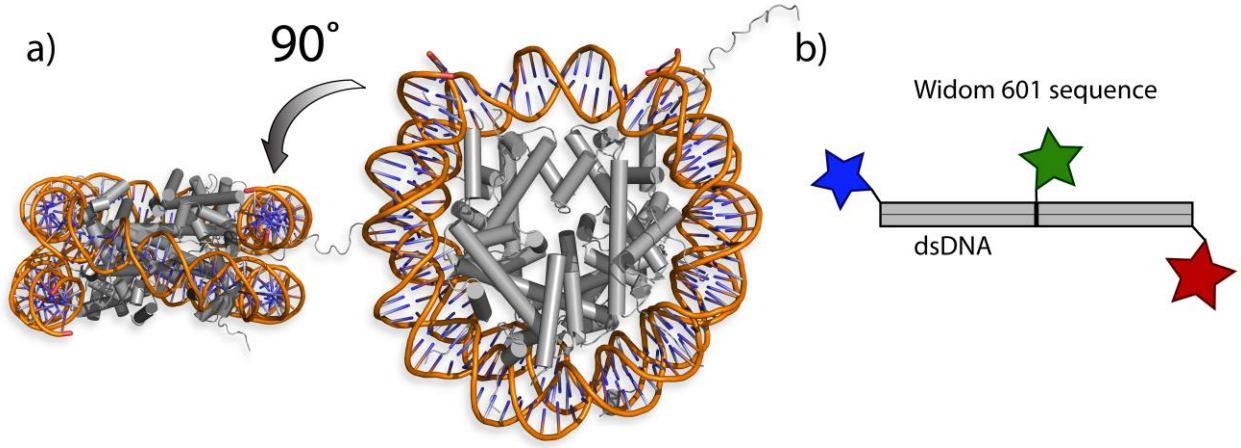

Figure 5.5: Structure and proposed labeling of a mononucleosome. (a) Structural view from the top and side of a mononucleosome. The histone core contains 8 proteins: two of each H2A H2B, H3 and H4 proteins. 147 basepairs of DNA wrap once and a half around the protein core. (b) Location of three proposed fluorophores/chromophores attachments on the Widom 601 DNA sequence, designed to bind the histone core.

The bacteriophytochrome study in chapter 2 is a great example of the path information that can be gleaned from 2DES. In that study, each sub-ensemble was analyzed individually and tracked as the waiting time in the experiment progressed. Therefore, the data was able to inform our understanding of the excited state pathway as it correlated to the initial starting point in the Franck-Condon region of the potential energy surface. Similar analysis will be vital to untangling the information in the chromophore-labeled mononucleosome experiments. For example, FRET rates and efficiencies can be tracked individually. That is, if the blue chromophore, attached to the 5' end of the sense strand of DNA, is exposed to more solvent because it has unwrapped from the histone core, it will likely have a slightly different transition energy than the same blue chromophore in a mononucleosome that is tightly wrapped at the time of the experiment. These two signals can be analyzed individually and FRET rates can be assigned to two populations of the same chromophore. Time resolved fluorescence experiments are capable of resolving multiple time constants in the energy transfer rate, but it not assign them to the correct population. By correlating input and output energies, 2DES gives us this extra information. Now, if we correlate energy transfer from the smaller transition energy of the blue chromophore to both the center and red end chromophores, we can assign it to the close conformation state.

Once the mononuceleosome is well characterized, there are many directions of inquiry to follow next. It is still unclear if dynamics change with the length of excess DNA on either end or how two or three linked nucleosomes may act. Depending on what is learned from the first set of experiments, it may be fruitful to follow by adding in transcription factors and assaying binding in addition to fluctuations. Arguably, the most important question to answer is what form is chromatin in when packaged in the cell nucleus. Is it highly structured, as it is when folded into chromosomes or is disordered in a polymer liquid-like state to allow better access to polymerases

and transcription factors? Gene expression is crucial to life so understanding the process *in vivo* is important to understanding life. 2DES of labeled chromatin would be tough experimentally but could lead towards fully understanding the process.

5.4 Conclusion

The work presented in this dissertation aims to understand how biology impacts photochemistry and vice versa. Therefore, it is natural that I propose experimental efforts to continue our understanding in both of these directions. A systematic, detailed spectroscopic study of mutations in bacteriorhodopsins will answer the unanswered questions from the bacteriophytochrome work in chapter 2. The bacteriophytochrome work provides evidence for the robustness of the photochemistry in the pigment-protein complex, but fails to identify the necessary pigment-protein interaction responsible for this. In the model system, bacteriorhodopsin, the fundamental principle of kinetic control through photoisomerization can be identified. Additionally, the larger question of how to exploit photo-physics to further understand biological processes and systems is directly addressed with my second future proposal. Armed with our knowledge and understanding of the impact of biology on the spectroscopic signatures of chromophores, we can use dye-labeled DNA-protein complexes, nucleosomes, to better understand the interaction and dynamics of physically unperturbed systems.

5.5 References

[1] P.D. Dahlberg, A.F. Fidler, J.R. Caram, P.D. Long, G.S. Engel, Energy Transfer Observed in Live Cells Using Two-Dimensional Electronic Spectroscopy, J Phys Chem Lett 4 (2013) 3636-3640.

[2] C. Dugave, L. Demange, Cis-trans isomerization of organic molecules and biomolecules: Implications and applications, Chem Rev 103 (2003) 2475-2532.

[3] P. Kukura, D.W. McCamant, S. Yoon, D.B. Wandschneider, R.A. Mathies, Structural observation of the primary isomerization in vision with femtosecond-stimulated Raman, Science 310 (2005) 1006-1009.

[4] M. Liebel, C. Schnedermann, G. Bassolino, G. Taylor, A. Watts, P. Kukura, Direct Observation of the Coherent Nuclear Response after the Absorption of a Photon, Phys Rev Lett 112 (2014).

[5] M.S. Braiman, T. Mogi, T. Marti, L.J. Stern, H.G. Khorana, K.J. Rothschild, Vibrational Spectroscopy of Bacteriorhodopsin Mutants - Light-Driven Proton Transport Involves Protonation Changes of Aspartic-Acid Residue-85, Residue-96, and Residue-212, Biochemistry 27 (1988) 8516-8520.

[6] M.S. Braiman, T. Mogi, L.J. Stern, N.R. Hackett, H.G. Khorana, K.J. Rothschild, Tyrosine-185 Acts as a Proton Acceptor during Bacteriorhodopsins Photocycle - Evidence from Ft-Ir Spectra of Site-Directed Mutants, Biophysical Journal 53 (1988) A442-A442.

[7] K.J. Rothschild, M.S. Braiman, Y.W. He, T. Marti, H.G. Khorana, Vibrational Spectroscopy of Bacteriorhodopsin Mutants - Evidence for the Interaction of Aspartic-Acid 212 with Tyrosine 185 and Possible Role in the Proton Pump Mechanism, J Biol Chem 265 (1990) 16985-16991.

[8] S. Subramaniam, T. Marti, H.G. Khorana, Protonation State of Asp (Glu)-85 Regulates the Purple-to-Blue Transition in Bacteriorhodopsin Mutants Arg-82-]Ala and Asp-85-]Glu - the Blue Form Is Inactive in Proton Translocation, Proceedings of the National Academy of Sciences of the United States of America 87 (1990) 1013-1017.

[9] K.J. Polach, J. Widom, Mechanism of Protein Access to Specific DNA-Sequences in Chromatin - a Dynamic Equilibrium-Model for Gene-Regulation, J Mol Biol 254 (1995) 130-149.

[10] J.D. Anderson, A. Thastrom, J. Widom, Spontaneous access of proteins to buried nucleosomal DNA target sites occurs via a mechanism that is distinct from nucleosome translocation, Mol Cell Biol 22 (2002) 7147-7157.

[11] W.J.A. Koopmans, R. Buning, T. Schmidt, J. van Noort, spFRET Using Alternating Excitation and FCS Reveals Progressive DNA Unwrapping in Nucleosomes, Biophysical Journal 97 (2009) 195-204.

[12] G. Li, M. Levitus, C. Bustamante, J. Widom, Rapid spontaneous accessibility of nucleosomal DNA, Nat Struct Mol Biol 12 (2005) 46-53.

[13] G.R. Fleming, M.H. Cho, Chromophore-solvent dynamics, Annu Rev Phys Chem 47 (1996) 109-134.

[14] M.H. Cho, S.J. Rosenthal, N.F. Scherer, L.D. Ziegler, G.R. Fleming, Ultrafast Solvent Dynamics - Connection between Time Resolved Fluorescence and Optical Kerr Measurements, J Chem Phys 96 (1992) 5033-5038.

[15] T.S. Yang, M.S. Chang, R. Chang, M. Hayashi, S.H. Lin, P. Vohringer, W. Dietz, N.F. Scherer, Femtosecond pump-probe study of molecular vibronic structures and dynamics of a cyanine dye in solution, J Chem Phys 110 (1999) 12070-12081.

[16] T.S. Yang, P. Vohringer, W. Dietz, N.F. Scherer, S.H. Lin, Molecular vibronic structures of HDITC in solutions studied by femtosecond wavelength-resolved pump-probe spectroscopy, J Chin Chem Soc-Taip 46 (1999) 409-416.

[17] J.R. Caram, A.F. Fidler, G.S. Engel, Excited and ground state vibrational dynamics revealed by two-dimensional electronic spectroscopy, J Chem Phys 137 (2012).

[18] J.R. Caram, G.S. Engel, Extracting dynamics of excitonic coherences in congested spectra of photosynthetic light harvesting antenna complexes, Faraday Discuss 153 (2011) 93-104.

[19] A.F. Fidler, E. Harel, P.D. Long, G.S. Engel, Two-Dimensional Spectroscopy Can Distinguish between Decoherence and Dephasing of Zero-Quantum Coherences, J Phys Chem A 116 (2012) 282-289.

[20] E. Hochuli, W. Bannwarth, H. Dobeli, R. Gentz, D. Stuber, Genetic Approach to Facilitate Purification of Recombinant Proteins with a Novel Metal Chelate Adsorbent, Bio-Technol 6 (1988) 1321-1325.

[21] P.T. Lowary, J. Widom, New DNA sequence rules for high affinity binding to histone octamer and sequence-directed nucleosome positioning, J Mol Biol 276 (1998) 19-42.

Chapter 6:

Conclusion

The study of photoactive proteins provides insight into the principles that control photochemistry. The mechanisms through which protein drive photochemistry and light harvesting are still not fully understood. The immediate solvation environment around the chromophore is static compared to a solvent like water and cannot rearrange in response to absorption of light and subsequent change in electronic structure. This structured solvation environment introduces opportunities for control not accessible to chemists worked in solvents. Therefore, proteins can push back on an excited dipole and have the potential to alter dynamics and outcome of the embedded photochemistry. To investigate the photochemistry itself, we need to determine the protein's influence on excited state dynamics of pigment-protein complexes. For example, a photon will drive isomerization of a chromophore, but that chromophore exerts force on the protein both sterically and electrostatically throughout this process. The protein then reacts to this force effectively creating feedback and intrinsically affecting the dynamics of the chromophore. In this manner, the relationship between the protein and the chromophore drives the photochemistry, and in this dissertation, I present experimental evidence of the fundamental photochemical design principles the protein exploits for its function.

In chapter 2, 2DES of bacteriophytochromes reveal the ability of the protein to retain its core, photochemical behavior in spite of heterogeneous conformations and fluctuations. The timescale of the nonradiative isomerization decay has been assigned time constants on the order of 30 ps[1], but isomerizations through conical intersections in other pigment-protein complexes such

as photoactive yellow protein and rhodopsin, have been assigned time constants on the order of 100 fs to 2 ps[2-5]. If bacteriophytochromes do not progress through a conical intersection decay, the isomerization must happen on the excited state and two very distinct *cis* and *trans* excited state pathways would be apparent in the 2DES of the excited state dynamics. The two dimensional nature of 2DES that correlates input and output energies allowed each sub-ensemble to be analyzed separately, thereby providing an analysis that can distinguish between one or two distinct excited state pathways. The result showed that despite the presence of ground state heterogeneity in transition energy to the excited state, only one dynamic pathway is observed indicating that isomerization is an excited to ground state process characteristic of a conical intersection.

The investigation of a synthetic light-harvesting pigment-protein complex in chapter 3 indicated that further design principles are necessary to recreate the coherent, ultrafast energy transfer characteristic of photosynthetic light harvesting. The synthetic light-harvesting complex is built of Tobacco Mosaic Virus capsid protein monomers that self assemble into a double layer disc. Each monomer is labeled with an Alexa Fluor 594 molecule, and the final result is a pigment-protein ring reminiscent of LH2 from *R. sphaeroides [6, 7]*. With a combination of linear absorption lineshape analysis and 2DES, there is indeed evidence of excited state interaction between neighboring chromophores, although in the regime of Förster resonance energy transfer rather than coherent resonance energy transfer found in photosynthetic light-harvesting complexes. The Forster regime result indicates that something is missing in this synthetic light-harvesting complex that is either the lack of full restriction of motion for the chromophores or the vibrational structure of the molecule, though in all likelihood, both influences are significant.

Lastly, in chapter 4, investigation of a series of reaction center mutants display the ability to retain ultrafast energy transfer despite highly disruptive mutations in proximity to the special pair of bacteriochlorophylls though fine tuning of the excitonic energy gaps and vibrational energy traps[8]. Efforts to perturb energy transfer dynamics with highly disruptive point mutations in the direct vicinity of the special pair bacteriochlorophylls lead to no significant changes. That is, the protein scaffold is better at preserving light-harvesting behavior than we are at perturbing it. By analyzing the coherences exhibited by sub-ensembles throughout the 2D spectrum, we are able to provide strong evidence that the balance between the protein scaffold and the vibrational structure of the ground and excited states in bacteriochlorophyll provide the resistance to disruption that had been observed.

The results from the experimental efforts in this dissertation highlight how simple chemistry is at the heart of complex biological systems. The delicate balance between protein scaffold and energy tuning and the response and vibrational structure of the chromophores are sufficient to drive ultrafast, stereospecific excited state dynamics and photochemistry. In light of these results, future work can shift focus from defining the protein's role in photo-induced processes to understanding the underlying properties. Biology has given us a valuable opportunity to learn about photochemistry in the form of full functional pigment-protein complexes; now that we have a clearer understanding of the protein's contribution, we can begin to study the fundamentals of photochemistry itself.

6.1 References

[1] Y. Yang, M. Linke, T. von Haimberger, J. Hahn, R. Matute, L. González, P. Schmieder, K. Heyne, Real-Time Tracking of Phytochrome's Orientational Changes During Pr Photoisomerization, Journal of the American Chemical Society 134 (2012) 1408-1411.

[2] E.E. Grintsevich, I.E. Adzerikho, A.G. Mrochek, D.I. Metelitza, Polydisulfides of substituted phenols as effective protectors of peroxidase against inactivation by ultrasonic cavitation, Biochemistry. Biokhimiia 66 (2001) 740-746.

[3] K. Pande, C.D.M. Hutchison, G. Groenhof, A. Aquila, J.S. Robinson, J. Tenboer, S. Basu, S. Boutet, D.P. DePonte, M.N. Liang, T.A. White, N.A. Zatsepin, O. Yefanov, D. Morozov, D. Oberthuer, C. Gati, G. Subramanian, D. James, Y. Zhao, J. Koralek, J. Brayshaw, C. Kupitz, C. Conrad, S. Roy-Chowdhury, J.D. Coe, M. Metz, P.L. Xavier, T.D. Grant, J.E. Koglin, G. Ketawala, R. Fromme, V. Srajer, R. Henning, J.C.H. Spence, A. Ourmazd, P. Schwander, U. Weierstall, M. Frank, P. Fromme, A. Barty, H.N. Chapman, K. Moffat, J.J. van Thor, M. Schmidt, Femtosecond structural dynamics drives the trans/cis isomerization in photoactive yellow protein, Science 352 (2016) 725-729.

[4] M.E. Vanbrederode, T. Gensch, W.D. Hoff, K.J. Hellingwerf, S.E. Braslavsky, Photoinduced Volume Change and Energy-Storage Associated with the Early Transformations of the Photoactive Yellow Protein from Ectothiorhodospira-Halophila, Biophysical Journal 68 (1995) 1101-1109.

[5] L.A. Peteanu, R.W. Schoenlein, Q. Wang, R.A. Mathies, C.V. Shank, The 1st Step in Vision Occurs in Femtoseconds - Complete Blue and Red Spectral Studies, Proc Natl Acad Sci U S A 90 (1993) 11762-11766.

[6] Y.Z. Ma, R.A. Miller, G.R. Fleming, M.B. Francis, Energy transfer dynamics in light-harvesting assemblies templated by the tobacco mosaic virus coat protein, J Phys Chem B 112 (2008) 6887-6892.

[7] R.A. Miller, A.D. Presley, M.B. Francis, Self-assembling light-harvesting systems from synthetically modified tobacco mosaic virus coat proteins, J Am Chem Soc 129 (2007) 3104-3109.

[8] M.L. Flanagan, P.D. Long, P.D. Dahlberg, B.S. Rolczynski, S.C. Massey, G.S. Engel, Mutations to R. sphaeroides Reaction Center Perturb Energy Levels and Vibronic Coupling but Not Observed Energy Transfer Rates, J Phys Chem A 120 (2016) 1479-1487.